Cancer Cell

Article

Intersection of immune and oncometabolic pathways drives cancer hyperprogression during immunotherapy

Graphical abstract

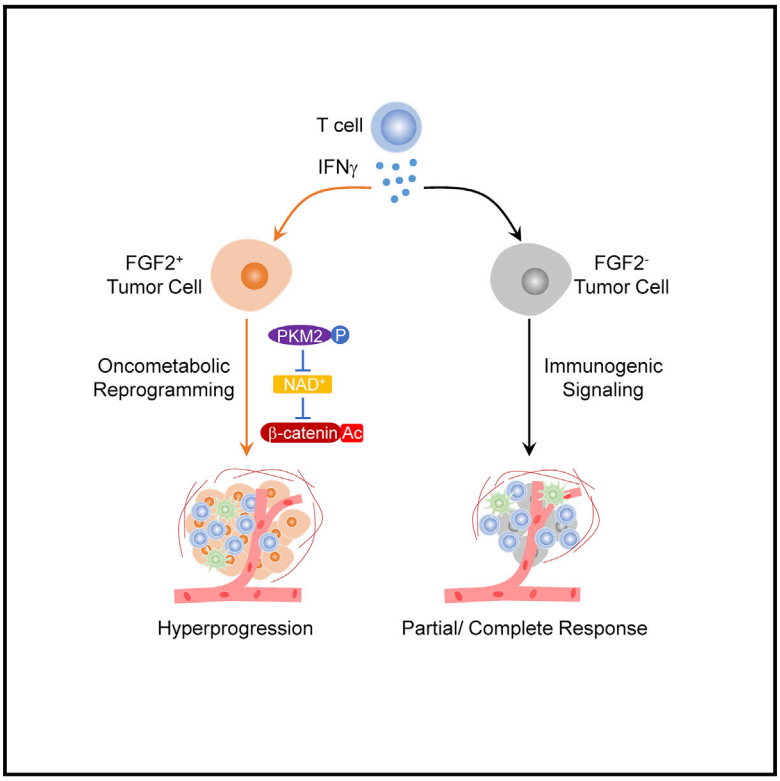

Highlights

- Hyperprogressive disease (HPD) occurs during immunotherapy
- HPD is associated with high levels of IFNγ, FGF2, and β-catenin signaling
- $CD8^+$ T cell derived IFNγ promotes HPD via rewiring cancer oncometabolic pathways
- High IFNγ-FGF2-β-catenin signature is a potential biomarker and target for HPD

Authors

Gaopeng Li, Jae Eun Choi, Ilona Kryczek, ..., Michael D. Green, Arul M. Chinnaiyan, Weiping Zou

Correspondence

migr@umich.edu (M.D.G.), wzou@umich.edu (W.Z.)

In brief

Li et al. uncover crosstalk between core immunogenic, metabolic, and oncogenic pathways in cancer cells during immunotherapy, which enables hyperprogressive disease (HPD) in preclinical models and correlates with immunotherapy-associated HPD in patients with cancer.

Li et al., 2023, Cancer Cell *41*, 304–322
February 13, 2023
https://doi.org/10.1016/j.ccell.2022.12.008

CellPress

CellPress

Cancer Cell

Article

Intersection of immune and oncometabolic pathways drives cancer hyperprogression during immunotherapy

Gaopeng Li,[1,2] Jae Eun Choi,[3,4] Ilona Kryczek,[1,2] Yilun Sun,[5,6] Peng Liao,[1,2] Shasha Li,[1,2] Shuang Wei,[1,2] Sara Grove,[1,2] Linda Vatan,[1,2] Reagan Nelson,[5] Grace Schaefer,[5] Steven G. Allen,[5] Kamya Sankar,[7] Leslie A. Fecher,[7] Mishal Mendiratta-Lala,[5] Timothy L. Frankel,[1] Angel Qin,[7] Jessica J. Waninger,[4,5] Alangoya Tezel,[5] Ajjai Alva,[2,7] Christopher D. Lao,[7] Nithya Ramnath,[7,8] Marcin Cieslik,[3,4,9] Paul W. Harms,[3] Michael D. Green,[2,5,8,11,12,*] Arul M. Chinnaiyan,[3,4,10] and Weiping Zou[1,2,3,11,12,13,*]

[1]Department of Surgery, University of Michigan, Ann Arbor, MI, USA
[2]Center of Excellence for Cancer Immunology and Immunotherapy, University of Michigan Rogel Cancer Center, Ann Arbor, MI, USA
[3]Department of Pathology, University of Michigan, Ann Arbor, MI, USA
[4]Michigan Center for Translational Pathology, University of Michigan, Ann Arbor, MI, USA
[5]Department of Radiation Oncology, University of Michigan, Ann Arbor, MI, USA
[6]Department of Biostatistics, University of Michigan, Ann Arbor, MI, USA
[7]Department of Internal Medicine, University of Michigan, Ann Arbor, MI, USA
[8]Veterans Affairs Ann Arbor Healthcare System, Ann Arbor, MI, USA
[9]Department of Computational Medicine & Bioinformatics, University of Michigan, Ann Arbor, MI, USA
[10]Howard Hughes Medical Institute, University of Michigan, Ann Arbor, MI, USA
[11]Graduate Program in Immunology, University of Michigan, Ann Arbor, MI, USA
[12]Graduate Program in Cancer Biology, University of Michigan, Ann Arbor, MI, USA
[13]Lead contact
*Correspondence: migr@umich.edu (M.D.G.), wzou@umich.edu (W.Z.)
https://doi.org/10.1016/j.ccell.2022.12.008

SUMMARY

Immune checkpoint blockade (ICB) can produce durable responses against cancer. We and others have found that a subset of patients experiences paradoxical rapid cancer progression during immunotherapy. It is poorly understood how tumors can accelerate their progression during ICB. In some preclinical models, ICB causes hyperprogressive disease (HPD). While immune exclusion drives resistance to ICB, counterintuitively, patients with HPD and complete response (CR) following ICB manifest comparable levels of tumor-infiltrating $CD8^+$ T cells and interferon γ (IFNγ) gene signature. Interestingly, patients with HPD but not CR exhibit elevated tumoral fibroblast growth factor 2 (FGF2) and β-catenin signaling. In animal models, T cell-derived IFNγ promotes tumor FGF2 signaling, thereby suppressing PKM2 activity and decreasing NAD^+, resulting in reduction of SIRT1-mediated β-catenin deacetylation and enhanced β-catenin acetylation, consequently reprograming tumor stemness. Targeting the IFNγ-PKM2-β-catenin axis prevents HPD in preclinical models. Thus, the crosstalk of core immunogenic, metabolic, and oncogenic pathways via the IFNγ-PKM2-β-catenin cascade underlies ICB-associated HPD.

INTRODUCTION

The molecular determinants of tumor response to immunotherapy are incompletely defined. Immune checkpoint blockade (ICB) therapy unleashes T cell-mediated anti-tumor immunity to promote partial or complete responses in a wide variety of cancers.[1–4] However, ICB can also result in atypical patterns of response, including pseudoprogression, in which an initial increase in tumor size is followed by subsequent clinical benefit from therapy.[5] Unfortunately, most patients with cancer develop stable or progressive disease on ICB.[2] More recently, it has been suggested that initiation of ICB may promote hyperprogressive disease (HPD),[6] which manifests as acceleration of cancer growth during ICB. Signaling induced by the ICB antibodies as well as amplification of *EGFR* or *MDM2/4* are associated with HPD.[7] Prior studies have identified T cell exclusion and immune signaling dysfunction as contributors to tumor progression on immunotherapy.[1–4] However, the importance of tumoral immune composition in atypical but clinically relevant patterns of response to ICB remains poorly defined.

Interferon γ (IFNγ) signaling is a key immunogenic pathway and plays a decisive role in spontaneous and ICB-induced anti-tumor immunity.[8] Host IFNγ signaling supports tumor antigen presentation, antigen-presenting cell (APC) activation, and effector T cell recruitment and directly affects tumor cell proliferation and survival.[1] Loss of IFNγ signaling in tumor cells results in

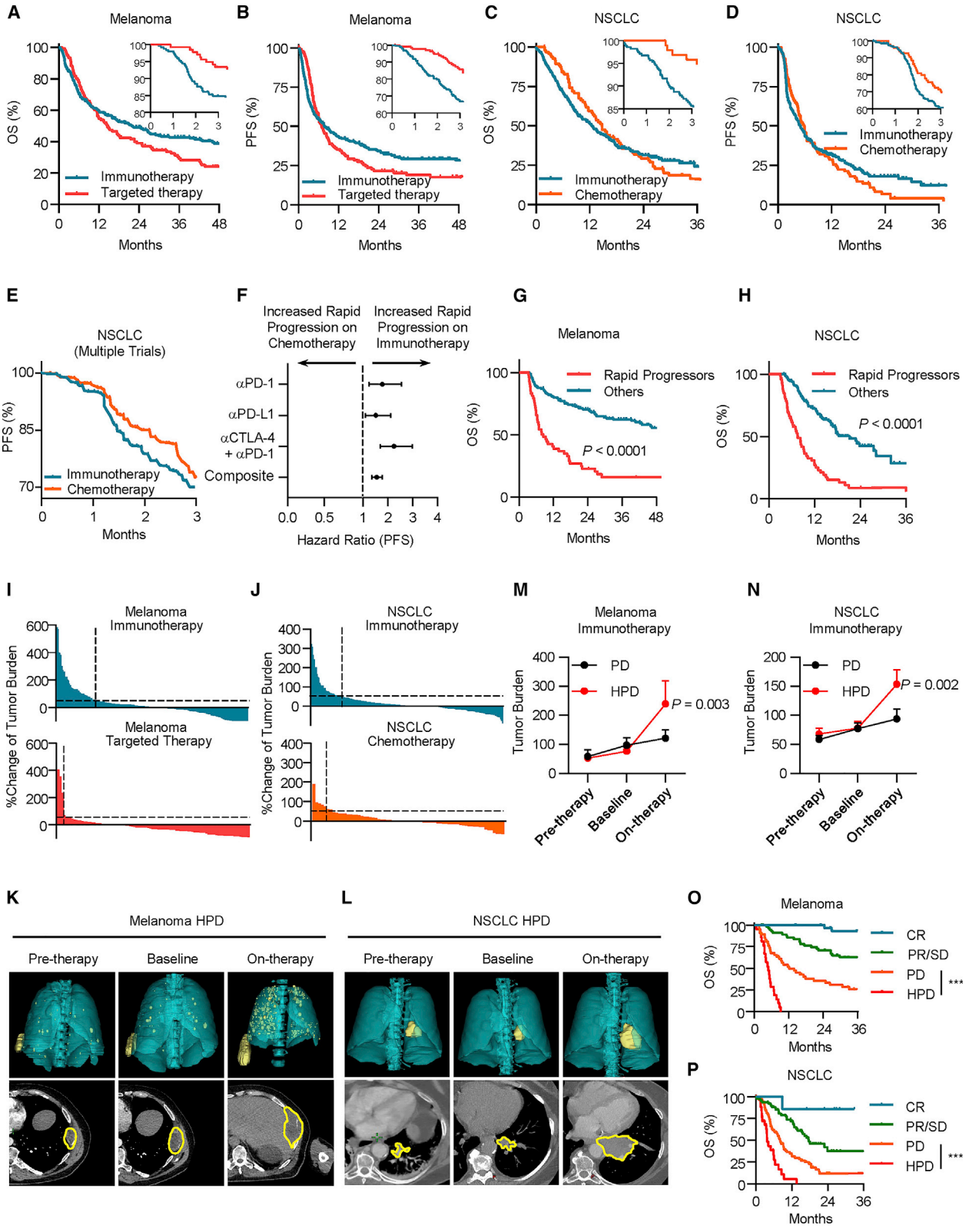

Figure 1. Rapid cancer progression occurs in a subset of patients during immunotherapy

(A) Overall survival (OS) of patients with metastatic melanoma (cohort 1) stratified by therapy type. Inset: 3-month OS. Immunotherapy, n = 251; targeted therapy, n = 138; restricted mean survival time (RMST) at 3 months, hazard ratio (HR) = 0.95, p < 0.0001 by log-rank test.

(legend continued on next page)

immune evasion and resistance to immunotherapy.[9–12] However, prolonged IFNγ exposure confers tumor resistance to ICB via multiple mechanisms, including PD-L1 induction and induction of cancer stemness.[13–16] Hence, IFNγ signaling can play a dual role in cancer immune responses. However, whether IFNγ can directly promote tumor progression in the context of immunotherapy remains unknown.

An intertwined network of oncogenic and metabolic programs works to support cancer growth and viability.[17–19] Oncogenes, including β-catenin, promote tumor stemness and invasiveness and increase metastatic potential.[20] Additionally, β-catenin signaling enhances tumor cell survival by inducing *MYC* and other genes.[21] Consequently, β-catenin signaling can promote resistance to immunotherapy.[13,22] Oncogenic programs also upregulate aerobic glycolysis to support cancer progression.[23] Furthermore, overexpression of tumor growth-stimulatory signals, including epidermal growth factor (EGF) and fibroblast growth factor (FGF), enables unchecked growth.[24,25] However, the importance and mechanism of how these oncogenic and metabolic drivers of cancer progression interact with immunogenic signaling induced by ICB therapy are poorly understood.

Here, we explored the interplay between key immunogenic (IFNγ), metabolic (glycolysis), and oncogenic (β-catenin) pathways in suspected ICB-associated HPD in tumor-bearing murine models and patients with cancer. We discover that core immunogenic, metabolic, and oncogenic pathway crosstalk provides a cellular and molecular basis for ICB-associated HPD. Our work suggests that targeting this crosstalk may prevent suspected iatrogenic cancer progression in patients receiving ICB.

RESULTS

Rapid cancer progression occurs in a subset of patients during immunotherapy

Immunotherapy has altered the landscape of cancer treatment. It is not fully understood whether there are differences in clinical response to immunotherapy compared with established cancer therapy. To explore this, we examined a cohort of patients with metastatic melanoma treated with ICB or targeted therapy at the University of Michigan (cohort 1, 389 patients; Table S1). ICB improved overall survival of patients compared with targeted therapy (Figure 1A). Surprisingly, a subset of patients treated with immunotherapy progressed rapidly within 3 months compared with those who received targeted therapy (Figure 1A, inset). Similarly, we noted that, although ICB improved the progression-free survival of patients with metastatic melanoma (Figure 1B), a subset of patients rapidly progressed after receipt of ICB compared with targeted therapy (Figure 1B, inset). To extend our studies, we examined a cohort of patients with non-small cell lung carcinoma (NSCLC) treated with ICB or chemotherapy at our institution (cohort 2, 375 patients; Table S2). Receipt of ICB was also associated with inferior overall and progression-free survival at 3 months in patients with NSCLC (Figures 1C and 1D). To substantiate this finding, we performed propensity score-matched multivariable modeling. After controlling for clinicopathologic variables, inferior overall survival and progression-free survival (Figures S1A–S1D) remained in patients with melanoma and NSCLC treated with ICB at 3 months compared with other systemic therapies. To externally validate

(B) Progression-free survival (PFS) of patients with metastatic melanoma stratified by therapy type. Inset: 3-month PFS. Progression-free RMST at 3 months, HR = 0.89; immunotherapy, n = 251; targeted therapy, n = 138, $p < 0.0001$ by log-rank test.

(C) OS of patients with metastatic NSCLC stratified by therapy type. Inset: 3-month OS. Immunotherapy, n = 279; chemotherapy, n = 96; RMST at 3 months, HR = 0.94, $p < 0.0001$ by log-rank test.

(D) PFS of patients with metastatic NSCLC stratified by therapy type. Inset: 3-month PFS. Immunotherapy, n = 279; chemotherapy, n = 96; progression-free RMST at 3 months, HR = 0.94, $p < 0.0001$ by log-rank test.

(E) PFS of patients with metastatic NSCLC treated with immunotherapy or chemotherapy and pooled analysis of Keynote-042, Poplar, and Checkmate 227 randomized control trials. Progression-free log-rank HR at 3 months = 0.616, $p = 0.0336$.

(F) HRs for 3-month PFS of patients with metastatic NSCLC treated with immunotherapy or chemotherapy and pooled analysis of Keynote-042, Poplar, and Checkmate 227 randomized control trials. Two-sided t test, $p = 0.0152$.

(G) OS of patients with metastatic melanoma treated with ICB (cohort 1), stratified by timing of progression. Other, n = 146; rapid progression (PFS < 3 months), n = 53; landmark analysis (3 months) HR = 0.291, $p < 0.0001$ by log-rank test.

(H) OS of patients with metastatic NSCLC treated with ICB (cohort 2), stratified by timing of progression. Other, n = 113; rapid progression (PFS < 3 months), n = 67; Landmark analysis (3 months) HR = 0.3251, $p < 0.0001$ by log-rank test.

(I) Waterfall plot showing change of tumoral burden from initiation of therapy to first surveillance imaging in patients with melanoma treated with the indicated therapy. Dotted line, greater than 50% increase in tumor burden; immunotherapy, n = 200; targeted therapy, n = 96; chi-square test = 19.53, $p < 0.0001$. Data are shown as percentage change.

(J) Waterfall plot showing change of tumoral burden from initiation of therapy to first surveillance imaging in patients with NSCLC treated with the indicated therapy. Dotted line, greater than 50% increase in tumor burden; immunotherapy, n = 212; chemotherapy, n = 68; chi-square test = 5.133; $p = 0.0235$. Data are shown as percentage change.

(K and L)Representative cross-sectional (bottom) and 3D reconstructed (top) computed tomography (CT) images of a patient with metastatic melanoma (K) and a patient with NSCLC (L) with HPD preceding receipt of immunotherapy (left), at baseline preceding immunotherapy (center), and at first reassessment following immunotherapy (right).

(M and N) Longitudinal tumor burden assessment in patients with melanoma (M) or NSCLC (N) who progressed while receiving ICB, stratified by pattern of response. Baseline, cross-sectional imaging immediately prior to ICB initiation; pre-therapy, imaging assessment prior to baseline evaluation; on therapy, next surveillance scan after baseline assessment. Patients with melanoma with PD (progressive disease; per RECIST 1.1, n = 48) and HPD (hyperprogressive disease, per Champiat et al.,[6] n = 21); patients with NSCLC with PD (n = 77) and HPD (n = 26), interrupted time series regression. Data are shown as mean ± SD. The p value is indicated.

(O) OS of patients with metastatic melanoma (cohort 1), stratified by best response. Complete response (CR), n = 31; partial/stable disease, n = 58; PD, n = 48; HPD, n = 21. Log-rank test, HPD versus PD HR = 0.3058, ***$p < 0.001$.

(P) OS of patients with metastatic NSCLC (cohort 2), stratified by best response. CR, n = 7; partial/stable disease, n = 77; PD, n = 77; HPD, n = 26. Log-rank test, HPD versus PD HR = 0.25, ***$p < 0.001$.

See also Figure S1 and Tables S1–S3.

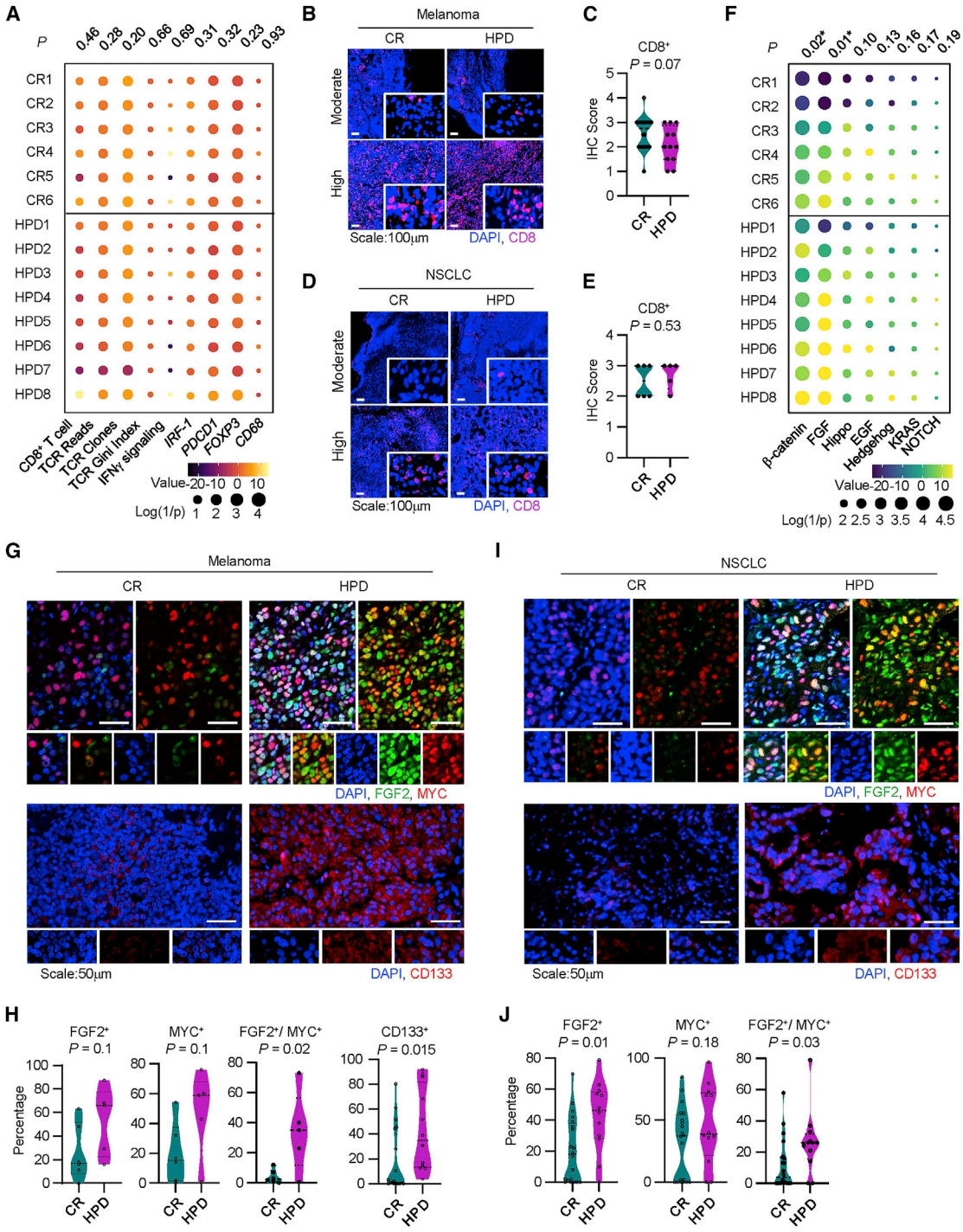

Figure 2. Immunogenic and oncogenic pathways correlate in patients with HPD

(A) Immune gene signature analysis of patients receiving immunotherapy who developed a CR or HPD per Champiat et al.[6] in cohort 3; individual patients are shown. The p values were generated from multivariate mixed-effect linear models controlling for biopsy site (fixed effect) and disease type (random effect).

(B and C) Representative immunofluorescence staining (B) and quantitation (C) for baseline tumor-infiltrating $CD8^+$ T cells in patients with melanoma with the indicated response to therapy. Frequency of positive cells is shown. CR, n = 20; HPD, n = 12. Two-sided t-test.

(D and E) Representative immunofluorescence staining (D) and quantitation (E) for baseline tumor-infiltrating $CD8^+$ T cells in patients with NSCLC with the indicated response to therapy. Frequency of positive cells is shown. CR, n = 20; HPD, n = 12. Two-sided t-test.

(F) Oncogenic gene signature analysis of patients receiving immunotherapy who developed a CR or HPD in cohort 3; individual patients are shown. The p values were generated from multivariate mixed-effect linear models controlling for biopsy site (fixed effect) and disease type (random effect).

(legend continued on next page)

these observations, we conducted a pooled analysis of the prospective, randomized controlled trials, which established the superiority of ICB over chemotherapy in metastatic NSCLC.[26–28] Again, receipt of ICB was associated with inferior initial progression-free survival at 3 months (Figure 1E). This inferior progression-free survival was observed regardless of whether anti-PD-1 (pembrolizumab), anti-PD-L1 (atezolizumab), or anti-CTLA-4 and anti-PD-1 (ipilimumab and nivolumab) were utilized (Figure 1F). Progression within 3 months was associated with significantly inferior overall survival in patients with melanoma and NSCLC receiving ICB (Figures 1G and 1H). Together, these data indicate that rapid cancer progression can occur in a subset of patients with cancer during immunotherapy.

Next, we evaluated the patterns of early/initial radiographic response to cancer therapies in patients with metastatic melanoma and NSCLC (cohorts 1 and 2). Immune-modified response evaluation criteria in solid tumors (imRECIST) criteria were utilized to exclude patients with pseudoprogression.[29] Quantitative evaluation revealed that a higher proportion of metastatic melanoma had a substantial (>50%) increase in tumor burden at the time of first surveillance imaging following receipt of ICB compared with receipt of targeted therapy (Figure 1I). Similarly, a subset of patients with metastatic NSCLC had a substantial increase in tumor burden after receipt of ICB (Figure 1J). Substantial increases in tumor burden were associated with significantly inferior overall survival in patients with melanoma and NSCLC receiving ICB (Figures S1E and S1F). These data collectively suggest that ICB is associated with a rapid and substantial increase in tumor burden in a subset of patients with cancer.

Multiple groups have suggested that cancer hyperprogression may occur following receipt of immunotherapy.[30] Tumor growth rate is a validated quantification of tumor kinetics over time.[31] We observed that a proportion of patients had an acceleration of their tumor growth rate after ICB, targeted therapy, or chemotherapy in melanoma and NSCLC (Figures S1G and S1H). We next applied previously reported definitions for HPD whose criteria include rapid time to failure, an increase in tumor burden, and tumor growth acceleration to our clinical cohorts (Table S3).[6,7,32–38] HPD occurred in ~11% patients with metastatic melanoma following receipt of ICB versus ~2% of patients following targeted therapy (Figure S1I). Likewise, we observed HPD in ~13% of patients with NSCLC following receipt of ICB and ~8% of patients following receipt of chemotherapy (Figure S1J). These proportions were similar regardless of which previously published definition of HPD was used.[6,7,32–38] These data collectively suggest that a small subset of patients with cancer may experience rapid progression upon immunotherapy.

HPD could represent unchecked intrinsic cancer growth in the face of ineffective therapy or a paradoxical acceleration of cancer progression induced by therapy. To evaluate these possibilities, we examined serial radiographic cross-sectional images from the period preceding and following ICB initiation in patients with metastatic melanoma and NSCLC. Cross-sectional and reconstructed 3D imaging showed that a subset of patients had significant increases in tumor burden after receipt of ICB (Figures 1K, 1L, S1K, and S1L). Longitudinal quantification of tumor burden demonstrated that a subset of patients with melanoma and NSCLC had significant increases in tumor burden following but not preceding initiation of ICB, as shown by individual patient growth curves (Figures S1M and S1N) as well as the composite values (Figures 1M and 1N). To understand whether these patients with potential HPD differed from patients with progressive disease (PD) as defined by imRECIST, we stratified patients by their radiographic response and compared their disease burden longitudinally. We observed that, unlike patients with PD, patients with HPD had dramatic increases in their tumor burden after receipt of ICB (Figures 1M and 1N). Interrupted time series analysis confirmed that patients with HPD were on a distinct disease trajectory after initiation of ICB compared with patients with PD. Metastatic melanoma and NSCLC patients with HPD had significantly diminished overall survival following receipt of ICB compared with patients with PD (Figures 1O and 1P). In patients with metastatic melanoma, HPD following immunotherapy occurred regardless of the age, sex, performance status, lines of prior therapy, receipt of single or dual ICB, melanoma histologic subtype, or BRAF mutational status (Figure S1O). In patients with metastatic NSCLC, HPD following ICB occurred regardless of age, sex, performance status, smoking status, histology, and receipt of immunotherapy alone or in combination with chemotherapy (Figure S1P). Of note, ICB-associated HPD was not associated with increased tumor growth rates in the pretreatment period (Figures S1Q and S1R). These data suggest that cancer may accelerate in a minority of patients following immunotherapy.

Immunogenic and oncogenic pathways correlate in patients with HPD

To investigate the molecular underpinnings of HPD in patients, we identified a cohort of patients who underwent comprehensive tumor and somatic sequencing, received ICB, and had evaluable cross-sectional imaging at our institution (cohort 3; Table S4).[39] Through longitudinal radiographic quantitation of tumor burden, we identified patients who had a complete response (CR) as well as patients who developed HPD in response to ICB (Figures S2A–S2D). Survival analysis confirmed that radiographic response to ICB impacted overall survival (Figure S2E). Limited IFNγ signaling and insufficient T cell infiltration are known to be associated with tumor progression and resistance to ICB.[1,2,4] We hypothesized that limited T cell responses would characterize the tumor immune microenvironment in patients who subsequently developed HPD. Unexpectedly, patients with CR and patients with HPD demonstrated comparable levels of IFNγ and *IRF1* as well as similar T cell clonal diversity, number of TCR clones, number of TCR reads, and $CD8^+$ T cell infiltration (Figure 2A). Regulatory T cells, myeloid dendritic cells (DCs), and macrophages mediate immunosuppression in the tumor

(G–J) Multiplex immunofluorescence staining was conducted in tumor tissues from patients with melanoma (G and H) and NSCLC (I and J). Representative images show FGF2-, MYC-, and CD133-expressing tumor cells in patients with HPD and CR (G and I). Percentages of single- or double-positive tumor cells are shown for patients with HPD and CR (H and J). Mean and interquartile range are shown. Melanoma patients with CR (n = 20) and HPD (n = 12); NSCLC patients with HPD (n = 5) and CR (n = 6). Two-sided t-test.
See also Figure S2 and Table S4.

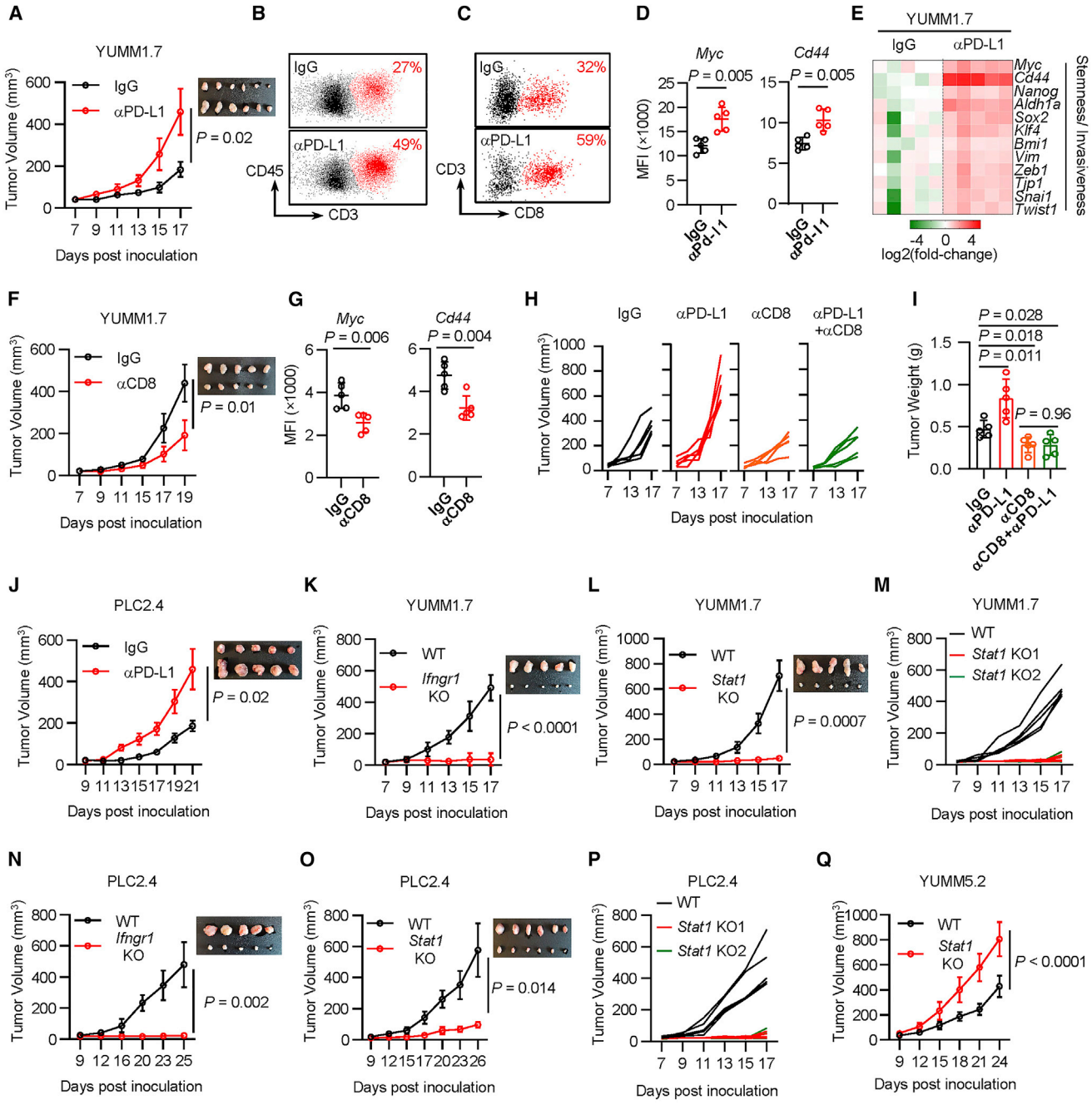

Figure 3. CD8⁺ T cells drive cancer hyperprogression via IFNγ

See also Figure S3.

(A–D) YUMM1.7 tumor-bearing C57BL/6 mice were treated with control (IgG) or PD-L1 antibody. Tumor growth curves were plotted (A). Fluorescence-activated cell sorting (FACS) analysis shows tumor T cell infiltration (B and C) and tumor *Myc* and *Cd44* expression (D). MFI, mean fluorescence intensity.

(E) YUMM1.7 tumor-bearing C57BL/6 mice were treated with control (IgG) or PD-L1 antibody. On day 14 after tumor inoculation, the indicated gene expression in tumors was determined by qPCR.

(F and G) YUMM1.7 tumor-bearing C57BL/6 mice were treated with control (IgG) or CD8 antibody. Tumor growth curves were plotted (F), and tumor *Myc* and *Cd44* expression (MFI) was determined by FACS (G).

(H and I) YUMM1.7 tumor-bearing mice were treated with control (IgG), PD-L1 antibody, CD8 antibody, or the combination of PD-L1 and CD8 antibodies. Tumor growth curves were plotted (H), and endpoint tumor weight (I) was scaled.

(J) PLC2.4 cells were inoculated in C57BL/6 WT mice. Mice were treated with control (IgG) or PD-L1 antibody. Tumor growth curves were plotted.

(K and L) WT and Ifngr1 KO (K) or Stat1 KO (L) YUMM1.7 cells were inoculated in C57BL/6 mice. Tumor growth curves were plotted.

(M) WT or 2 single clones of Stat1 KO YUMM1.7 cells were inoculated in C57BL/6 mice. Tumor growth curves were plotted.

(legend continued on next page)

microenvironment via multiple mechanisms, such as the PD-L1-PD-1 pathway.[40,41] Surprisingly, the levels of *PDCD1* (PD-1), *FOXP3*, and *CD68* were also comparable between patients who had CR and HPD in response to ICB (Figure 2A). To orthogonally confirm this observation, we evaluated $CD8^+$ T cells in tumors from metastatic melanoma (cohort 1) and NSCLC patients (cohort 2) who had available tissues. Multiplex immunohistochemistry showed comparable levels of tumor $CD8^+$ T cell infiltration between CR and HPD patients with melanoma (Figures 2B and 2C) and NSCLC (Figures 2D and 2E). These data indicate that patients with HPD are unexpectedly not immune excluded.

Given the lack of significant differences in the immune composition of patients who responded completely versus those who developed HPD following receipt of ICB, we then evaluated common oncogenic pathways.[18] Gene signatures for several common oncogenic signaling pathways, including Sonic Hedgehog, Hippo, KRAS, NOTCH, and EGF, were similarly expressed in patients with HPD and CR (Figure 2F). Interestingly, we found that FGF2 and Wnt-β-catenin gene signatures were highly expressed in patients who developed HPD compared with patients who underwent a CR (Figures 2F and S2F). We detected comparable levels of expression of *EGFR*, *MDM2*, and *MDM4* but higher levels of tumor stemness and invasiveness in HPD compared with CR (Figure S2G). We found one case with *BRAF* mutation and no cases with *MDM2*, *MDM4*, and *EGFR* amplification in this cohort (Figure S2H). The results suggest that FGF2, Wnt-β-catenin, and stemness/invasiveness pathways may be activated in patients with HPD. To validate this finding, we examined FGF2 and MYC, surrogates for FGF signaling and β-catenin signaling, in tumors from patients with melanoma and NSCLC who had CR or HPD following receipt of ICB. Multiplex immunohistochemistry revealed nuclear FGF2 indicative of active FGF2 signal transduction[42] and MYC expression (Figure 2G, top panel). Quantitation revealed higher levels of $FGF2^+MYC^+$ melanoma cells in patients with a HPD phenotype compared with patients with a CR phenotype (Figure 2H). Similar results were obtained in patients with NSCLC (Figures 2I, top panel, and 2J). Furthermore, we performed multiplex immunofluorescence staining for CD133, a marker for stemness in cancer tissues from patients with CR and HPD. There was higher frequency of $CD133^{high}$ tumor cells (Figures 2G and 2I, bottom panels, and 2H) and $FGF2^{high}CD133^{high}$ tumor cells (Figures S2I and S2J) in HPD patients compared with CR patients. The data suggest that immunotherapy-associated HPD is associated with activation of the FGF2 and β-catenin oncogenic pathways as well as increased tumor stemness.

$CD8^+$ T cells drive cancer hyperprogression via IFNγ

Preclinical models mimicking ICB-triggered HPD have not been developed. To resolve whether ICB may trigger HPD in melanoma, we sought to establish a melanoma murine model with HPD features by testing 4 cell lines: B16-F0, B16-F10, YUMM1.7, and YUMM5.2. We inoculated the 4 cell lines into C57BL/6 mice and treated them with anti-PD-L1 monoclonal antibody (mAb) (αPd-l1). αPD-L1 therapy showed a minimal anti-tumor effect in mice bearing B16 melanoma[43,44] and YUMM5.2 tumors (Figure S3A). To our surprise, tumors progressed faster in YUMM1.7 melanoma-bearing mice under ICB (Figure 3A). In line with this, αCTLA-4 treatment also promoted YUMM1.7 tumor growth (Figure S3B). αPD-L1 resulted in increased tumor T cell infiltration in the YUMM1.7 model (Figures 3B and 3C) as well as enhanced multiple tumor stemness- and invasiveness-associated genes, such as *Myc* and *Cd44* proteins (Figure 3D) and transcripts (Figure 3E). In contrast, αPD-L1 therapy did not modulate these genes in the YUMM5.2 model (Figure S3C). Notably, previous studies have revealed inconsistent efficacy of ICB in YUMM1.7 tumor-bearing mice.[45,46] To elucidate the necessity of immune activation as demonstrated in patients with cancer (Figure 2) and recapitulate tumor stemness potential *in vivo* (Figures 1 and 2), we inoculated a limited number of tumor cells into animals and initiated treatment at an early time point.

Because melanoma from HPD patients harbored activated $CD8^+$ T cells (Figure 2), we wondered whether $CD8^+$ T cells unexpectedly support tumor progression in the YUMM1.7 melanoma-bearing model. We treated YUMM1.7 melanoma-bearing mice with a CD8-depleting mAb (αCD8) (Figure S3D). We observed that αCD8 slowed YUMM1.7 tumor progression (Figure 3F) and reduced tumoral *Myc* and *Cd44* expression (Figures 3G and S3E). The data suggest that $CD8^+$ T cells may activate oncogenic pathways in tumor cells. We further tested this possibility in the setting of ICB. We treated YUMM1.7 tumor-bearing mice with αPD-L1, αCD8, or the combination of αPD-L1 and αCD8. Again, αPD-L1 promoted tumor growth but failed to do so when $CD8^+$ T cells were depleted, as determined by tumor growth measurements (Figure 3H) and tumor weights (Figure 3I). These data suggest that ICB may enhance tumor growth in a $CD8^+$ T cell-dependent manner.

To explore how $CD8^+$ T cells activate oncogenic pathways, we cultured YUMM1.7 cells with activated $CD8^+$ T cells or activated T cell medium (TCM). T cells (Figure S3F) and TCM (Figure S3G) induced expression of *Myc* in YUMM1.7 cells in a dose-dependent manner. Moreover, TCM promoted YUMM1.7 tumor sphere formation compared with control medium (Figure S3H). The data suggest that $CD8^+$ T cell-derived factor(s) may stimulate tumorigenesis. IFNγ is a key effector cytokine released by $CD8^+$ T cells that signals through IFNγ receptor 1 (IFNGR1) and induces STAT1 phosphorylation.[8] We hypothesized a potential role of IFNγ in inducing T cell-mediated tumorigenesis. To this end, we established *Ifngr1* knockout (KO) YUMM1.7 cells and treated them with TCM. We found that TCM induced expression of *Myc* and *Cd44* in wild type (WT) YUMM1.7 cells but not in *Ifngr1* KO YUMM1.7 cells (Figures S3I and S3J). The data suggest that T cell-derived IFNγ may promote tumorigenesis. As a validation, we knocked out *Stat1*, the transcription factor responsible for IFNγ signaling, in YUMM1.7 cells. IFNγ strongly induced *Cd44* expression and tumor sphere formation in YUMM1.7 WT cells

(N and O) PLC2.4 WT and Ifngr1 KO (N) or Stat1 KO (O) cells were inoculated in C57BL/6 WT mice. Tumor growth curves were plotted. n = 5 (N), n = 6 (O).
(P) WT or 2 single clones of Stat1 KO PLC2.4 cells were inoculated in C57BL/6 mice. Tumor growth curves were plotted.
(Q) WT or Stat1 KO YUMM5.2 cells were inoculated in C57BL/6 mice. Tumor growth curves were plotted.
n = 5 unless otherwise indicated. Data are shown as mean ± SD, two-tailed t test. See also Figure S3.

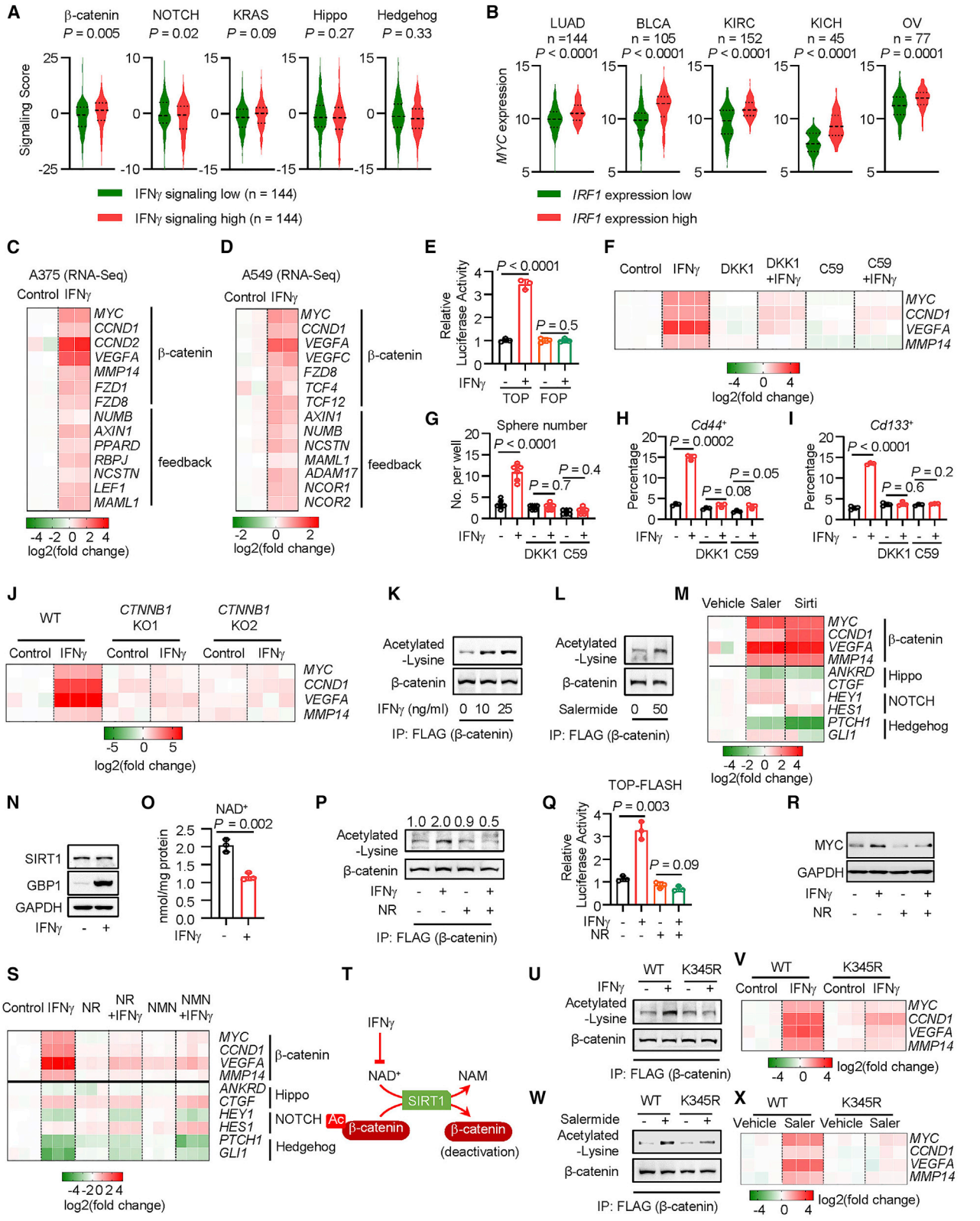

Figure 4. IFNγ reduces NAD+ to activate β-catenin acetylation

(A) Correlation between the IFNγ and oncogenic signaling gene scores in lung adenocarcinoma in TCGA datasets. The expression of the indicated oncogenic gene signaling scores was plotted based on the top and bottom 25th percentiles of the IFNγ gene signaling scores; p value by two-tailed t test.

(legend continued on next page)

but not in *Stat1* KO cells (Figures S3K and S3L). The data indicate that CD8$^+$ T cell-derived IFNγ signaling may promote tumor stemness, thereby enhancing tumorigenic potential. To solidify this finding, we examined the effect of recombinant IFNγ on YUMM1.7 and YUMM5.2 cancer cells *in vitro*. Treatment with IFNγ induced more spheres (Figures S3M and S3N); higher expression of stemness markers, including *Cd44* and *Cd133* (Figures S3O and S3P), on the cancer cell membrane; and multiple stemness gene transcripts (Figure S3Q) in YUMM1.7 cells but not in YUMM5.2 cells. Furthermore, we tested whether the effect of IFNγ on tumor stemness depended on tumor cell density. We cultured YUMM1.7 cells at different densities and observed that IFNγ strongly induced *Myc* and *Cd44* expression in YUMM1.7 cells cultured at low density (10%–30%) but not at high density (>60%) (Figures S3R and S3S). Similar results were obtained in YUMM1.7 cell sphere formation at low density (Figures S3T and S3U). The data suggest that different melanoma cancer models, such as YUMM1.7 and YUMM5.2, can differentially respond to IFNγ and/or ICB.

To extend our observation to a lung cancer model, we inoculated Lewis lung carcinoma (LLC) cells into C57BL/6 mice and treated these mice with αPD-L1. In line with our previous results,[44] LLC-bearing mice were resistant to ICB. We isolated multiple tumor clones (PLC1.1–PLC1.4 and PLC2.1–PLC2.4) from mice bearing progressive LLC (PLC) and treated them with IFNγ. IFNγ stimulated *Myc* expression in all PLC clones (Figure S3V). We inoculated PLC2.4 cells into C57BL/6 mice and treated these mice with αPD-L1. Again, checkpoint blockade induced tumor progression (Figure 3J). Altogether, the results reveal an oncogenic role of IFN signaling in some mouse tumor models. We then stimulated multiple human melanoma and lung cancer cell lines with IFNγ. IFNγ was able to induce *MYC* expression in a minority of the cancer cell lines we examined (Figures S3W and S3X). To extend these findings, we inoculated A375 human melanoma cells into NSG mice, treated these mice with recombinant human IFNγ, and observed that treatment with IFNγ supported tumor progression (Figure S3Y).

To determine a direct role of the IFNγ signaling pathway in YUMM1.7 tumor progression *in vivo*, we pooled 3 different *Ifngr1* KO YUMM1.7 clones and 3 different *Stat1* KO YUMM1.7 clones and inoculated these KO clones and WT cells into WT C57BL/6 mice. We observed that WT tumors progressed rapidly on treatment, while *Ifngr1* KO (Figure 3K) and *Stat1* KO (Figure 3L) tumors grew slowly. Similar results were obtained when individual *Stat1* KO YUMM1.7 cell clones were studied *in vivo* (Figure 3M). The data indicate that IFNγ signaling facilitates YUMM1.7 tumor progression *in vivo*. Moreover, pooled *Ifngr1* KO (Figure 3N) or *Stat1* KO (Figure 3O) PLC2.4 tumors progressed more slowly compared with WT PLC2.4 tumors *in vivo*. Similar results were observed in individual *Stat1* KO PLC2.4 clones (Figure 3P). Thus, IFNγ signaling promotes tumor growth in the PLC2.4 model. As an additional control, we generated *Stat1* KO YUMM5.2 cells and performed similar *in vivo* experiments. Contrary to the results from the *Stat1* KO YUMM1.7 tumor model, the *Stat1* KO YUMM5.2 tumors grew faster than their WT counterparts (Figure 3Q). Thus, IFNγ signaling may promote tumor progression in a subset of preclinical models.

(B) Correlation between the *IRF1* and *MYC* signaling gene scores in several cancer types in TCGA datasets. The expression of the *MYC* gene signaling scores was plotted based on the top and bottom 25th percentiles of the *IRF1* gene signaling scores; p value by two-tailed t test. LUAD, lung adenocarcinoma; BLCA, bladder urothelial carcinoma; KIRC, kidney renal clear cell carcinoma; OV, ovarian cancer.
(C and D) Based on the RNA-seq datasets (GSE99299), the indicated gene expression is shown in A375 (C) or A549 (D) cells in the presence or absence of IFNγ. n = 2.
(E) A375 cells were transfected with the β-catenin signaling reporter TOP-FLASH or the mutant vector (FOP-FLASH). Cells were treated with IFNγ for 48 h. Results are expressed as relative luciferase activity. Data are shown as mean ± SD, n = 3, p value by two-tailed t test.
(F) A375 cells were treated with IFNγ and recombinant DKK1 or Wnt-C59 (C59) for 48 h. The indicated gene expression was determined by qPCR; n = 3.
(G)YUMM1.7 cells were treated with IFNγ and DKK1 or Wnt-C59 (C59) for 48 h, followed by 3D sphere culture. Spheres were counted on day 7 after sphere culture. Data are shown as mean ± SD; n = 6, two-tailed t test.
(H and I) YUMM1.7 cells were treated with IFNγ and DKK1 or Wnt-C59 (C59) for 48 h. Percentages of *Cd44*$^+$ (H) or *Cd133*$^+$ (I) cells were determined by FACS. Data are shown as mean ± SD; n = 3, two-tailed t test.
(J) WT or 2 clones of CTNNB1 KO A375 cells were treated with IFNγ for 48 h. The indicated gene expression was determined by qPCR; n = 3.
(K)FLAG-tagged β-catenin-expressing A375 cells were treated with IFNγ for 24 h. Co-immunoprecipitation (coIP) was performed with FLAG antibody. Acetylated lysine and β-catenin were detected in the IP products. 1 of 2 western blots is shown.
(L) FLAG-tagged β-catenin-expressing A375 cells were treated with salermide for 10 h. Acetylated lysine and β-catenin were determined in the coIP products with FLAG antibody. 1 of 2 blots is shown.
(M) A375 cells were treated with salermide (Saler) or sirtinol (Sirti) for 24 h. The indicated gene expression was determined by qRT-PCR; n = 3.
(N) A375 cells were treated with IFNγ for 24 h. SIRT1 and GBP1 (positive control) proteins were detected by western blot. 1 of 2 western blots is shown.
(O) A375 cells were treated with IFNγ for 24 h. NAD$^+$ levels were determined by quantitation kit. Data are shown as mean ± SD; n = 3, two-tailed t test.
(P) FLAG-tagged β-catenin-expressing A375 cells were treated with IFNγ in the presence or absence of 0.7 mM nicotinamide riboside (NR) for 24 h. Acetylated lysine and β-catenin were detected in the coIP products with FLAG antibody. 1 of 2 western blots is shown.
(Q) A375 cells carrying TOP-FLASH were treated with IFNγ in the presence or absence of 0.7 mM NR for 24 h. Luciferase activity of the β-catenin signaling reporter was determined. Data are shown as mean ± SD; n = 3, two-tailed t test.
(R) A375 cells were treated with IFNγ and NR for 24 h. MYC and GAPDH proteins were determined by western blot. 1 of 3 western blots is shown.
(S) A375 cells were treated with IFNγ and NR or β-nicotinamide mononucleotide (NMN) for 48 h. The indicated gene expression was determined by qPCR; n = 3.
(T) Schematic showing that IFNγ reduces NAD$^+$ to suppress SIRT1-mediated β-catenin deacetylation, thereby activating β-catenin.
(U and V) WT or CTNNB1 K345R mutant A375 cells were treated with IFNγ. 24 h after treatment, acetylated β-catenin was determined by western blotting following FLAG-β-catenin coIP (U). 48 h after treatment, the indicated gene expression was determined by qPCR (V). 1 of 2 western blots is shown; n = 3 for qPCR.
(W and X) WT or CTNNB1 K345R mutant A375 cells were treated with Saler. 12 h after treatment, acetylated β-catenin was determined by western blotting following FLAG-β-catenin coIP (W). 24 h after treatment, the indicated gene expression was determined by qPCR (X). 1 of 2 western blots is shown; n = 3 for qPCR.
See also Figure S4.

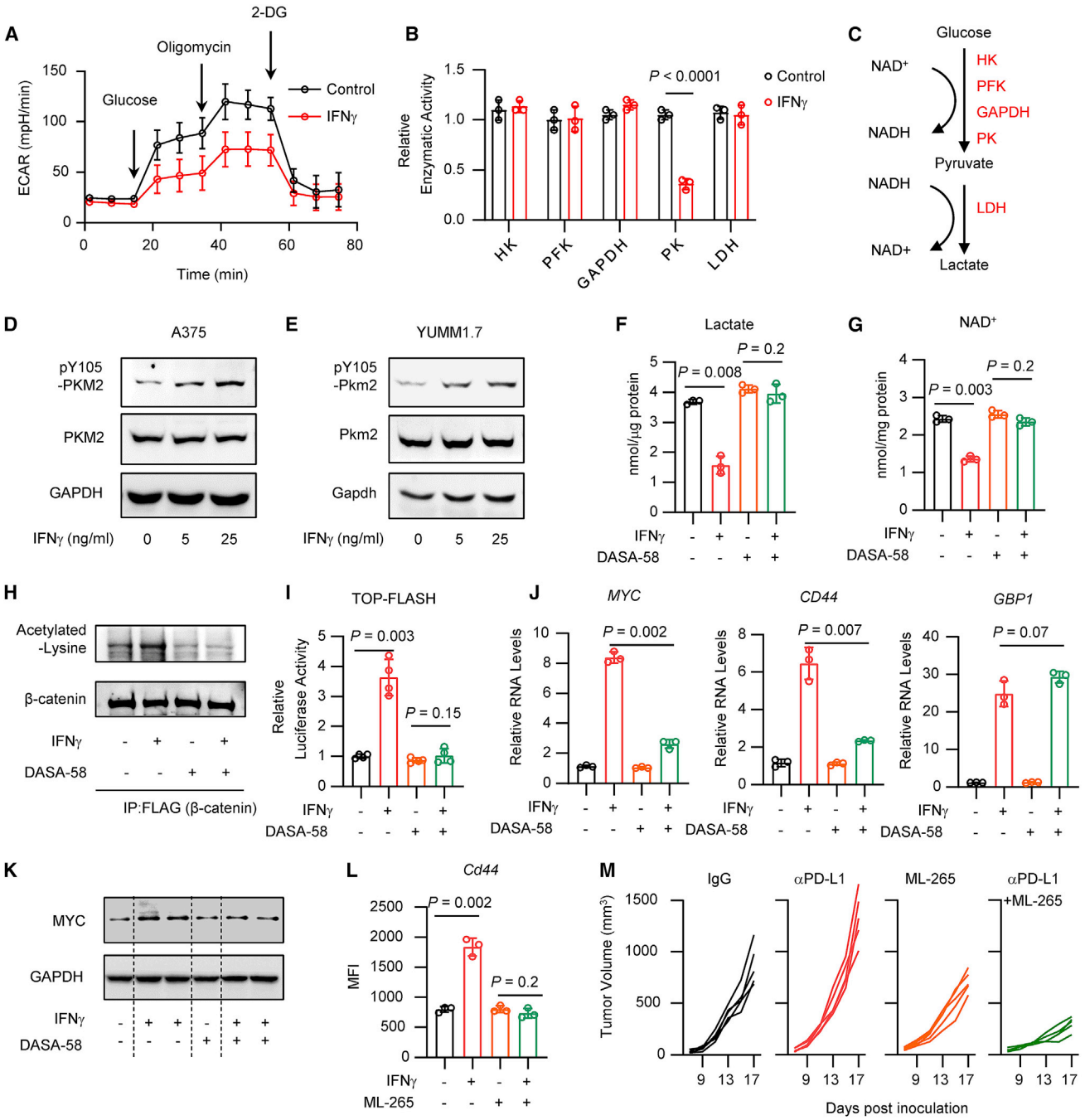

Figure 5. IFNγ regulates PKM2 phosphorylation to alter NAD⁺/β-catenin signaling

(A) A375 cells were treated with IFNγ for 24 h. Seahorse analysis showed the extracellular acidification rate (ECAR) in control cells and IFNγ-treated cells in the presence of glucose, oligomycin, or 2-DG. Data are shown as mean ± SD; n = 3.

(B) A375 cells were treated with IFNγ for 24 h. Catalytic activities of glycolysis rate-limiting enzymes were determined by quantitation kits. Data are shown as mean ± SD; n = 3, two-tailed t test.

(C) Schematic showing the glycolysis pathway and the NAD⁺/NADH balance.

(D and E) A375 (D) or YUMM1.7 (E) cells were treated with IFNγ for 24 h. Phosphorylated or total protein levels of PKM2 were detected by western blot. 1 of 2 western blots is shown.

(F and G) A375 cells were treated with IFNγ in the presence or absence of DASA-58 for 48 h. Lactate production (F) or intracellular levels of NAD⁺ (G) were determined by quantitation kit. Data are shown as mean ± SD; n = 3, two-tailed t test.

(H) A375 cells carrying FLAG-tagged β-catenin were treated with IFNγ in the presence or absence of DASA-58. Acetylated lysine and β-catenin were detected in the coIP products with FLAG antibody. 1 of 2 western blots is shown.

(legend continued on next page)

Altogether, the data suggest that, in a small subset of cancer models, IFN signaling may activate oncogenic pathways and that ICB may promote rapid tumor progression via the T cell-IFNγ signaling-activated oncogenic pathway.

IFNγ reduces NAD$^+$ to activate β-catenin acetylation

We then explored the oncogenic pathway(s) activated by IFNγ and ICB. We analyzed the established oncogenic signaling genes in the lung cancer TCGA datasets.[18] We found that IFNγ signaling positively and negatively correlated with the β-catenin and NOTCH signaling pathways, respectively. However, there was no correlation between the IFNγ signaling pathway and the KRAS, Hippo, and Hedgehog signaling pathways (Figure 4A). Furthermore, expression of *IRF1* and *MYC*, target genes in the IFNγ and β-catenin signaling pathways, respectively, correlated positively across multiple cancer types in TCGA datasets (Figure 4B). This evidence, along with our observations of the relationship between CD8$^+$ T cells/IFNγ and oncogenic gene expression in mouse models and patients (Figures 2 and 3), suggest potential crosstalk between IFNγ and β-catenin signaling pathways in tumors. In line with this finding, real-time PCR (Figure S4A) and RNA sequencing data (Figures 4C and 4D) demonstrated that IFNγ activated β-catenin signaling genes in A375 and A549 cells. We tested a role of IFNγ in modulating β-catenin signaling using a reporter. We treated the human melanoma cell line A375 with IFNγ. IFNγ treatment induced the luciferase activity of the β-catenin signaling reporter TOP-FLASH but not the control reporter FOP-FLASH (Figure 4E). In line with this, IFNγ treatment resulted in nuclear translocation of β-catenin protein (Figure S4B) as well as induction of *MYC*, *CCND1*, *VEGFA*, and *MMP14*, classic target genes of β-catenin signaling (Figures 4C, 4D, and S4A). To determine whether the increased gene expression was dependent on Wnt/ β-catenin signaling, we cultured A375 and YUMM1.7 cells with the Wnt-β-catenin signaling inhibitors DKK1 and Wnt-C59 in the presence of IFNγ. The two inhibitors diminished IFNγ-mediated expression of β-catenin signaling genes (Figure 4F), formation of tumor spheres (Figure 4G), and surface expression of the stemness markers *Cd44* and *Cd133* (Figures 4H and 4I). Furthermore, we established β-catenin KO A375 cells (Figure S4B). IFNγ activated expression of *MYC*, *CCND1*, *VEGFA*, and *MMP14* in WT cells but not in *CTNNB1* KO cells (Figure 4J). Collectively, these data indicate that IFNγ activates β-catenin signaling in tumor cells.

To dissect how IFNγ activates β-catenin, we investigated the expression and post-translational modification of β-catenin. IFNγ treatment did not alter the protein levels of total and phosphorylated β-catenin (Figures S4C and S4D) but increased β-catenin acetylation in A375 cells (Figure 4K). Acetylation of β-catenin increases its activity to stimulate gene transcription. P300 and Sirtuins are the main enzymes to catalyze acetylation and deacetylation of β-catenin, respectively.[47–49] We treated A375 cells with L002, an inhibitor of P300,[50] in the presence of IFNγ. As expected, L002 treatment reduced *MYC* expression. However, IFNγ was still able to increase *MYC* expression in L002-pretreated A375 cells, suggesting that P300 may not be involved in IFNγ-induced β-catenin signaling (Figure S4E). Then, we treated A375 cells with salermide, a Sirtuin inhibitor.[51] We observed that salermide treatment induced β-catenin acetylation (Figure 4L) and target gene expression (Figure 4M). In addition, IFNγ failed to increase the expression of β-catenin target genes in cells co-treated with salermide (Figures S4F–S4I). In line with this, sirtinol, another Sirtuin inhibitor, also induced β-catenin signaling gene expression (Figure 4M). Notably, salermide and sirtinol failed to trigger signaling gene expression of Hippo, NOTCH, and Hedgehog (Figure 4M). The Wnt-β-catenin signaling inhibitors DKK1 and Wnt-C59 abolished the effect of salermide on expression of *MYC*, *CCND1*, *VEGFA*, and *MMP14* (Figure S4J). The data suggest that IFNγ may induce β-catenin signaling via reducing Sirtuin-mediated β-catenin deacetylation. Sirtuins are a class of NAD$^+$-dependent deacetylases.[52] IFNγ stimulated guanylate binding protein (GBP) 1 expression (positive control),[53] had no effect on SIRT1 expression (Figure 4N), but reduced the intracellular level of NAD$^+$ (Figure 4O). To restore NAD$^+$ and Sirtuin activity, we treated A375 cells with nicotinamide riboside (NR), an NAD$^+$ precursor. Interestingly, NR treatment diminished IFNγ-altered β-catenin acetylation (Figure 4P), TOP-FLASH reporter activity (Figure 4Q), and β-catenin target gene expression (Figures 4R and 4S) compared with vehicle controls. Similarly, treatment with nicotinamide mononucleotide (NMN), also diminished the effect of IFNγ on expression of β-catenin signaling genes, while expression of other oncogenic pathways, such as Hippo, NOTCH, and Hedgehog signaling, were not affected by NR or NMN (Figure 4S). Altogether, these data suggest that IFNγ enhances β-catenin acetylation by reducing NAD$^+$ levels (Figure 4T). β-Catenin can be acetylated at K49 and K345. We found that IFNγ did not affect the expression of K49-acetylated β-catenin (Figure S4K). Sirtuin may catalyze deacetylation of β-catenin at K345.[47] We established stable cells carrying the K345R β-catenin mutation. Upon IFNγ (Figures 4U and 4V) and salermide (Figures 4W and 4X) treatment, β-catenin acetylation (Figures 4U and 4W) and downstream gene activation (Figures 4V and 4X) were largely abrogated in K345R mutant cells. The data suggest that IFNγ may affect β-catenin acetylation at K345 by reducing Sirtuin activity. As an additional control, we treated non-HPD-prone mouse YUMM5.2 cells with IFNγ. IFNγ had no effect on

(I) A375 cells carrying TOP-FLASH were treated with IFNγ, in the presence or absence of DASA-58 for 24 hours. Relative luciferase activity was determined. Data are shown as mean ± SD; n = 4, two-tailed t test.
(J) A375 cells were treated with IFNγ in the presence or absence of DASA-58 for 24 h. β-Catenin signaling genes and IFNγ signaling gene (GBP1) (positive control) were determined by qRT-PCR. Data are shown as mean ± SD; n = 3, two-tailed t test.
(K) A375 cells were treated with IFNγ in the presence or absence of DASA-58 for 48 h. MYC and GAPDH proteins were determined by western blot. 1 of 2 western blots is shown.
(L) YUMM1.7 cells were treated with IFNγ in the presence or absence of ML-265 for 48 h. Surface expression of *Cd44* was determined by FACS. Data are shown as mean ± SD; n = 3, two-tailed t test.
(M) YUMM1.7 tumor-bearing C57BL/6 mice were treated with anti-PD-L1, ML-265, or the combination of anti-PD-L1 and ML-265. Tumor growth curves were plotted. n = 5/group.
See also Figure S5.

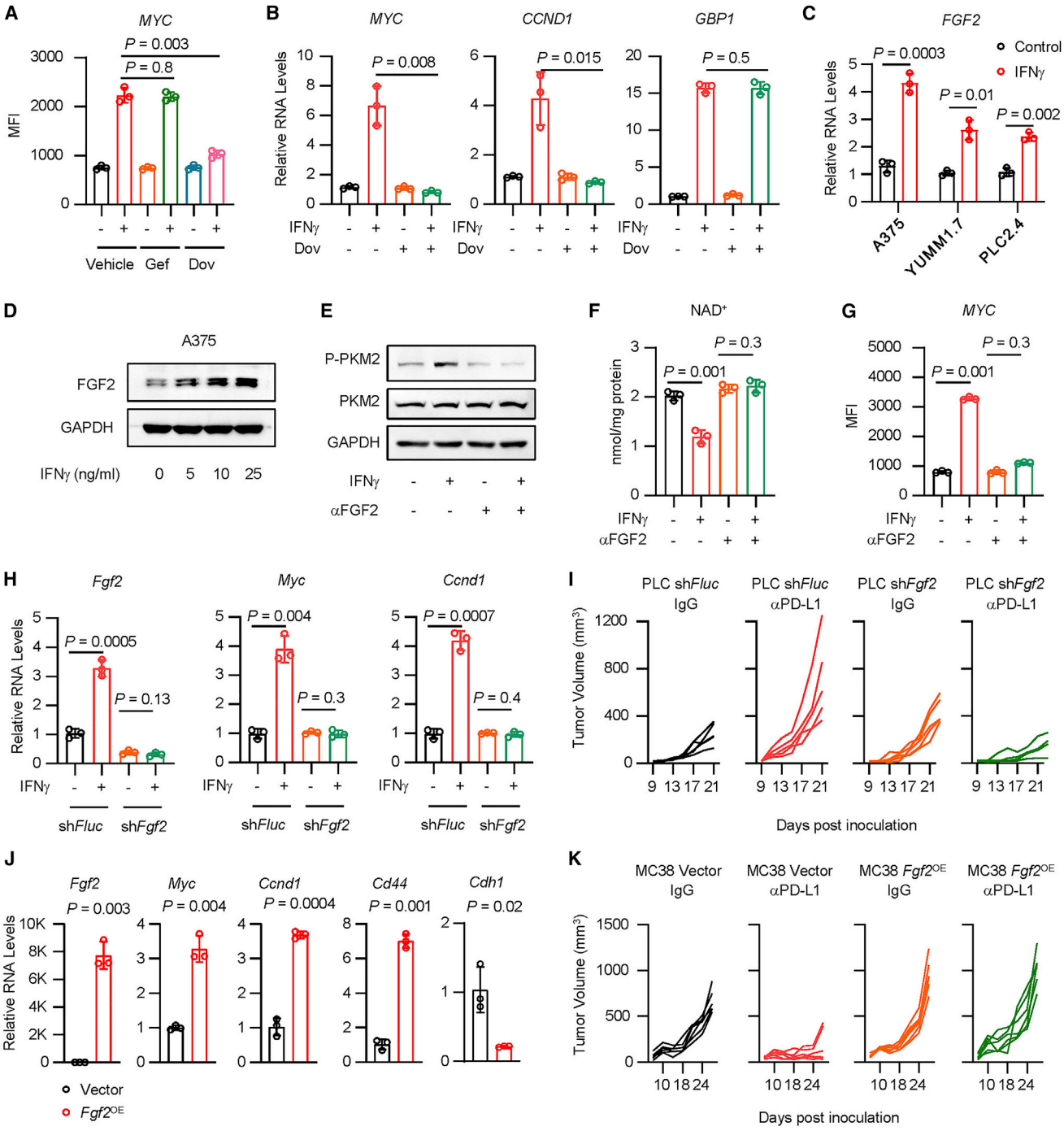

Figure 6. IFNγ induces FGF2 to control PKM2/NAD$^+$/β-catenin signaling

(A) A375 cells were treated with IFNγ in the presence of gefitinib (Gef) or dovitinib (Dov) for 36 h. MYC protein was determined by FACS. Data are shown as mean ± SD; n = 3, two-tailed t test.

(B) A375 cells were treated with IFNγ in the presence of Dov for 48 h. β-Catenin signaling genes (*MYC* and *CCND1*) and the IFNγ signaling gene (*GBP1*) were determined by qRT-PCR. Data are shown as mean ± SD; n = 3, two-tailed t test.

(C) FGF2 transcripts were quantified by qRT-PCR in IFNγ-treated A375, YUMM1.7, and PLC2.4 cells. Data are shown as mean ± SD; n = 3, two-tailed t test.

(D) FGF2 protein was determined by western blot in A375 cells treated with IFNγ. 1 of 2 western blots is shown.

(E and G) A375 cells were treated with IFNγ in the presence or absence of an FGF2-neutralizing antibody (αFGF2). Phosphorylated (Y105) and total protein levels of PKM2 were determined at 24 h by western blot (E). Cellular NAD$^+$ levels were quantified at 24 h by kit (F). *MYC* expression was determined at 48 h by FACS (G). 1 of 2 western blots is shown (E). Data are shown as mean ± SD; n = 3, two-tailed t test (F and G).

(H) *Fgf2*, Myc, or *Ccnd1* transcripts were detected by qRT-PCR in PLC2.4 sh*Fluc* or sh*Fgf2* cells. Data are shown as mean ± SD; n = 3, two-tailed t test.

(I) sh*Fluc* or sh*Fgf2* PLC2.4 tumor-bearing C57BL/6 mice were treated with anti-PD-L1 and isotype IgG. Tumor growth curves were plotted. n = 5 animals.

(legend continued on next page)

β-catenin signaling activity (Figure S4L) and intracellular NAD^+ levels (Figure S4M). Thus, IFNγ selectively alters the NAD^+-β-catenin signaling activities in HPD-prone tumor models.

IFNγ regulates PKM2 phosphorylation to alter NAD^+ and β-catenin signaling

Glycolysis ferments glucose into lactate, functioning as a metabolic regulator of NAD^+/NADH in cancer cells.[54] We investigated whether IFNγ regulates tumor glycolysis, thereby altering NAD^+ and the β-catenin signaling pathway. Seahorse experiments revealed that IFNγ treatment resulted in a lower glycolytic rate in A375 cells, as shown by the extracellular acidification rate (ECAR). This effect was abolished by 2-DG, a glycolysis inhibitor (Figures 5A, S5A, and S5B). To determine whether IFNγ-regulated glycolysis is related to tumor cell proliferation, we treated A375 cells with IFNγ in the presence or absence of different concentrations of palbociclib, a CDK4/6 inhibitor. IFNγ reduced tumor lactate production regardless of palbociclib treatment (Figure S5C). Additionally, IFNγ diminished lactate production in WT A375 cells but not in *STAT1* KO A375 cells (Figure S5D). Thus, IFNγ signaling abrogates tumor glycolysis.

To validate this observation in the context of T cells, we co-cultured A375 cells with TCM. Consistent with our prior findings, TCM reduced lactate production in WT A375 cells but not *IFNGR1* KO A375 cells (Figure S5E). The data suggest that T cells regulate tumor glycolysis via IFNγ. To understand how IFNγ affects glycolysis, we measured the catalytic activities of the rate-limiting enzymes in the glycolysis pathway. Interestingly, IFNγ impaired the activity of pyruvate kinase (PK) but not that of hexokinase (HK), phosphofructokinase (PFK), glyceraldehyde-3-phosphate dehydrogenase (GAPDH), or lactate dehydrogenase (LDH) (Figure 5B). Inhibition of PK diminishes pyruvate production, in turn decreasing the reaction by LDH, in which pyruvate and NADH will be converted into lactate and NAD^+, respectively (Figure 5C). Indeed, we detected reduced levels of pyruvate in A375 cells treated with IFNγ compared with the control (Figure S5F). PKM2 is the predominant isotype of PK in tumor cells.[55] IFNγ failed to regulate lactate production in sh*PKM2* A375 cells (Figure S5G). Thus, IFNγ regulates tumor glycolysis in a PK-dependent manner.

We observed that IFNγ induced PKM2 phosphorylation without altering total PKM2 expression in A375 and YUMM1.7 cells (Figures 5D and 5E). Notably, IFNγ induced phosphorylation of PKM2 at Y105 (Figures 5D and 5E) but not at S37[56] (Figure S5H). Phosphorylation of PKM2 at Y105 inhibits formation of active, tetrameric PKM2 by disrupting binding of the PKM2 cofactor fructose-1,6-bisphosphate, thereby reducing its catalytic activity.[57] To link PKM2 with NAD^+-β-catenin signaling, we knocked down *Pkm2* with shRNA in YUMM1.7 cells and PLC2.4 cells. We detected a decrease in the levels of pyruvate, lactate, and NAD^+ (Figures S5I–S5K) and an increase in the levels of Myc (Figure S5L) in sh*Pkm2* YUMM1.7 cells and sh*Pkm2* PLC2.4 cells compared with controls. Moreover, knocking down *Pkm2* enhanced *Cd44* expression, and NR blocked this effect (Figure S5M). The data suggest that knocking down *PKM2* can activate β-catenin signaling and promote tumorigenesis. To validate this observation in an *in vivo* system, we inoculated sh*Pkm2* YUMM1.7 and sh*Pkm2* PLC2.4 cells into C57BL/6 mice. As expected, sh*Pkm2* tumors progressed faster than control tumors (Figures S5N and S5O). Thus, restriction of PKM2 activity could promote β-catenin signaling and accelerate tumor progression.

To rescue the effect of IFNγ on PKM2, we applied DASA-58, a selective activator of PKM2.[58] We treated A375 cells with DASA-58 in the presence of IFNγ. DASA-58 treatment reversed the effect of IFNγ on lactate production (Figure 5F), NAD^+ (Figure 5G), β-catenin acetylation (Figure 5H), TOP-FLASH reporter activity (Figure 5I), and β-catenin signaling gene expression (Figures 5J and 5K). Notably, DASA-58 failed to alter the impact of IFNγ on *GBP1* expression (Figure 5J). The data suggest that DASA-58 blocks β-catenin activation by IFNγ rather than the blockade of global IFNγ signaling. Similarly, ML-265, another PKM2 activator,[58] diminished the effect of IFNγ on *Cd44* expression in YUMM1.7 cells (Figure 5L). Collectively, PKM2 activation blocks IFNγ-mediated β-catenin signaling activation. To extend this observation *in vivo*, we treated YUMM1.7 tumor-bearing mice with αPD-L1, ML-265, and the combination of αPD-L1 and ML-265. Although αPD-L1 alone promoted tumor progression, ML-265 alone inhibited tumor growth, and the combination therapy completely reversed αPD-L1-mediated HPD, resulting in potent tumor inhibition (Figure 5M). As an experimental control, we observed that IFNγ had no effect on lactate production (Figure S5P) and PKM2 phosphorylation (Figure S5Q) in non-HPD prone YUMM5.2 cells. Altogether, targeting PKM2 blocks β-catenin activation and subverts ICB-triggered HPD.

IFNγ targets FGF2 to control PKM2-NAD^+-β-catenin signaling

Next, we explored the upstream signaling genes involved in regulation of the PKM2-NAD^+-β-catenin axis by IFNγ. Several kinases, such as EGF receptor (EGFR) and FGF receptor (FGFR), can induce PKM2 phosphorylation.[56,57] We treated A375 cells with gefitinib, an EGFR inhibitor, and dovitinib, a FGFR inhibitor. We found that inhibition of FGFR, but not EGFR, abolished the stimulatory effect of IFNγ on *MYC* expression (Figure 6A). In addition to *MYC*, dovitinib diminished the effect of IFNγ on expression of *CCND1* but had no impact on *GBP1* expression (Figure 6B). RNA sequencing (RNA-seq) datasets demonstrated that IFNγ induced expression of *FGF2*, but not the other FGF/FGFR family members, in A375 melanoma cells, while IFNγ failed to induce FGF2 in non-HPD-prone B16F10 melanoma cells (Table S5). In support of these data, we observed that IFNγ stimulated *FGF2* mRNA and protein expression in A375, YUMM1.7, and PLC2.4 cells (Figures 6C and 6D). IRF1 was enriched in the promoter of *FGF2* in the chromatin immunoprecipitation sequencing (ChIP-seq) datasets on K562 cells (Figure S6A). The IRF1 motif was conserved across human and mouse species (Figure S6A). We inserted the *FGF2* promoter and exon 1 sequence upstream of the luciferase coding sequence in

(J) MC38 cells were forced to express *Fgf2* ($Fgf2^{OE}$). RNA levels of *Fgf2*, β-catenin signaling genes (*Myc*, *Ccnd1*, and *Cd44*), and an epithelial marker gene (*Cdh1*) were determined by qRT-PCR. Data are shown as mean ± SD; n = 3, two-tailed t test.
(K) $Fgf2^{OE}$ MC38 tumor-bearing C57BL/6 mice were treated with anti-PD-L1 and isotype IgG. Tumor growth curves were plotted. n = 6 animals.
See also Figures S6 and S7 and Table S5.

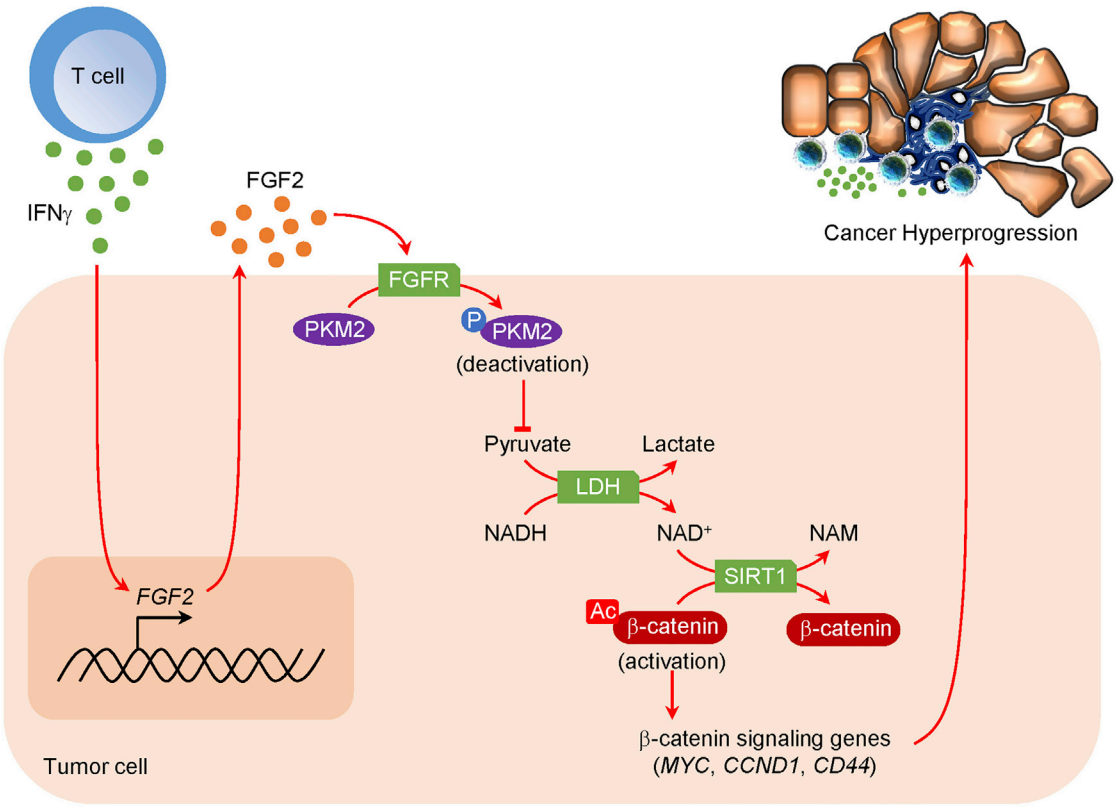

Figure 7. Oncometabolic reprogramming drives cancer hyperprogression during immunotherapy

Shown is a mechanistic scheme of HPD development. IFNγ produced by ICB-activated T cells targets tumor *FGF2* signaling, inducing PKM2 phosphorylation at Y105 and decreasing NAD^+ levels, thereby diminishing SIRT1 activity and lessening β-catenin deacetylation. Consequently, the β-catenin signaling pathway is activated, resulting in enhanced oncogenic potential and HPD.

PGL3-basic plasmid and generated a *FGF2* promoter reporter. We found that IFNγ induced the luciferase activity of the *FGF2* promoter and failed to do so when the IRF1 binding site was deleted (Figure S6B). Thus, IFNγ activates *FGF2* transcription via IRF1.

To determine the involvement of FGF2 in the effect of IFNγ on β-catenin, we treated A375 cells with IFNγ in the presence or absence of an FGF2-neutralizing antibody (αFGF2). αFGF2 abrogated the effect of IFNγ on PKM2 phosphorylation, NAD^+, and β-catenin signaling gene expression (Figures 6E–6G) and had no effect on the levels of total and phosphorylated STAT1 (Figure S6C). In line with this, treatment with recombinant FGF2 protein induced expression of phosphorylated-PKM2, MYC, and CD44 and reduced the levels of NAD^+ (Figures S6D–S6F). Moreover, knockdown of *FGF2* resulted in reduced expression of *Myc* and *Cd44* induced by IFNγ in PLC2.4 and YUMM1.7 cells (Figures 6H, S6G, and S6H). In addition, we treated multiple mouse and human cancer cell lines with IFNγ. Consistent with *MYC* activation (Figures 3D, S3C, S3S, S3U, and S3V), IFNγ stimulated FGF2 protein in a minority of cancer cell lines (Figures S6I and S6K). IFNγ promotes FGF2 signaling to control PKM2-NAD^+-β-catenin signaling in tumor cells.

To determine whether FGF2 expression is involved in ICB-triggered HPD, we inoculated shFGF2 PLC2.4 cells into C57BL/6 mice and treated these mice with αPD-L1. As expected, αPD-L1 accelerated tumor progression in WT PLC2.4 tumors but inhibited sh*Fgf2* PLC2.4 tumor progression (Figure 6I). The data suggest that FGF2 signaling contributes to ICB-triggered HPD. To solidify this finding, we overexpressed *Fgf2* ($Fgf2^{OE}$) in MC38 cells. We found that $Fgf2^{OE}$ MC38 cells expressed higher levels of *Myc*, *Ccnd1*, and *Cd44* and lower levels of *Cdh1* compared with vector carrying MC38 cells (Figure 6J). We inoculated $Fgf2^{OE}$ MC38 tumors into C57BL/6 mice and treated these mice with αPD-L1. αPD-L1 slowed down control MC38 tumor progression but failed to control $Fgf2^{OE}$ MC38 tumors (Figure 6K). Collectively, these data suggest that tumor FGF2 activates oncogenic signaling and shapes immunotherapy outcome.

Oncometabolic reprogramming drives cancer hyperprogression during immunotherapy

Finally, we evaluated whether oncogenic and immunogenic signaling pathways converged in patients with PD on ICB.[59–62] While radiographic quantification required for HPD ascertainment is not available in public datasets, we hypothesized that a subset of patients with PD would have HPD. We confirmed that IFNγ signaling strongly correlated with $CD8^+$ T cell infiltration in these cohorts (Figure S7A). Our data suggest that FGF may regulate Wnt signaling in preclinical models of cancer HPD (Figures 6A–6K). Interestingly, we observed a positive correlation between FGF and Wnt-β-catenin signaling signatures in

patients receiving immunotherapy (Figure S7B). Our experimental work also suggests that IFNγ signaling promotes FGF and β-catenin signaling in HPD. Interestingly, in patients who received ICB and develop PD, we found that FGF and Wnt-β-catenin signaling scores were increased in the subset of patients with elevated IFNγ signaling (Figure S7C). In contrast, there was no elevation of FGF or Wnt-β-catenin in patients who developed a CR (Figure S7D). We confirmed that, within PD patients, a triple-high (IFNγ/FGF/β-catenin) gene signature score was associated with diminished overall survival compared with patients with triple-low signatures (Figure S7E). In line with this, we analyzed a single-cell RNA-seq dataset from patients with cutaneous malignancies treated with ICB.[63] Tumors from non-responders manifested higher levels of IFNγ^{high}FGF^{high}β-catenin^{high} (triple-high) gene signatures compared with responders (Figure S7F). Interestingly, there existed 2 distinct tumor cell subtypes within the same tumor: one population that was sensitive to ICB and another one that was resistant to ICB (Figure S7G). The triple-high gene signature was enriched in the ICB-resistant subtype (Figure S7H). The data suggest that immunotherapy fails to eradicate tumor cells expressing the triple-high gene signature. Thus, CD8$^+$/IFNγ immunogenic signaling and FGF2/β-catenin oncogenic signaling is enriched in patients who derive limited benefits from ICB (Figure 7).

DISCUSSION

In this work, we conducted comprehensive sequencing, immunological, clinical, and radiographic evaluations in multiple cohorts of patients receiving ICB. These analyses demonstrate that HPD likely occurs in a small subset of patients. In addition, we established syngeneic immunocompetent animal models of HPD, enabling dissection of the cellular, molecular, and immunological mechanisms of accelerated cancer progression because of ICB. We report that the interplay between core immunogenic, metabolic, and oncogenic mechanisms enables cancer hyperprogression via the IFNγ-PKM2-β-catenin signaling cascade in preclinical models and patients.

Heterogeneity of response to cancer therapeutics is frequently observed. While ICB improves progression-free and overall survival at a population level, we found that in prospective[26–28] and institutional cohorts, a minority of patients develop hyperprogression after receipt of ICB. This is similar to previous reports demonstrating an association between HPD and ICB.[6,7,32] It remains to be prospectively validated whether HPD is enriched in patients receiving ICB. Although medically challenging, in the future, generation of a humanized mouse with tumors and matched autologous T cells from patients experiencing HPD could enable additional mechanistic insights. Our data suggest that, akin to ICB-triggered autoimmune reactions, HPD may be an immune-related adverse event.

Given the prognostic impact of HPD, it is extremely important to define molecular mechanisms and identify molecular biomarkers for this clinical outcome. By integrating information from comprehensive sequencing with clinical and radiographic platforms at the University of Michigan Rogel Cancer Center,[39,64,65] we immunologically and genetically characterized HPD. Previous clinical reports suggest amplification of oncogenic genes, including *EGFR*, *MDM2*, and *MDM4*,[7] and enriched Foxp3$^+$ regulatory T (Treg) cells[66] in HPD tumors. Myeloid cells and the PD-L1-PD-1 pathway are also known to mediate immunosuppression in the human tumor microenvironment.[40,41,67] However, we detected comparable levels of *EGFR*, *MDM2*, *MDM4*, *FOXP3*, *CD68*, and *PDCD1* expression in tumors from patients with CR and HPD. Moreover, it has been speculated that the Fc region of ICB antibodies may be involved in HPD development.[68] However, HPD has been observed in patients treated with anti-PD-L1, anti-PD-1, and anti-CTLA4 mAbs in different isotypes, including immunoglobulin G1 (IgG1), IgG2, and IgG4 (demonstrated in this work).[33,69–79] Thus, prior to our study, the cellular and molecular basis of HPD remained elusive.

Our experiments demonstrate that HPD is driven by the interplay among core immunogenic, metabolic, and oncogenic pathways via the IFNγ-PKM2-β-catenin molecular cascade. Immune exclusion and mutations in the IFNγ and MHC genes are known resistance mechanisms to immunotherapy, promoting disease progression. It is commonly assumed that HPD tumors are "cold" with poor immune infiltration. To our surprise, we discovered that intratumoral CD8$^+$ T cells and active IFNγ signaling are required for HPD in preclinical models. This mirrors the unexpected finding that patients with HPD and CR had similar tumoral T cell infiltration and IFNγ signaling. This extends previous reports that highlight the duality of IFN signaling in promoting antitumor immunity and enabling tumor immune evasion.[80] Hence, CD8$^+$ T cells and IFNγ signaling may unexpectedly contribute to HPD in mouse models and patients with cancer.

We observed that CD8$^+$ T cell-derived IFNγ targets FGF2 to selectively inhibit PKM2, a dominant rate-limiting enzyme in glycolysis, resulting in reduced NAD$^+$ production. Consequently, β-catenin activity is increased in tumor cells, promoting cancer stemness and tumorigenic potential. Corroborating this mechanism, patients with HPD had increases in *MYC* and *FGF2* pathway activities, accompanied by high levels of invasiveness and stemness gene signatures and expression of the cancer stem-like marker CD133. In line with this, it has been reported that tumor cells with stem-like properties manifest high metastatic potential[81,82] and are resistant to T cell-mediated cytotoxicity.[83,84]

It has been observed previously that FGF and β-catenin signaling pathways promote T cell exclusion and resistance to immunotherapy.[85] In contrast, we uncovered a previously unappreciated mode of action of IFNγ controlling an intertwined metabolic and oncogenic signaling pathway: IFNγ targets PKM2 to diminish Sirtuin-mediated β-catenin deacetylation via NAD$^+$ reduction, causing β-catenin acetylation and activation. These data suggest that, similar to oncogene addiction, there is a state of IFN addiction where tumor cells can be supported by and dependent on immune signaling axes. While tumoral regulation of T cell metabolism to promote immunosuppression is well established, our work suggests that T cells may also regulate tumoral metabolism. Further, this work suggests that tumor glycolysis is not only a downstream effect of oncogenic signaling but also an upstream regulator of oncogenesis. In line with this, FGF2 and β-catenin oncogenic signatures were enriched in patients with HPD. Hence, we suggest a causal link between immune activation and accelerated tumor progression during immunotherapy. Collectively, our data suggest that HPD is a form of immunopathology.

In addition to its scientific importance, our work may be translationally meaningful. We identify a triple-high (IFNγ/FGF/β-catenin)

gene signature score associated with HPD in patients. This may serve as a surrogate marker for HPD, enabling prediction of HPD. In addition, our study may inform the development of therapeutic strategies to limit the devastating consequences of cancer hyperprogression. Mechanistically, IFNγ-FGF2-PKM2-β-catenin signaling promotes HPD. FGF2R inhibitors are approved as antioncologic agents in cholangiocarcinoma and urothelial carcinoma.[86] PKM2 activators are currently being clinically pursued (ClinicalTrials.gov: NCT04328740). Our studies highlight that these agents may be repurposed to limit HPD. Thus, our molecular studies provide insight and justification for future clinical trials to further our understanding of ICB-associated HPD to search for biomarker(s) and improve clinical management of patients with HPD.

In summary, our work demonstrates that ICB is likely associated with HPD in a small subset of patients. The interaction between the core immunogenic, metabolic, and oncogenic pathways via the IFNγ-FGF2-β-catenin axis is a plausible mechanism and may serve as potential biomarkers for HPD. This work suggests that targeting this axis may prevent development of HPD in patients receiving immunotherapy and provides a rationale for investigating this in prospective clinical studies.

STAR★METHODS

Detailed methods are provided in the online version of this paper and include the following:

- KEY RESOURCES TABLE
- RESOURCE AVAILABILITY
  - Lead contact
  - Materials availability
  - Data and code availability
- EXPERIMENTAL MODEL AND SUBJECT DETAILS
  - Human studies
  - Cell lines
  - Tumor models
- METHOD DETAILS
  - Multiplex immunofluorescence staining and analysis
  - Animal experiments
  - Cell culture
  - Plasmids
  - Luciferase activity assay
  - Flow cytometry analysis (FACS)
  - Extracellular acidification (ECAR) and oxygen consumption rate (OCR)
  - Quantification of enzymatic activity
  - Quantification of lactate, NAD^+/NADH, and pyruvate
  - Quantitative PCR (qPCR)
  - Western blotting
  - Co-Immunoprecipitation (Co-IP)
  - Intratumoral immune cell profiling
  - Signature score computation
  - Statistical analysis

SUPPLEMENTAL INFORMATION

Supplemental information can be found online at https://doi.org/10.1016/j.ccell.2022.12.008.

ACKNOWLEDGMENTS

We thank our laboratory members for intellectual input. This work was supported in part by NIH/NCI R01 grants (CA217648, CA123088, CA099985, CA193136, and CA152470), the VA (VA150CU000182 and I01BX005267), foundations (MRA689853 and L863220), and the NIH/NCI through the University of Michigan Rogel Cancer Center (CA46592).

AUTHOR CONTRIBUTIONS

G.L., M.D.G., and W.Z. conceived the idea, designed the experiments, and composed the paper. G.L. conducted experiments. I.K. contributed to multiplex immunofluorescence staining and analysis. J.E.C., S.L., and M.C. contributed to RNA-seq datasets analysis. M.D.G., Y.S., R.N., G.S., S.G.A., K.S., L.A.F., M.M.-L., T.L.F., A.Q., J.J.W., A.T., A.A., C.D.L., N.R., and P.W.H. facilitated acquisition of clinical information and samples. P.L., S.W., S.G., and L.V. assisted with animal experiments. A.M.C. contributed to RNA-seq datasets and the interpretation of the results. W.Z. supervised the project.

DECLARATION OF INTERESTS

W.Z. has served as a scientific advisor or consultant for NGM, CrownBio, Cstone, ProteoVant, Hengenix, NextCure, and Intergalactic. L.A.F receives clinical trial support from Array, Kartos, BMS, EMD Serono, and Pfizer and is a consultant for Elsevier. C.D.L. receives clinical trial support from BMS, Merck, and Novartis. A.Q. has research funding from Merck and Clovis. A.A. serves as a consultant for Merck, AstraZeneca, Bristol-Myers Squibb, and Pfizer/EMD Serono. A.A. receives research funding through the University of Michigan from Merck, Genentech, Prometheus Laboratories, Mirati Therapeutics, Roche, Bayer, Progenics, Astellas Pharma, Arcus Biosciences, AstraZeneca, Bristol-Myers Squibb, and Clovis Oncology.

INCLUSION AND DIVERSITY

We support inclusive, diverse, and equitable conduct of research.

Received: July 8, 2022
Revised: November 7, 2022
Accepted: December 20, 2022
Published: January 12, 2023

REFERENCES

1. Sharma, P., Hu-Lieskovan, S., Wargo, J.A., and Ribas, A. (2017). Primary, adaptive, and acquired resistance to cancer immunotherapy. Cell *168*, 707–723. https://doi.org/10.1016/j.cell.2017.01.017.
2. Robert, C., Marabelle, A., Herrscher, H., Caramella, C., Rouby, P., Fizazi, K., and Besse, B. (2020). Immunotherapy discontinuation - how, and when? Data from melanoma as a paradigm. Nat. Rev. Clin. Oncol. *17*, 707–715. https://doi.org/10.1038/s41571-020-0399-6.
3. Topalian, S.L., Drake, C.G., and Pardoll, D.M. (2015). Immune checkpoint blockade: a common denominator approach to cancer therapy. Cancer Cell *27*, 450–461. https://doi.org/10.1016/j.ccell.2015.03.001.
4. Zou, W., Wolchok, J.D., and Chen, L. (2016). PD-L1 (B7-H1) and PD-1 pathway blockade for cancer therapy: mechanisms, response biomarkers, and combinations. Sci. Transl. Med. *8*, 328rv4. https://doi.org/10.1126/scitranslmed.aad7118.
5. Chiou, V.L., and Burotto, M. (2015). Pseudoprogression and immune-related response in solid tumors. J. Clin. Oncol. *33*, 3541–3543. https://doi.org/10.1200/JCO.2015.61.6870.
6. Champiat, S., Dercle, L., Ammari, S., Massard, C., Hollebecque, A., Postel-Vinay, S., Chaput, N., Eggermont, A., Marabelle, A., Soria, J.C., and Ferté, C. (2017). Hyperprogressive disease is a new pattern of progression in cancer patients treated by anti-PD-1/PD-L1. Clin. Cancer Res. *23*, 1920–1928. https://doi.org/10.1158/1078-0432.CCR-16-1741.
7. Kato, S., Goodman, A., Walavalkar, V., Barkauskas, D.A., Sharabi, A., and Kurzrock, R. (2017). Hyperprogressors after immunotherapy: analysis of genomic alterations associated with accelerated growth rate. Clin.

Cancer Res. *23*, 4242–4250. https://doi.org/10.1158/1078-0432.CCR-16-3133.

8. Castro, F., Cardoso, A.P., Gonçalves, R.M., Serre, K., and Oliveira, M.J. (2018). Interferon-Gamma at the crossroads of tumor immune surveillance or evasion. Front. Immunol. *9*, 847. https://doi.org/10.3389/fimmu.2018.00847.

9. Shin, D.S., Zaretsky, J.M., Escuin-Ordinas, H., Garcia-Diaz, A., Hu-Lieskovan, S., Kalbasi, A., Grasso, C.S., Hugo, W., Sandoval, S., Torrejon, D.Y., et al. (2017). Primary resistance to PD-1 blockade mediated by JAK1/2 mutations. Cancer Discov. *7*, 188–201. https://doi.org/10.1158/2159-8290.CD-16-1223.

10. Gao, J., Shi, L.Z., Zhao, H., Chen, J., Xiong, L., He, Q., Chen, T., Roszik, J., Bernatchez, C., Woodman, S.E., et al. (2016). Loss of IFN-gamma pathway genes in tumor cells as a mechanism of resistance to anti-CTLA-4 therapy. Cell *167*, 397–404.e9. https://doi.org/10.1016/j.cell.2016.08.069.

11. Manguso, R.T., Pope, H.W., Zimmer, M.D., Brown, F.D., Yates, K.B., Miller, B.C., Collins, N.B., Bi, K., LaFleur, M.W., Juneja, V.R., et al. (2017). In vivo CRISPR screening identifies Ptpn2 as a cancer immunotherapy target. Nature *547*, 413–418. https://doi.org/10.1038/nature23270.

12. Du, W., Hua, F., Li, X., Zhang, J., Li, S., Wang, W., Zhou, J., Wang, W., Liao, P., Yan, Y., et al. (2021). Loss of optineurin drives cancer immune evasion via palmitoylation-dependent IFNGR1 lysosomal sorting and degradation. Cancer Discov. *11*, 1826–1843. https://doi.org/10.1158/2159-8290.

13. Spranger, S., and Gajewski, T.F. (2018). Impact of oncogenic pathways on evasion of antitumour immune responses. Nat. Rev. Cancer *18*, 139–147. https://doi.org/10.1038/nrc.2017.117.

14. Benci, J.L., Johnson, L.R., Choa, R., Xu, Y., Qiu, J., Zhou, Z., Xu, B., Ye, D., Nathanson, K.L., June, C.H., et al. (2019). Opposing functions of interferon coordinate adaptive and innate immune responses to cancer immune checkpoint blockade. Cell *178*, 933–948.e14. https://doi.org/10.1016/j.cell.2019.07.019.

15. Benci, J.L., Xu, B., Qiu, Y., Wu, T.J., Dada, H., Twyman-Saint Victor, C., Cucolo, L., Lee, D.S.M., Pauken, K.E., Huang, A.C., et al. (2016). Tumor interferon signaling regulates a multigenic resistance program to immune checkpoint blockade. Cell *167*, 1540–1554.e12. https://doi.org/10.1016/j.cell.2016.11.022.

16. Singh, S., Kumar, S., Srivastava, R.K., Nandi, A., Thacker, G., Murali, H., Kim, S., Baldeon, M., Tobias, J., Blanco, M.A., et al. (2020). Loss of ELF5-FBXW7 stabilizes IFNGR1 to promote the growth and metastasis of triple-negative breast cancer through interferon-gamma signalling. Nat. Cell Biol. *22*, 591–602. https://doi.org/10.1038/s41556-020-0495-y.

17. Hanahan, D., and Weinberg, R.A. (2011). Hallmarks of cancer: the next generation. Cell *144*, 646–674. https://doi.org/10.1016/j.cell.2011.02.013.

18. Sanchez-Vega, F., Mina, M., Armenia, J., Chatila, W.K., Luna, A., La, K.C., Dimitriadoy, S., Liu, D.L., Kantheti, H.S., Saghafinia, S., et al. (2018). Oncogenic signaling pathways in the cancer genome atlas. Cell *173*, 321–337.e10. https://doi.org/10.1016/j.cell.2018.03.035.

19. Hanahan, D., and Weinberg, R.A. (2000). The hallmarks of cancer. Cell *100*, 57–70. https://doi.org/10.1016/s0092-8674(00)81683-9.

20. Clevers, H., and Nusse, R. (2012). Wnt/beta-catenin signaling and disease. Cell *149*, 1192–1205. https://doi.org/10.1016/j.cell.2012.05.012.

21. MacDonald, B.T., Tamai, K., and He, X. (2009). Wnt/beta-catenin signaling: components, mechanisms, and diseases. Dev. Cell *17*, 9–26. https://doi.org/10.1016/j.devcel.2009.06.016.

22. Spranger, S., Bao, R., and Gajewski, T.F. (2015). Melanoma-intrinsic beta-catenin signalling prevents anti-tumour immunity. Nature *523*, 231–235. https://doi.org/10.1038/nature14404.

23. Gatenby, R.A., and Gillies, R.J. (2004). Why do cancers have high aerobic glycolysis? Nat. Rev. Cancer *4*, 891–899. https://doi.org/10.1038/nrc1478.

24. Turner, N., and Grose, R. (2010). Fibroblast growth factor signalling: from development to cancer. Nat. Rev. Cancer *10*, 116–129. https://doi.org/10.1038/nrc2780.

25. Normanno, N., De Luca, A., Bianco, C., Strizzi, L., Mancino, M., Maiello, M.R., Carotenuto, A., De Feo, G., Caponigro, F., and Salomon, D.S. (2006). Epidermal growth factor receptor (EGFR) signaling in cancer. Gene *366*, 2–16. https://doi.org/10.1016/j.gene.2005.10.018.

26. Hellmann, M.D., Paz-Ares, L., Bernabe Caro, R., Zurawski, B., Kim, S.W., Carcereny Costa, E., Park, K., Alexandru, A., Lupinacci, L., de la Mora Jimenez, E., et al. (2019). Nivolumab plus ipilimumab in advanced non-small-cell lung cancer. N. Engl. J. Med. *381*, 2020–2031. https://doi.org/10.1056/NEJMoa1910231.

27. Mok, T.S.K., Wu, Y.L., Kudaba, I., Kowalski, D.M., Cho, B.C., Turna, H.Z., Castro, G., Jr., Srimuninnimit, V., Laktionov, K.K., Bondarenko, I., et al. (2019). Pembrolizumab versus chemotherapy for previously untreated, PD-L1-expressing, locally advanced or metastatic non-small-cell lung cancer (KEYNOTE-042): a randomised, open-label, controlled, phase 3 trial. Lancet *393*, 1819–1830. https://doi.org/10.1016/S0140-6736(18)32409-7.

28. Fehrenbacher, L., Spira, A., Ballinger, M., Kowanetz, M., Vansteenkiste, J., Mazieres, J., Park, K., Smith, D., Artal-Cortes, A., Lewanski, C., et al. (2016). Atezolizumab versus docetaxel for patients with previously treated non-small-cell lung cancer (POPLAR): a multicentre, open-label, phase 2 randomised controlled trial. Lancet *387*, 1837–1846. https://doi.org/10.1016/S0140-6736(16)00587-0.

29. Hodi, F.S., Ballinger, M., Lyons, B., Soria, J.C., Nishino, M., Tabernero, J., Powles, T., Smith, D., Hoos, A., McKenna, C., et al. (2018). Immune-modified response evaluation criteria in solid tumors (imRECIST): refining guidelines to assess the clinical benefit of cancer immunotherapy. J. Clin. Oncol. *36*, 850–858. https://doi.org/10.1200/JCO.2017.75.1644.

30. Ferté, C., Fernandez, M., Hollebecque, A., Koscielny, S., Levy, A., Massard, C., Balheda, R., Bot, B., Gomez-Roca, C., Dromain, C., et al. (2014). Tumor growth rate is an early indicator of antitumor drug activity in phase I clinical trials. Clin. Cancer Res. *20*, 246–252. https://doi.org/10.1158/1078-0432.CCR-13-2098.

31. Park, H.J., Kim, K.W., Won, S.E., Yoon, S., Chae, Y.K., Tirumani, S.H., and Ramaiya, N.H. (2021). Definition, incidence, and challenges for assessment of hyperprogressive disease during cancer treatment with immune checkpoint inhibitors: a systematic review and meta-analysis. JAMA Netw. Open *4*, e211136. https://doi.org/10.1001/jamanetworkopen.2021.1136.

32. Matos, I., Martin-Liberal, J., García-Ruiz, A., Hierro, C., Ochoa de Olza, M., Viaplana, C., Azaro, A., Vieito, M., Braña, I., Mur, G., et al. (2020). Capturing hyperprogressive disease with immune-checkpoint inhibitors using RECIST 1.1 criteria. Clin. Cancer Res. *26*, 1846–1855. https://doi.org/10.1158/1078-0432.CCR-19-2226.

33. Ferrara, R., Mezquita, L., Texier, M., Lahmar, J., Audigier-Valette, C., Tessonnier, L., Mazieres, J., Zalcman, G., Brosseau, S., Le Moulec, S., et al. (2018). Hyperprogressive disease in patients with advanced non-small cell lung cancer treated with PD-1/PD-L1 inhibitors or with single-agent chemotherapy. JAMA Oncol. *4*, 1543–1552. https://doi.org/10.1001/jamaoncol.2018.3676.

34. Kim, C.G., Kim, K.H., Pyo, K.H., Xin, C.F., Hong, M.H., Ahn, B.C., Kim, Y., Choi, S.J., Yoon, H.I., Lee, J.G., et al. (2019). Hyperprogressive disease during PD-1/PD-L1 blockade in patients with non-small-cell lung cancer. Ann. Oncol. *30*, 1104–1113. https://doi.org/10.1093/annonc/mdz123.

35. Saâda-Bouzid, E., Defaucheux, C., Karabajakian, A., Coloma, V.P., Servois, V., Paoletti, X., Even, C., Fayette, J., Guigay, J., Loirat, D., et al. (2017). Hyperprogression during anti-PD-1/PD-L1 therapy in patients with recurrent and/or metastatic head and neck squamous cell carcinoma. Ann. Oncol. *28*, 1605–1611. https://doi.org/10.1093/annonc/mdx178.

36. Kim, Y., Kim, C.H., Lee, H.Y., Lee, S.H., Kim, H.S., Lee, S., Cha, H., Hong, S., Kim, K., Seo, S.W., et al. (2019). Comprehensive clinical and genetic characterization of hyperprogression based on volumetry in advanced non-small cell lung cancer treated with immune checkpoint inhibitor. J. Thorac. Oncol. *14*, 1608–1618. https://doi.org/10.1016/j.jtho.2019.05.033.

37. Tunali, I., Gray, J.E., Qi, J., Abdalah, M., Jeong, D.K., Guvenis, A., Gillies, R.J., and Schabath, M.B. (2019). Novel clinical and radiomic predictors of rapid disease progression phenotypes among lung cancer patients

treated with immunotherapy: an early report. Lung Cancer *129*, 75–79. https://doi.org/10.1016/j.lungcan.2019.01.010.

38. Petrioli, R., Mazzei, M.A., Giorgi, S., Cesqui, E., Gentili, F., Francini, G., Volterrani, L., and Francini, E. (2020). Hyperprogressive disease in advanced cancer patients treated with nivolumab: a case series study. Anti Cancer Drugs *31*, 190–195. https://doi.org/10.1097/CAD.0000000000000864.
39. Robinson, D.R., Wu, Y.M., Lonigro, R.J., Vats, P., Cobain, E., Everett, J., Cao, X., Rabban, E., Kumar-Sinha, C., Raymond, V., et al. (2017). Integrative clinical genomics of metastatic cancer. Nature *548*, 297–303. https://doi.org/10.1038/nature23306.
40. Zou, W. (2005). Immunosuppressive networks in the tumour environment and their therapeutic relevance. Nat. Rev. Cancer *5*, 263–274. https://doi.org/10.1038/nrc1586.
41. Curiel, T.J., Wei, S., Dong, H., Alvarez, X., Cheng, P., Mottram, P., Krzysiek, R., Knutson, K.L., Daniel, B., Zimmermann, M.C., et al. (2003). Blockade of B7-H1 improves myeloid dendritic cell-mediated antitumor immunity. Nat. Med. *9*, 562–567. https://doi.org/10.1038/nm863.
42. Maher, P.A. (1996). Nuclear Translocation of fibroblast growth factor (FGF) receptors in response to FGF-2. J. Cell Biol. *134*, 529–536. https://doi.org/10.1083/jcb.134.2.529.
43. Wang, W., Green, M., Choi, J.E., Gijón, M., Kennedy, P.D., Johnson, J.K., Liao, P., Lang, X., Kryczek, I., Sell, A., et al. (2019). CD8(+) T cells regulate tumour ferroptosis during cancer immunotherapy. Nature *569*, 270–274. https://doi.org/10.1038/s41586-019-1170-y.
44. Lin, H., Wei, S., Hurt, E.M., Green, M.D., Zhao, L., Vatan, L., Szeliga, W., Herbst, R., Harms, P.W., Fecher, L.A., et al. (2018). Host expression of PD-L1 determines efficacy of PD-L1 pathway blockade-mediated tumor regression. J. Clin. Invest. *128*, 1708. https://doi.org/10.1172/JCI120803.
45. Nikbakht, N., Tiago, M., Erkes, D.A., Chervoneva, I., and Aplin, A.E. (2019). BET inhibition modifies melanoma infiltrating T cells and enhances response to PD-L1 blockade. J. Invest. Dermatol. *139*, 1612–1615. https://doi.org/10.1016/j.jid.2018.12.024.
46. Homet Moreno, B., Zaretsky, J.M., Garcia-Diaz, A., Tsoi, J., Parisi, G., Robert, L., Meeth, K., Ndoye, A., Bosenberg, M., Weeraratna, A.T., et al. (2016). Response to programmed cell death-1 blockade in a murine melanoma syngeneic model requires costimulation, CD4, and CD8 T cells. Cancer Immunol. Res. *4*, 845–857. https://doi.org/10.1158/2326-6066.CIR-16-0060.
47. Chocarro-Calvo, A., García-Martínez, J.M., Ardila-González, S., De la Vieja, A., and García-Jiménez, C. (2013). Glucose-induced beta-catenin acetylation enhances Wnt signaling in cancer. Mol. Cell *49*, 474–486. https://doi.org/10.1016/j.molcel.2012.11.022.
48. Wolf, D., Rodova, M., Miska, E.A., Calvet, J.P., and Kouzarides, T. (2002). Acetylation of beta-catenin by CREB-binding protein (CBP). J. Biol. Chem. *277*, 25562–25567. https://doi.org/10.1074/jbc.M201196200.
49. Simic, P., Zainabadi, K., Bell, E., Sykes, D.B., Saez, B., Lotinun, S., Baron, R., Scadden, D., Schipani, E., and Guarente, L. (2013). SIRT1 regulates differentiation of mesenchymal stem cells by deacetylating beta-catenin. EMBO Mol. Med. *5*, 430–440. https://doi.org/10.1002/emmm.201201606.
50. Yang, H., Pinello, C.E., Luo, J., Li, D., Wang, Y., Zhao, L.Y., Jahn, S.C., Saldanha, S.A., Chase, P., Planck, J., et al. (2013). Small-molecule inhibitors of acetyltransferase p300 identified by high-throughput screening are potent anticancer agents. Mol. Cancer Therapeut. *12*, 610–620. https://doi.org/10.1158/1535-7163.MCT-12-0930.
51. Lara, E., Mai, A., Calvanese, V., Altucci, L., Lopez-Nieva, P., Martinez-Chantar, M.L., Varela-Rey, M., Rotili, D., Nebbioso, A., Ropero, S., et al. (2009). Salermide, a Sirtuin inhibitor with a strong cancer-specific proapoptotic effect. Oncogene *28*, 781–791. https://doi.org/10.1038/onc.2008.436.
52. Imai, S.i., and Guarente, L. (2014). NAD+ and sirtuins in aging and disease. Trends Cell Biol. *24*, 464–471. https://doi.org/10.1016/j.tcb.2014.04.002.
53. Li, G., Kryczek, I., Nam, J., Li, X., Li, S., Li, J., Wei, S., Grove, S., Vatan, L., Zhou, J., et al. (2021). LIMIT is an immunogenic lncRNA in cancer immunity and immunotherapy. Nat. Cell Biol. *23*, 526–537. https://doi.org/10.1038/s41556-021-00672-3.
54. Liberti, M.V., and Locasale, J.W. (2016). The warburg effect: how does it benefit cancer cells? Trends Biochem. Sci. *41*, 211–218. https://doi.org/10.1016/j.tibs.2015.12.001.
55. Anastasiou, D., Poulogiannis, G., Asara, J.M., Boxer, M.B., Jiang, J.K., Shen, M., Bellinger, G., Sasaki, A.T., Locasale, J.W., Auld, D.S., et al. (2011). Inhibition of pyruvate kinase M2 by reactive oxygen species contributes to cellular antioxidant responses. Science *334*, 1278–1283. https://doi.org/10.1126/science.1211485.
56. Yang, W., Xia, Y., Ji, H., Zheng, Y., Liang, J., Huang, W., Gao, X., Aldape, K., and Lu, Z. (2011). Nuclear PKM2 regulates beta-catenin transactivation upon EGFR activation. Nature *480*, 118–122. https://doi.org/10.1038/nature10598.
57. Hitosugi, T., Kang, S., Vander Heiden, M.G., Chung, T.W., Elf, S., Lythgoe, K., Dong, S., Lonial, S., Wang, X., Chen, G.Z., et al. (2009). Tyrosine phosphorylation inhibits PKM2 to promote the Warburg effect and tumor growth. Sci. Signal. *2*, ra73. https://doi.org/10.1126/scisignal.2000431.
58. Anastasiou, D., Yu, Y., Israelsen, W.J., Jiang, J.K., Boxer, M.B., Hong, B.S., Tempel, W., Dimov, S., Shen, M., Jha, A., et al. (2012). Pyruvate kinase M2 activators promote tetramer formation and suppress tumorigenesis. Nat. Chem. Biol. *8*, 839–847. https://doi.org/10.1038/nchembio.1060.
59. Nathanson, T., Ahuja, A., Rubinsteyn, A., Aksoy, B.A., Hellmann, M.D., Miao, D., Van Allen, E., Merghoub, T., Wolchok, J.D., Snyder, A., and Hammerbacher, J. (2017). Somatic mutations and neoepitope homology in melanomas treated with CTLA-4 blockade. Cancer Immunol. Res. *5*, 84–91. https://doi.org/10.1158/2326-6066.CIR-16-0019.
60. Riaz, N., Havel, J.J., Makarov, V., Desrichard, A., Urba, W.J., Sims, J.S., Hodi, F.S., Martín-Algarra, S., Mandal, R., Sharfman, W.H., et al. (2017). Tumor and microenvironment evolution during immunotherapy with nivolumab. Cell *171*, 934–949.e16. https://doi.org/10.1016/j.cell.2017.09.028.
61. Van Allen, E.M., Miao, D., Schilling, B., Shukla, S.A., Blank, C., Zimmer, L., Sucker, A., Hillen, U., Foppen, M.H.G., Goldinger, S.M., et al. (2015). Genomic correlates of response to CTLA-4 blockade in metastatic melanoma. Science *350*, 207–211. https://doi.org/10.1126/science.aad0095.
62. Abril-Rodriguez, G., Torrejon, D.Y., Liu, W., Zaretsky, J.M., Nowicki, T.S., Tsoi, J., et al. (2020). PAK4 inhibition improves PD-1 blockade immunotherapy. Nat. Can. *1*, 46–58. https://doi.org/10.1038/s43018-019-0003-0.
63. Yost, K.E., Satpathy, A.T., Wells, D.K., Qi, Y., Wang, C., Kageyama, R., McNamara, K.L., Granja, J.M., Sarin, K.Y., Brown, R.A., et al. (2019). Clonal replacement of tumor-specific T cells following PD-1 blockade. Nat. Med. *25*, 1251–1259. https://doi.org/10.1038/s41591-019-0522-3.
64. Yu, J., Green, M.D., Li, S., Sun, Y., Journey, S.N., Choi, J.E., Rizvi, S.M., Qin, A., Waninger, J.J., Lang, X., et al. (2021). Liver metastasis restrains immunotherapy efficacy via macrophage-mediated T cell elimination. Nat. Med. *27*, 152–164. https://doi.org/10.1038/s41591-020-1131-x.
65. Robinson, D., Van Allen, E.M., Wu, Y.M., Schultz, N., Lonigro, R.J., Mosquera, J.M., Montgomery, B., Taplin, M.E., Pritchard, C.C., Attard, G., et al. (2015). Integrative clinical genomics of advanced prostate cancer. Cell *161*, 1215–1228. https://doi.org/10.1016/j.cell.2015.05.001.
66. Tay, C., Qian, Y., and Sakaguchi, S. (2020). Hyper-progressive disease: the potential role and consequences of T-regulatory cells foiling anti-PD-1 cancer immunotherapy. Cancers *13*, 48. https://doi.org/10.3390/cancers13010048.
67. Tan, C.L., Kuchroo, J.R., Sage, P.T., Liang, D., Francisco, L.M., Buck, J., Thaker, Y.R., Zhang, Q., McArdel, S.L., Juneja, V.R., et al. (2021). PD-1 restraint of regulatory T cell suppressive activity is critical for immune tolerance. J. Exp. Med. *218*, e20182232. https://doi.org/10.1084/jem.20182232.
68. Lo Russo, G., Moro, M., Sommariva, M., Cancila, V., Boeri, M., Centonze, G., Ferro, S., Ganzinelli, M., Gasparini, P., Huber, V., et al. (2019). Antibody-fc/FcR interaction on macrophages as a mechanism for hyperprogressive disease in non-small cell lung cancer subsequent to

PD-1/PD-L1 blockade. Clin. Cancer Res. *25*, 989–999. https://doi.org/10.1158/1078-0432.CCR-18-1390.

69. Bosch-Barrera, J., Oliva, E., Sais, E., Vásquez, C.A., Roselló, A., and Menéndez, J.A. (2019). Hyperprogression after first dose of immunotherapy in a patient with radioresistant metastasis from nonsmall cell lung cancer. Anti Cancer Drugs *30*, 1067–1070. https://doi.org/10.1097/CAD.0000000000000837.
70. Fricke, J., Mambetsariev, I., Pharaon, R., Subbiah, S., Rajurkar, S., and Salgia, R. (2020). Hyperprogression on immunotherapy with complete response to chemotherapy in a NSCLC patient with high PD-L1 and STK11: a case report. Medicine (Baltim.) *99*, e22323. https://doi.org/10.1097/MD.0000000000022323.
71. Peng, Y., Zhang, L., Zeng, T., Liu, L., Liu, X., Yang, Y., Zhang, H., and Ruan, Z. (2020). Characterization of hyperprogression after immunotherapy in a lung adenocarcinoma patient with strong expression of programmed death ligand 1. J. Thorac. Oncol. *15*, e4–e8. https://doi.org/10.1016/j.jtho.2019.08.007.
72. Bernal Vaca, L., Mendoza, S.D., Vergel, J.C., Rueda, X., and Bruges, R. (2019). Hyperprogression in pediatric melanoma metastatic to the breast treated with a checkpoint inhibitor. Cureus *11*, e3859. https://doi.org/10.7759/cureus.3859.
73. Schuiveling, M., Tonk, E.H.J., Verheijden, R.J., and Suijkerbuijk, K.P.M. (2021). Hyperprogressive disease rarely occurs during checkpoint inhibitor treatment for advanced melanoma. Cancer Immunol. Immunother. *70*, 1491–1496. https://doi.org/10.1007/s00262-020-02716-3.
74. Yilmaz, M., and Akovali, B. (2020). Hyperprogression after nivolumab for melanoma: a case report. J. Oncol. Pharm. Pract. *26*, 244–251. https://doi.org/10.1177/1078155219845436.
75. Forschner, A., Hilke, F.J., Bonzheim, I., Gschwind, A., Demidov, G., Amaral, T., Ossowski, S., Riess, O., Schroeder, C., Martus, P., et al. (2020). MDM2, MDM4 and EGFR amplifications and hyperprogression in metastatic acral and mucosal melanoma. Cancers *12*, 540. https://doi.org/10.3390/cancers12030540.
76. Wang, J., Wang, X., Yang, X., Zhao, H., and Huo, L. (2020). FDG PET findings of hyperprogression during immunotherapy in a patient with hepatocellular carcinoma. Clin. Nucl. Med. *45*, 92–93. https://doi.org/10.1097/RLU.0000000000002849.
77. Hoshal, S.G., Wickwire, P.C., Gandour-Edwards, R.F., Rajappa, P., and Cates, D.J. (2021). Metastatic renal cell carcinoma presenting as a rapidly enlarging endotracheal mass due to hyperprogression on anti-PD1 immunotherapy. Ear Nose Throat J. *100*, 905S–907S. https://doi.org/10.1177/0145561320931215.
78. Chan, A.S., Ng, V.Y., Snider, J., Kallen, M.E., and Miller, K.D. (2020). Hyperprogression of liver metastasis with neoadjuvant immunotherapy for soft tissue sarcoma. Cureus *12*, e8575. https://doi.org/10.7759/cureus.8575.
79. Ji, Z., Peng, Z., Gong, J., Zhang, X., Li, J., Lu, M., Lu, Z., and Shen, L. (2019). Hyperprogression after immunotherapy in patients with malignant tumors of digestive system. BMC Cancer *19*, 705. https://doi.org/10.1186/s12885-019-5921-9.
80. Forys, J.T., Kuzmicki, C.E., Saporita, A.J., Winkeler, C.L., Maggi, L.B., Jr., and Weber, J.D. (2014). ARF and p53 coordinate tumor suppression of an oncogenic IFN-beta-STAT1-ISG15 signaling axis. Cell Rep. *7*, 514–526. https://doi.org/10.1016/j.celrep.2014.03.026.
81. Chen, J., Li, Y., Yu, T.S., McKay, R.M., Burns, D.K., Kernie, S.G., and Parada, L.F. (2012). A restricted cell population propagates glioblastoma growth after chemotherapy. Nature *488*, 522–526. https://doi.org/10.1038/nature11287.
82. Oshimori, N., Oristian, D., and Fuchs, E. (2015). TGF-beta promotes heterogeneity and drug resistance in squamous cell carcinoma. Cell *160*, 963–976. https://doi.org/10.1016/j.cell.2015.01.043.
83. Paczulla, A.M., Rothfelder, K., Raffel, S., Konantz, M., Steinbacher, J., Wang, H., Tandler, C., Mbarga, M., Schaefer, T., Falcone, M., et al. (2019). Absence of NKG2D ligands defines leukaemia stem cells and mediates their immune evasion. Nature *572*, 254–259. https://doi.org/10.1038/s41586-019-1410-1.
84. Boiko, A.D., Razorenova, O.V., van de Rijn, M., Swetter, S.M., Johnson, D.L., Ly, D.P., Butler, P.D., Yang, G.P., Joshua, B., Kaplan, M.J., et al. (2010). Human melanoma-initiating cells express neural crest nerve growth factor receptor CD271. Nature *466*, 133–137. https://doi.org/10.1038/nature09161.
85. Sweis, R.F., Spranger, S., Bao, R., Paner, G.P., Stadler, W.M., Steinberg, G., and Gajewski, T.F. (2016). Molecular drivers of the non-T-cell-inflamed tumor microenvironment in urothelial bladder cancer. Cancer Immunol. Res. *4*, 563–568. https://doi.org/10.1158/2326-6066.CIR-15-0274.
86. Loriot, Y., Necchi, A., Park, S.H., Garcia-Donas, J., Huddart, R., Burgess, E., Fleming, M., Rezazadeh, A., Mellado, B., Varlamov, S., et al. (2019). Erdafitinib in locally advanced or metastatic urothelial carcinoma. N. Engl. J. Med. *381*, 338–348. https://doi.org/10.1056/NEJMoa1817323.
87. Eisenhauer, E.A., Therasse, P., Bogaerts, J., Schwartz, L.H., Sargent, D., Ford, R., Dancey, J., Arbuck, S., Gwyther, S., Mooney, M., et al. (2009). New response evaluation criteria in solid tumours: revised RECIST guideline (version 1.1). Eur. J. Cancer *45*, 228–247. https://doi.org/10.1016/j.ejca.2008.10.026.
88. Li, J., Wang, W., Zhang, Y., Cieślik, M., Guo, J., Tan, M., Green, M.D., Wang, W., Lin, H., Li, W., et al. (2020). Epigenetic driver mutations in ARID1A shape cancer immune phenotype and immunotherapy. J. Clin. Invest. *130*, 2712–2726. https://doi.org/10.1172/JCI134402.

STAR★METHODS

KEY RESOURCES TABLE

REAGENT or RESOURCE	SOURCE	IDENTIFIER
Antibodies		
anti-FGF2	Abcam	Cat # ab92337, RRID: AB_2049652
anti-phospho-PKM2 (Y105)	Cell Signaling Technology	Cat # 3827, RRID: AB_1950369
anti-phospho-PKM2 (S37)	Signalway	Cat # 11456
anti-PKM2	Proteintech	Cat # 15822, RRID: AB_1851537
anti-GBP1	Proteintech	Cat # 15303, RRID: AB_2247448
anti-GBP2	Proteintech	Cat # 11854, RRID: AB_2109336
anti-SIRT1	Cell Signaling Technology	Cat # 2028, RRID: AB_1196631
anti-phospho-STAT1	Cell Signaling Technology	Cat # 9167, RRID: AB_561284
anti-STAT1	Cell Signaling Technology	Cat # 9172, RRID: AB_2198300
anti-MYC	Cell Signaling Technology	Cat # 13987, RRID: AB_2631168
anti-acetylated-lysine	Cell Signaling Technology	Cat # 9441, RRID: AB_331805
anti-acetyl-β-catenin (K49)	Cell Signaling Technology	Cat # 9030, RRID: AB_2797689
anti-non-phospho-β-catenin	Cell Signaling Technology	Cat # 8814, RRID: AB_11127203
anti-CD44	Cell Signaling Technology	Cat # 37259, RRID: AB_2750879
anti-Histone H3	Cell Signaling Technology	Cat # 4499, RRID: AB_10544537
anti-Tubulin	Cell Signaling Technology	Cat # 2148, RRID: AB_2288042
anti-GAPDH	Proteintech	Cat # 60004, RRID: AB_2107436
V500 Rat Anti-Mouse CD45	BD Biosciences	Cat # 561487, RRID: AB_10697046
PE Rat Anti-Mouse CD44	BD Biosciences	Cat # 561860, RRID: AB_10895375
APC anti-mouse CD133	Biolegend	Cat # 141207, RRID: AB_10898121
FITC Rat Anti-Mouse CD90.2	BD Biosciences	Cat # 553004, RRID: AB_394543
PerCP-Cy5.5 Anti-Mouse CD3e	BD Biosciences	Cat # 551163, RRID: AB_394082
APC-Cy7 Anti-Mouse CD4	BD Biosciences	Cat # 552051, RRID: AB_394331
Alexa Fluor 700 Rat Anti-Mouse CD8a	BD Biosciences	Cat # 557959; RRID: AB_396959
anti-mouse PD-L1	Bio X Cell	Cat # BE0101, RRID: AB_10949073
rat IgG2b isotype control	Bio X Cell	Cat # BE0090, RRID: AB_1107780
anti-mouse CTLA-4	Bio X Cell	Cat # BE0131, RRID: AB_10950184
anti-mouse CD8α	Bio X Cell	Cat # BE0117, RRID: AB_10950145
anti-Human CD8	Abcam	Cat # ab17147, RRID: AB_443686
anti-Human FGF2	Abcam	Cat # ab92337, RRID: AB_2049652
anti-Human MYC	Abcam	Cat # ab32072, RRID: AB_731658
anti-Human CD133	Miltenyi Biotec	Cat # 130-090-422, RRID: AB_244339
Chemicals, peptides, and recombinant proteins		
DASA-58	Cayman Chemical	Cat # 13941
ML-265	Cayman Chemical	Cat # 13942
L002	Cayman Chemical	Cat # 17778
Wnt-C59	Cayman Chemical	Cat # 16644
Nicotinamide riboside	Cayman Chemical	Cat # 23132
β-Nicotinamide Mononucleotide	Cayman Chemical	Cat # 16411
Sirtinol	Cayman Chemical	Cat # 10523
Salermide	Cayman Chemical	Cat # 13178
Palbociclib	Cayman Chemical	Cat # 16273
human IFNγ	R&D Systems	Cat # 285-IF
mouse IFNγ	R&D Systems	Cat # 485-MI

(*Continued on next page*)

Continued

REAGENT or RESOURCE	SOURCE	IDENTIFIER
human DKK1	R&D Systems	Cat # 5439-DK
mouse DKK1	R&D Systems	Cat # 5897-DK
human FGF2	R&D Systems	Cat # 233-FB
Critical commercial assays		
Lactate Assay Kit	Sigma-Aldrich	Cat # MAK064
NAD/NADH Quantitation Kit	Sigma-Aldrich	Cat # MAK037
Pyruvate Assay Kit	Sigma-Aldrich	Cat # MAK071
Hexokinase Colorimetric Assay Kit	Sigma-Aldrich	Cat # MAK091
Phosphofructokinase (PFK) Activity Colorimetric Assay Kit	Sigma-Aldrich	Cat # MAK093
GAPDH Activity Assay Kit	Sigma-Aldrich	Cat # MAK277
Pyruvate Kinase Activity Assay Kit	Sigma-Aldrich	Cat # MAK072
Lactate Dehydrogenase Activity Assay Kit	Sigma-Aldrich	Cat # MAK066
Deposited data		
Gene expression profile of patient samples	[39,64,65]	dbGaP: phs000673.v2. p1
Gene expression profile of patient samples	[60]	GEO datasets: GSE91061
Gene expression profile of patient samples	[62]	dbGaP: phs001919. v1.p1
Gene expression profile of cell samples	[11]	GEO datasets: GSE99299
Gene expression profile of single cell patient samples	[63]	GEO datasets: GSE123814
Experimental models: Cell lines		
Human Cell line: A375	ATCC	Cat # CRL-1619
Human Cell line: MeWo	ATCC	Cat # HTB-65
Human Cell line: A2058	ATCC	Cat # CRL-11147
Human Cell line: CHL-1	ATCC	Cat # CRL-9446
Human Cell line: Malme-3M	ATCC	Cat # HTB-64
Human Cell line: G361	ATCC	Cat # CRL-1424
Human Cell line: SKMEL-1	ATCC	Cat # HTB-67
Human Cell line: SKMEL-2	ATCC	Cat # HTB-68
Human Cell line: SKMEL-5	ATCC	Cat # HTB-70
Human Cell line: SKMEL-28	ATCC	Cat # HTB-72
Human Cell line: A549	ATCC	Cat # CCL-185
Human Cell line: H1299	ATCC	Cat # CRL-5803
Human Cell line: H292	ATCC	Cat # CRL-1848
Human Cell line: H23	ATCC	Cat # CRL-5800
Human Cell line: H69	ATCC	Cat # HTB-119
Human Cell line: H460	ATCC	Cat # HTB-177
Human Cell line: H661	ATCC	Cat # HTB-183
Human Cell line: H1437	ATCC	Cat # CRL-5872
Human Cell line: H1975	ATCC	Cat # CRL-5908
Mouse Cell line: YUMM1.7	ATCC	Cat # CRL-3362
Mouse Cell line: YUMM5.2	ATCC	Cat # CRL-3367
Mouse Cell line: B16-F0	ATCC	Cat # CRL-6322
Mouse Cell line: LLC	ATCC	Cat # CRL-1642
Human Cell line: 293T	ATCC	Cat # CRL-3216
Mouse Cell line: MC38	[44]	N/A
Experimental models: Organisms/strains		
Mouse: C57BL/6J	The Jackson Laboratory	Cat # JAX: 000664
Mouse: NSG	The Jackson Laboratory	Cat # JAX: 005557
Oligonucleotides		

(*Continued on next page*)

Continued

REAGENT or RESOURCE	SOURCE	IDENTIFIER
Primers	Integrated DNA Technologies	See Tables S6–S8
Recombinant DNA		
PGL-3 Basic	Promega	Cat # E1751
PCI-neo	Promega	Cat # E1841
TOP-FLASH	Addgene	Cat # 12456
FOP-FLASH	Addgene	Cat # 12457
FLAG-β-catenin	Addgene	Cat # 16828
PLKO.1	Addgene	Cat # 10879
PX459	Addgene	Cat # 48139
Fgf2 promoter and exon1	Origene	N/A
Software and algorithms		
BD FACSDiva Software	BD Biosciences	https://www.bdbiosciences.com/en-us/products/software/instrument-software/bd-facsdiva-software#Overview
Graphpad Prism 8.0 software	GraphPad Software	http://www.graphpad.com/scientificsoftware/prism/
ImageJ	NIH	https://imagej.nih.gov/ij/

RESOURCE AVAILABILITY

Lead contact

Further information and requests for materials should be directed to the lead contact: Weiping Zou (wzou@umich.edu)

Materials availability

This study did not generate new unique reagents.

Data and code availability

The expression sequencing from the University of Michigan cohort was previously deposited (National Center for Biotechnology Information database of Genotypes and Phenotypes (dbGaP) under accession number phs000673.v2. p1.).[39,64,65] The expression sequencing data and corresponding clinical annotation for patients receiving ICB was previously deposited (Gene Expression Omnibus (GEO) under accession number GSE91061; National Center for Biotechnology Information database of Genotypes and Phenotypes (dbGaP) under accession number phs001919. v1.p1.[59–62] The expression profile of cell lines was previously deposited (Gene Expression Omnibus (GEO) under accession number GSE99299).[11] The single cell RNA sequencing data of cancer patients upon immunotherapy was previously deposited (Gene Expression Omnibus (GEO) under accession number GSE123814).[63] All raw data supporting the findings of this study are available from the corresponding authors upon request.

EXPERIMENTAL MODEL AND SUBJECT DETAILS

Human studies

Patients were recruited through the University of Michigan Hospital, Ann Arbor, MI, USA. All clinical records in this study were obtained with the approval of Institutional Review Boards and patients' consents was waived following Institutional Review Board protocol review (HUM00146400, HUM00139259, HUM00163915, HUM00161860, and HUM00046018). Cohort 1 represents metastatic melanoma patients who received treatment at the University of Michigan from 2013–2020. Cohort 2 represents metastatic NSCLC patients who received treatment at the University of Michigan from 2013–2019. Cohort 3 represents patients at the University of Michigan who have undergone comprehensive tumor and somatic bulk RNA sequencing as previously described who received immunotherapy and had evaluable cross-sectional imaging.[39] Tumor radiographic response and tumor growth rate were evaluated at the first imaging assessment preceding and following therapy initiation in the subset of patients with evaluable longitudinal cross-sectional imaging. Radiologists blinded to the hypothesis conducted evaluation of clinical imaging to define tumor burden and all measurements were validated by a board-certified radiation oncologist. Patients with pseudoprogression were identified by using imRECIST criteria[29] and excluded from all cohorts. RECIST1.1[87] was utilized for response assessment. Hyperprogression was defined as previously published (Table S3); analysis using Champiat et al. criteria are displayed. Tumor burden was defined as

the sum of the longest cross-sectional diameters of lesions noted on radiographic studies. Progression-free survival and overall survival were calculated from initiation of therapy. 3D reconstructions were constructed in Eclipse within the ARIA Oncology Information System (Varian Oncology, Version 15).

Cell lines

Human melanoma cell lines included A375 (CRL-1619), MeWo (HTB-65), A2058 (CRL-11147), CHL-1(CRL-9446), Malme-3M (HTB-64), G361 (CRL-1424), SKMEL-1 (HTB-67), SKMEL-2 (HTB-68), SKMEL-5 (HTB-70), and SKMEL-28 (HTB-72). Human lung cancer cell lines included A549 (CCL-185), H1299 (CRL-5803), H292 (CRL-1848), H23 (CRL-5800), H69 (HTB-119), H460 (HTB-177), H661 (HTB-183), H1437 (CRL-5872), and H1975 (CRL-5908). Mouse melanoma cell lines were YUMM1.7 (CRL-3362), YUMM5.2 (CRL-3367), and B16-F0 (CRL-6322). Mouse lung cancer cell lines were Lewis lung carcinoma (LLC, CRL-1642) and its subclones. Human embryonic kidney cell 293T (CRL-3216) was used in the study. These cell lines were from the American Type Culture Collection (ATCC). Mouse colon cancer cell line MC38 from previously studies was used.[44,88] To generate LLC subclones, LLC tumor bearing mice were treated with anti-PD-L1. Tumor cells were dissected from these mice bearing ICB-resistant tumors and serially diluted and seeded into 96 well plates. Ten days after seeding, single cell clones (PLC1.1-PLC2.4) were collected by trypsinization. Using CRISPR Cas9, *IFNGR1* KO and *STAT1* KO A375 cells, *Ifngr1* KO and *Stat1* KO YUMM1.7 cells and PLC2.4 cells, and *Stat1* KO YUMM5.2 cell lines were generated in this study. YUMM1.7 cells were maintained at low confluence (less than 70%) to avoid clumping. All cell lines were tested for mycoplasma contamination routinely and confirmed negative for mycoplasma. Cells were cultured in pyruvate-free medium supplemented with 10% FBS. A375, MeWo, A2058, CHL-1, Malme-3M, SKMEL-1, SKMEL-2, SKMEL-5, SKMEL-28, A549, 293T, LLC, and PLC2.4 cells were cultured in DMEM (Gibco #11965), H1299, H292, H23, H69, H460, H661, H1437, H1975 YUMM1.7, YUMM5.2, B16, and MC38 cells were cultured in RPMI (Gibco #11875). G361 cells were cultured in McCoy's 5a medium (Gibco #16600). All cells were maintained in 37°C and 5% CO_2.

Tumor models

Six- to eight-week-old female C57BL/6 (C57BL/6J, Stock# 000664) and NSG (#005557) mice were obtained from the Jackson Laboratory. All mice were maintained under pathogen-free conditions. The animal room is a controlled environment: temperature (18–23°C), humidity (40–60%), and a 12-hour light/dark cycle. YUMM1.7 (10^5), YUMM5.2 (10^5), PLC2.4 (10^5), and MC38 (2.5×10^6) cells were subcutaneously injected into the right flank of C57BL/6 mice. A375 (5×10^5) cells were subcutaneously injected into the right flank of NSG mice. Tumor diameters were measured using calipers. Tumor volume was calculated by Length × Width × Width/2. Tumor weight was measured with an analytical balance. Animal studies were conducted under the approval of the Institutional Animal Care and Use Committee at the University of Michigan (PRO00008278). The study is compliant with all relevant ethical regulations regarding animal research. In none of the experiments did xenograft tumor size surpass 2 cm in any dimensions, and no animal had severe abdominal distension (≥10% original body weight increase). Sample size was chosen based on preliminary data. After tumor inoculation, mice were randomized and assigned to different groups for treatment.

METHOD DETAILS

Multiplex immunofluorescence staining and analysis

Multiplex immunofluorescence staining was performed on pretreatment formalin fixed paraffin embedded (FFPE) human melanoma or non-small cell lung carcinoma sections with OPAL 4-Color IHC kits (Akoya Biosciences, NEL810001KT). Antibodies against human CD8 (C8/144B, Abcam, 1:100), FGF2 (EP1735, Abcam, 1:500), MYC (Y69, Abcam, 1:200), and CD133 (AC133, Miltenyi Biotec, 1:50) were used in the study. Imaging was completed using the Mantra Quantitative Pathology Workstation. Tissue core images were captured at x4 and ×40 magnifications. All cube filters were used for each image capture (DAPI, CY3, CY5, Texas Red). The incorporated saturation protection feature was set at an exposure time of 250 ms. Images were analyzed using in Form Cell Analysis software (Perkin Elmer). Images were batch analyzed using a subset of randomly chosen tissue core images. Using the inform software, both tissue and cell compartments were identified and segmented. Tissue was segmented into stroma and epithelial cancer compartments, while cells were segmented into nucleus compartments. DAPI counterstain was used to determine the size and shape of each nucleus. After cell segmentation, based on single staining, $CD8^+$ T cells and tumor cells were determined and quantified using the inform software after selected cells were manually assigned.

Animal experiments

Six- to eight-week-old female C57BL/6 (C57BL/6J, Stock# 000664) and NSG (#005557) mice were obtained from the Jackson Laboratory. All mice were maintained under pathogen-free conditions. The animal room is a controlled environment: temperature (18–23°C), humidity (40–60%), and a 12-hour light/dark cycle. YUMM1.7 (10^5), YUMM5.2 (10^5), PLC2.4 (10^5), and MC38 (2.5×10^6) cells were subcutaneously injected into the right flank of C57BL/6 mice. A375 (5×10^5) cells were subcutaneously injected into the right flank of NSG mice. For anti-PD-L1 treatment in MC38 model, 5 mg/kg anti-PD-L1 (*InVivo*MAb, 10F.9G2) and control antibody (*InVivo*MAb, LTF-2) were intraperitoneally administered on day 6, 9, and 12 post tumor inoculation. For anti-PD-L1 treatment in YUMM1.7 and PLC2.4 model, 5 mg/kg anti-PD-L1 (*InVivo*MAb, 10F.9G2) and control antibody (*InVivo*MAb, LTF-2) were intraperitoneally administered on day 0, 3, 6, 9, 12, and 15 post tumor inoculation. For anti-CTLA4 treatment in YUMM1.7 model, 5 mg/kg anti-CTLA4 (*InVivo*MAb, 9H10) and control antibody (*InVivo*MAb, LTF-2) were intraperitoneally administered on day 0, 3, 6, 9, 12, and

15 post tumor inoculation. For anti-CD8 treatment in YUMM1.7 model, 5 mg/kg anti-CD8α (InVivoMAb, YTS169.4) and control antibody (*InVivo*MAb, LTF-2) were intraperitoneally administered on day −1, 2, 5, and 8 post tumor inoculation. For IFNγ treatment in A375 model, 0.5 μg IFNγ (R&D, 285-IF) was intraperitoneally administered every 3 days post tumor inoculation. For ML-265 treatment in YUMM1.7 model, 50 mg/kg ML-265 was intraperitoneally administered every other day post tumor inoculation. Tumor diameters were measured using calipers. Tumor volume was calculated by Length × Width × Width/2. Tumor weight was measured with an analytical balance. Animal studies were conducted under the approval of the Institutional Animal Care and Use Committee at the University of Michigan (PRO00008278). The study is compliant with all relevant ethical regulations regarding animal research. In none of the experiments did xenograft tumor size surpass 2 cm in any dimensions, and no animal had severe abdominal distension (≥10% original body weight increase). Sample size was chosen based on preliminary data. After tumor inoculation, mice were randomized and assigned to different groups for treatment.

Cell culture

To generate knock down cell lines, lentiviral particles were produced by transfection of PLKO.1 shRNA plasmid with psPAX2 (Addgene #12260) and pMD2.G (Addgene #12259) (4:3:1) into 293T cells, and subsequently transduced into tumor cells with polybrene (Sigma-Aldrich, 8 μg/mL) overnight. 48 hours after transfection, cells were selected with puromycin (1–2 μg/mL) for an additional 2 weeks. To establish knock out cell lines, PX459-sgRNA plasmids were transfected into tumor cells for 2 days and selected by puromycin (1–2 μg/mL) for an additional 2 days. The cells were then serially diluted and seeded into 96 well plates. After 2–3 weeks, single cell colonies were dissociated and re-plated into 6 well plates. Upon cell confluency, half of the cells were harvested and validated for knock out (KO) efficiency via Western blotting. β-catenin K345R mutant plasmid was expressed in CTNNB1 KO cells to generate β-catenin K345R mutant cells. All transfections were conducted with lipofectamine 2000 (Thermo Fisher) at a ratio of 1 μg plasmid: 2 μL transfection regent. The transfection dosage was determined by titration.

Plasmids

To generate FGF2 promoter luciferase reporter, DNA sequences corresponding to Fgf2 promoter and exon1 were synthesized (Origene) and inserted into PGL3-basic plasmid (Promega). TOP-FLASH (#12456), FOP-FLASH (#12457), and FLAG-β-catenin (#16828) were obtained from Addgene. Site directed mutagenesis was conducted to generate β-catenin K345R mutant plasmid. To force mouse Fgf2 expression, the coding sequence of Fgf2 was PCR amplified from cDNA generated from IFNγ-treated YUMM1.7 cells and subsequently inserted into PCI-Flag plasmid. PCI-Flag plasmid was prepared by inserting the Kozak sequence plus Flag tag plus 5 × Glycine sequence into the PCI-neo plasmid (Promega) between NheI and XhoI. To knock down *Pkm2* and *Fgf2*, shRNAs were designed and inserted into PLKO.1 plasmid (Addgene #10879). The shRNA targeting firefly luciferase (sh*Fluc*) served as a negative control. To knock out IFNGR1 and STAT1, sgRNA was designed and inserted into PX459 plasmid (Addgene #48139). The target sequences are listed in Table S6. The primer sequences are listed in Table S7.

Luciferase activity assay

A375 cells were transfected with TOP-FLASH or FOP-FLASH, along with PRL-SV40P (Addgene #27163) for 24 hours, then treated with IFNγ, NR, and DASA-58 for additional 24 hours. Luciferase activity for firefly luciferase (TOP-FLASH) and renilla luciferase (PRL-SV40P) was measured with Dual-Luciferase Reporter Assay System (Promega). Relative firefly luciferase activity was normalized with renilla luciferase activity.

Flow cytometry analysis (FACS)

Cells were trypsinized and washed with MACS buffer (PBS, 2%FBS, 1 mM EDTA). Surface staining was performed by adding the following antibodies to the cell suspension in 50 μL MACS buffer: anti-CD45 (30-F11, BD Biosciences), anti-CD44 (IM7, BD Biosciences), and anti-CD133 (315-2C11, BioLegend). For intracellular staining, cell suspension was incubated with anti-MYC (D3N8F, Cell Signaling Technology), followed by washing and incubating with secondary antibody (#A-11011, Invitrogen). After 30 minutes incubation, cells were washed with MACS buffer and analyzed on BD Fortessa flow cytometer.

Extracellular acidification (ECAR) and oxygen consumption rate (OCR)

ECAR and OCR were measured in control cells or IFNγ-treated cells with a Seahorse XF96 Analyzer (Seahorse Bioscience, Billerica, MA, USA). In brief, 3×10^5 A375 cells were seeded in RPMI-1640 with 10% FBS and incubated for 1 to 2 hours to allow cell adhesion. The media were removed and replaced with Seahorse assay media with 2 mM glutamine without glucose. The plates containing cells were incubated for 1 hour at 37°C without CO2. Extracellular flux analysis was performed at 37°C without CO_2 in the XF96 analyzer (Seahorse Bioscience) following the manufacturer's instructions. Port additions and times are indicated in the figures. Glucose (10 mM), Oligomycin (1.25 μM), and 2-DG (5 mM), were injected where relevant, and ECAR (mpH/min) or OCR (pmol O_2/min) were measured in real time.

Quantification of enzymatic activity

A375 cells were treated with 10 ng/mL IFNγ for 36 hours. Cells were collected and the catalytic activity of glycolysis rate-limiting enzymes were quantitated by Hexokinase Colorimetric Assay Kit (MAK091, Sigma-Aldrich), Phosphofructokinase (PFK) Activity Colorimetric Assay Kit (MAK093, Sigma-Aldrich), GAPDH Activity Assay Kit (MAK277, Sigma-Aldrich), Pyruvate Kinase Activity Assay Kit

(MAK072, Sigma-Aldrich), and Lactate Dehydrogenase Activity Assay Kit (MAK066, Sigma-Aldrich), respectively, according to the manufacturer's instructions.

Quantification of lactate, NAD^+/NADH, and pyruvate

To analyze the metabolites, cells were washed with warm fresh medium and incubated in warm fresh medium for 1 hour to balance the metabolites. Then, extracellular lactate was measured with a Lactate Assay Kit (MAK064, Sigma-Aldrich). Intracellular NAD^+/NADH and pyruvate were measured with a NAD^+/NADH quantification kit (MAK037, Sigma-Aldrich) and Pyruvate assay kit (MAK071, Sigma-Aldrich), respectively, according to the manufacturer's instructions.

Quantitative PCR (qPCR)

Total RNA was isolated from cells by column purification (Direct-zol RNA Miniprep Kit, Zymo Research) with DNase treatment. cDNA was synthesized using RevertAid First Strand cDNA Synthesis Kit (Thermo Fisher Scientific) with random hexamer primers. Quantitative PCR (qPCR) was performed on cDNA using Fast SYBR Green Master Mix (Thermo Fisher Scientific) on a StepOnePlus Real-Time PCR System (Thermo Fisher Scientific). Gene expression was quantified using the primers listed in Table S8. Fold changes in mRNA expression were calculated by the ΔΔCt method using ACTB as an endogenous control. Results are expressed as fold change by normalizing to the controls.

Western blotting

Cells were washed in cold PBS and lysed in 1 × RIPA lysis buffer (Pierce) with 1 × protease inhibitor (Pierce). Lysates were incubated on ice for 10 min and cleared by centrifugation at 15,000g for 15 minutes. Protein concentration was quantified using a BCA protein assay kit (Thermo Fisher). Thirty microgram protein was mixed with sample buffer (Thermo Fisher) with β-ME and denatured at 95°C for 5 minutes. Sample was separated by SDS–PAGE and transferred to a Nitrocellulose Membrane (Bio-Rad). Membranes were blocked with 5% w/v non-fat dry milk and incubated with primary antibodies overnight at 4°C and HRP-conjugated secondary antibodies (CST) for 1 hour at room temperature. Signal was detected using Clarity and Clarity Max Western ECL Blotting Substrates (Bio-Rad) and captured using ChemiDoc Imaging System (Bio-Rad). Antibodies were as follows: anti-FGF2 (Abcam, #EP1735, 1:1000), anti-phosphorylated PKM2 (Y105) (CST, #3827, 1: 1000), anti-phosphorylated PKM2 (S37) (Signalway, #11456, 1:1000), anti-PKM2 (Proteintech, #15822-1-AP, 1:1000), anti-GBP1 (Proteintech, #15303, 1: 1,000), anti-GBP2 (Proteintech, #11854, 1:1000), anti-SIRT1 (CST, #2028, 1: 1,000), anti-phospho-STAT1 (CST, #9167, 1:1000), anti-STAT1 (CST, #9172, 1: 1,000), anti-MYC (CST, #13987, 1:1,000), anti-acetylated-lysine (CST, #9441, 1:1000), anti- acetyl-β-catenin (K49) (CST, #9030, 1:1000), anti-non-phospho (Active) β-catenin (CST, #8814, 1:1000), anti-CD44 (CST, #37259, 1:1000), anti-Histone H3 (CST, #4499, 1:1000), anti-Tubulin (CST, #2148, 1:1000), and anti-GAPDH (Proteintech, #60004, 1: 5,000). Subcellular fractionation was performed with NE-PER™ Nuclear and Cytoplasmic Extraction Reagents (Thermo Scientific, #78833).

Co-Immunoprecipitation (Co-IP)

Cells were collected with IP lysis buffer (Pierce, 87787) plus protease inhibitor. Protein concentration was determined with BCA protein assay kit. 200–500 μg protein samples were added with 20 μL EZview Red ANTI-FLAG M2 Affinity Gel (Sigma Aldrich), then incubated with gentle rocking at 4°C overnight. Samples were then centrifuged at 7500 ×g for 30 seconds at 4°C. Cell pellets were washed 4 times with IP lysis buffer, resuspended with 40 μL 2 × sample buffer with β-ME, and heated for 5 minutes at 95°C. The denatured protein samples were analyzed by Western blot.

Intratumoral immune cell profiling

To analyze intratumoral T cells, single-cell suspensions were prepared from fresh tumor tissues by physically passing through 100 μm cell strainers. Immune cells were enriched by density gradient centrifugation. 2–3 μL of Anti-CD45 (30-F11, BD Biosciences), anti-CD90 (53–2.1, BD Biosciences), anti-CD3 (145-2C11, BD Biosciences), anti-CD4 (GK1.5, BD Biosciences), and anti-CD8 (53–6.7, BD Biosciences) antibodies were added for 20 minutes for surface staining. The cells were then washed and resuspended in 1 mL of freshly prepared Fix/Perm solution (BD Biosciences) at 4°C overnight, followed by washing with Perm/Wash buffer (BD Biosciences). All samples were read on an LSR Fortessa cytometer and analyzed with FACS DIVA software v. 8.0 (BD Biosciences).

Signature score computation

We used normalized expression of genes (Z-score) to define the following signatures: $CD8^+$ T cell infiltration (*CD8A*, *CD8B*, *PRF1*, and *GZMB*), IFNγ signaling (*IFNG*, *STAT1*, *IRF1*, *GBP1*, *CXCL9*, *IFIT1*, *IFITM1*, and *IFI35*), FGF signaling (*FGF2*, *FGFR1*, *FRS2*, *GRB2*, *SOS1*, *FOS*, *MET*, *RUNX2*, *SHC1*, *PTK2B*, *RPS6KA1*, and *SSH1*), β-catenin signaling (*CTNNB1*, *MYC*, *CCND2*, *LEF1*, *TCF7*, *ADAM17*, *AXIN1*, *AXIN2*, *CUL1*, *DKK1*, *DKK4*, *DVL2*, *FZD1*, *FZD8*, *MAML1*, *NCOR2*, *NCSTN*, *NKD1*, *NUMB*, *PPARD*, *PSEN2*, *RBPJ*, and *SKP2*), Shh signaling (*GLI1*, *PTCH1*, *TLE1*, *SHH*, *SCG2*, *RTN1*, *SLIT1*, *OPHN1*, and *NRCAM*), Hippo signaling (*YAP1*, *WTIP*, *AMOT*, *WWC1*, *WWTR1*, *LATS2*, *SCHIP1*, *MARK3*, *WWC2*, *LATS1*, and *PJA1*), KRAS signaling (*ABCB1*, *AKAP12*, *APOD*, *ARG1*, *BMP2*, *BTBD3*, *CBL*, *EPHB2*, and *MAP7*), NOTCH signaling (*NOTCH1*, *HEY1*, *HEY2*, *JAG1*, *JAG2*, *HES1*, *SKP1*, *KAT2A*, *MAML2*), EGF signaling (*EGF*, *EGFR*, *ETS2*, *IER3*, *EGR1*, *IER2*, *NEDD9*, *EGR3*, *EGR4*, *ID1*, *ID3*, *ARC*, *NAB2*, and *NAP1L1*), and stemness/invasiveness gene signature (*MYC*, *CD44*, *NANOG*, *SOX2*, *KLF4*, *BMI1*, *VIM*, *ZEB1*, *FN1*, *TJP1*, *SNAI1*, *SNAI2*, and *TWIST1*).

Statistical analysis

For cell-based experiments, biological triplicates were performed in each single experiment, unless otherwise stated. For animal studies, no less than 5 replicates per group were employed. Animals were randomized into different groups after tumor cell inoculation. The investigators were not blinded to allocation during experiments and outcome assessment. Data are shown as mean values with standard derivation. Statistical analysis was performed using GraphPad Prism8 software (GraphPad Software, Inc.) or in R. Two-tailed t-test was used to compare treatment groups with control groups; Survival function was estimated by Kaplan–Meier methods and log-rank test was used to calculate statistical differences. In cases with non-proportional hazards, the restricted mean survival time was utilized. Inverse-probability weighted (IPW) estimator was used for multivariable modeling. The weights were estimated using the covariate balancing propensity score method with consideration for age, gender, histology, performance status, number of lines of prior therapy, BRAF mutational status (Cohort 1 only), and smoking status (Cohort 2 only). For all tests, $p < 0.05$ was considered significant. Sample size was not predetermined. Unless noted, samples were independent biological replicates.

Cancer Cell, Volume *41*

Supplemental information

Intersection of immune and oncometabolic pathways drives cancer hyperprogression during immunotherapy

Gaopeng Li, Jae Eun Choi, Ilona Kryczek, Yilun Sun, Peng Liao, Shasha Li, Shuang Wei, Sara Grove, Linda Vatan, Reagan Nelson, Grace Schaefer, Steven G. Allen, Kamya Sankar, Leslie A. Fecher, Mishal Mendiratta-Lala, Timothy L. Frankel, Angel Qin, Jessica J. Waninger, Alangoya Tezel, Ajjai Alva, Christopher D. Lao, Nithya Ramnath, Marcin Cieslik, Paul W. Harms, Michael D. Green, Arul M. Chinnaiyan, and Weiping Zou

Table S1: Clinical characteristics of melanoma patients (Cohort 1), Related to Figure 1.

	Total Cohort	Immune Checkpoint Blockade	Targeted Therapy	
Number of Patients	389	251	138	
Age at Immunotherapy (Average)	59.6	60.9	57.2	P= 0.019
Gender				
Male	257 (66%)	163 (65%)	94 (68%)	P=0.527
Female	132 (34%)	88 (35%)	44 (32%)	
ECOG Performance Status				P=0.001
0-1	359 (92%)	240 (96%)	119 (86%)	
2+	30 (8%)	11 (4%)	19 (14%)	
Histology				
Melanoma	389(100%)	251 (100%)	138(100%)	
BRAF V600 Mutant	233 (43%)	95 (38%)	138(100%)	P<0.001
Stage at Therapy				
IV	389(100%)	251 (100%)	138(100%)	
Prior Lines of Therapy				
0	295 (76%)	216 (86%)	79 (57%)	P<0.001
1+	94 (24%)	35 (14%)	59 (43%)	
Disease Origin				
Cutaneous	326 (84%)	200 (80%)	126 (91%)	P<0.001
Mucosal	20 (5%)	20 (8%)	0 (0%)	
Ocular	31 (8%)	27 (11%)	4 (3%)	
Unknown	12 (3%)	4 (1%)	8 (6%)	
Therapy				
Dabrafenib	14 (3%)		14 (10%)	
Trametinib	4 (1%)		4 (3%)	
Vemurafenib	36 (9%)		36 (26%)	
Encorafenib	1 (0%)		1 (1%)	
DTIC	1 (0%)		1 (1%)	
Dabrafenib and Trametinib	77 (20%)		77 (56%)	
Vemurafenib and Cobimetinib	3 (1%)		3 (2%)	
Encorafenib and Binimetinib	2 (1%)		2 (1%)	
Nivolumab	38 (10%)	38 (15%)		
Pembrolizumab	96 (25%)	96 (38%)		
Ipilimumab	45 (12%)	45 (18%)		
Ipilimumab and Nivolumab	72 (1%)	72 (29%)		

Abbreviations:
ECOG- Eastern Cooperative Oncology Group

Table S2: Clinical characteristics of NSCLC patients (Cohort 2), Related to Figure 1.

	Total Cohort	Immune Checkpoint Blockade	Chemotherapy	
Number of Patients	375	279	96	
Average Age	66.0	66.0	65.9	P=0.88
Gender				
Male	165 (44%)	109 (39%)	56 (58%)	P=0.001
Female	210 (56%)	170 (61%)	40 (42%)	
ECOG Performance Status				P=0.001
0-1	301 (80%)	213 (76%)	88 (92%)	
2+	74 (20%)	66 (24%)	8 (8%)	
Smoking Status				P=0.159
Never	50 (13%)	37 (13%)	13 (13%)	
Former	279 (75%)	213 (76%)	66 (69%)	
Current	46 (12%)	29 (11%)	17 (18%)	
Stage at Therapy				
IV	375 (100%)	279(100%)	96 (100%)	
Tumor Histology				
Adenocarcinoma	282 (75%)	201 (72%)	81 (85%)	P=0.003
Squamous Cell Carcinoma	66 (18%)	60 (22%)	6 (6%)	
Other	27 (7%)	18 (6%)	9 (9%)	
Prior Lines of Therapy				P<0.001
0	174 (46%)	109 (39%)	65 (68%)	
1	104 (28%)	88 (32%)	16 (17%)	
2+	97 (26%)	82 (29%)	15 (15%)	
Therapy				
Platinum doublet	54 (14%)		54 (56%)	
Gemcitabine	8 (2%)		8 (8%)	
Pemetrexed	12 (3%)		12 (13%)	
Taxane	5 (1%)		5 (5%)	
Other	17 (5%)		17 (18%)	
Atezolizumab	47 (13%)	47 (17%)		
Nivolumab	81 (22%)	81 (29%)		
Pembrolizumab	50 (13%)	50 (18%)		
Carboplatin, pemetrexed, pembrolizumab	82 (22%)	82 (29%)		
Paclitaxel, pemetrexed, pembrolizumab	19 (5%)	19 (7%)		

Abbreviations:
ECOG- Eastern Cooperative Oncology Group

Table S3: HPD definitions, Related to Figure 1.

Authors	Cancer Type	Definition	DOI
Champiat S, et al.	Multiple Cancer Types	TGR ratio > 2 and PD at 1st assessment	10.1158/1078-0432.CCR-16-1741
Ferrara R, et al.	NSCLC	Delta TGR > 50%	10.1001/jamaoncol.2018.3676
Kim CG, et al.	NSCLC	PD, TTF < 2 months, TGK ratio >2 and TGR ratio >2	10.1093/annonc/mdz123
Kato S, et al.	Multiple Cancer Types	TTF < 2 months, >50% RECIST, >2 fold increase in progression pace	10.1158/1078-0432.CCR-16-3133
Saâda-Bouzid E, et al.	Head and Neck Cancer	TGK ratio > 2	10.1093/annonc/mdx178
Kim Y, et al.	NSCLC	TTF < 2 months, >50% volume increase, TGK >2	10.1016/j.jtho.2019.05.033
Matos I, et al.	Multiple Cancer Types	PD in < 8 weeks, 1.4x increase from baseline or 1.2x increase from baseline with involvement of 2 new organs	10.1158/1078-0432.CCR-19-2226
Tunali I, et al.	NSCLC	TGR ratio >2, TTF < 2 months, AND PD on 1st scan	10.1016/j.lungcan.2019.01.010
Petrioli R, et al.	Multiple Cancer Types	TGR ratio > 2	10.1097/CAD.0000000000000864

Abbreviations:
HPD- Hyperprogressive Disease
NSCLC- Non-small Cell Lung Cancer
PD- Progressive Disease
RECIST- Response Evaluation Criteria In Solid Tumors
TGK- Tumor Growth Kinetics
TGR- Tumor Growth Rate
TTF- Time to Treatment Failure

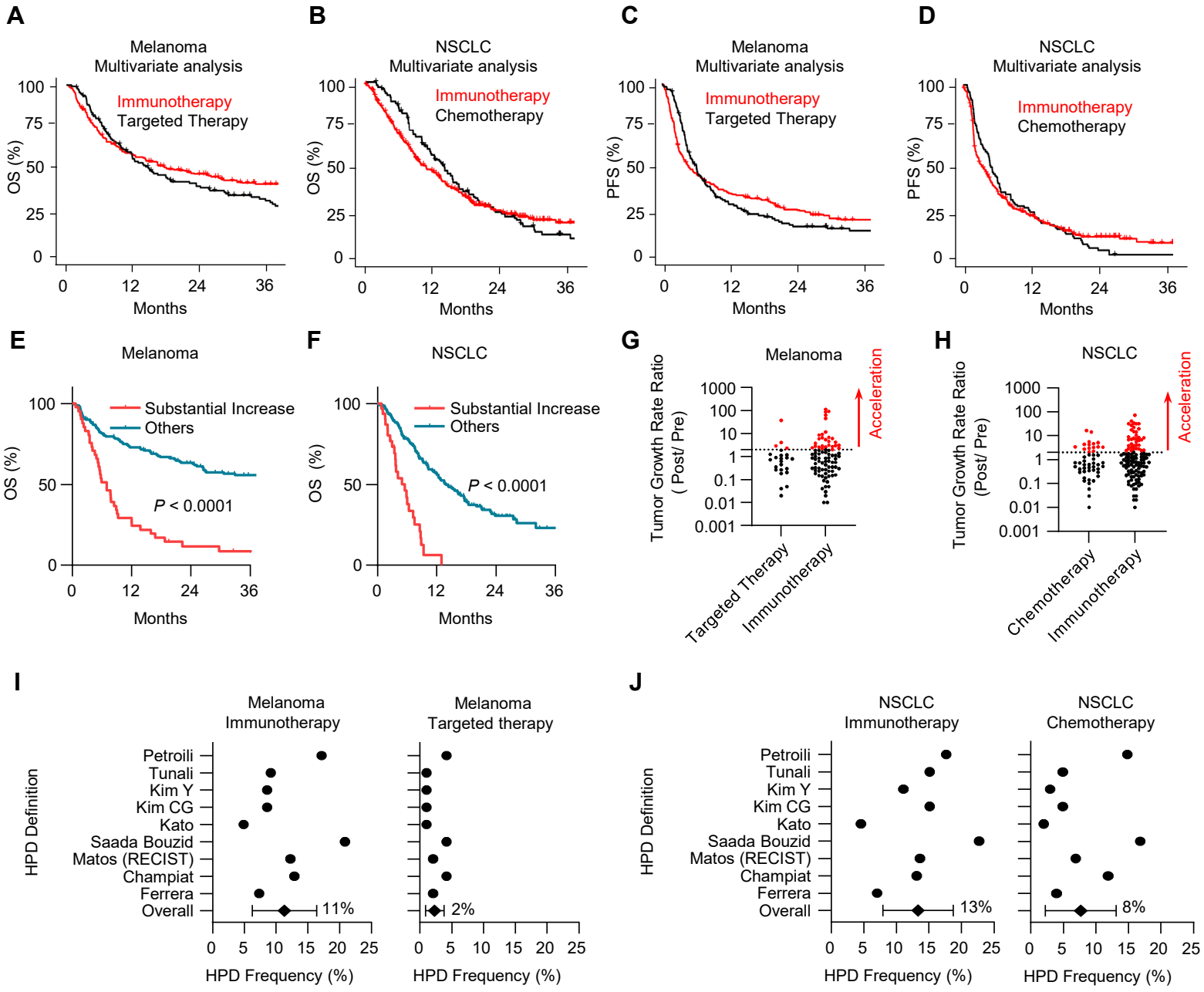
A
Melanoma
Multivariate analysis
Immunotherapy
Targeted Therapy
OS (%)
Months
B
NSCLC
Multivariate analysis
Immunotherapy
Chemotherapy
OS (%)
Months
C
Melanoma
Multivariate analysis
Immunotherapy
Targeted Therapy
PFS (%)
Months
D
NSCLC
Multivariate analysis
Immunotherapy
Chemotherapy
PFS (%)
Months
E
Melanoma
Substantial Increase
Others
P < 0.0001
OS (%)
Months
F
NSCLC
Substantial Increase
Others
P < 0.0001
OS (%)
Months
G
Melanoma
Tumor Growth Rate Ratio
(Post/ Pre)
Acceleration
Targeted Therapy
Immunotherapy
H
NSCLC
Tumor Growth Rate Ratio
(Post/ Pre)
Acceleration
Chemotherapy
Immunotherapy
I
Melanoma
Immunotherapy
Melanoma
Targeted therapy
HPD Definition
Petroili
Tunali
Kim Y
Kim CG
Kato
Saada Bouzid
Matos (RECIST)
Champiat
Ferrera
Overall
11%
2%
HPD Frequency (%)
HPD Frequency (%)
J
NSCLC
Immunotherapy
NSCLC
Chemotherapy
HPD Definition
Petroili
Tunali
Kim Y
Kim CG
Kato
Saada Bouzid
Matos (RECIST)
Champiat
Ferrera
Overall
13%
8%
HPD Frequency (%)
HPD Frequency (%)

K

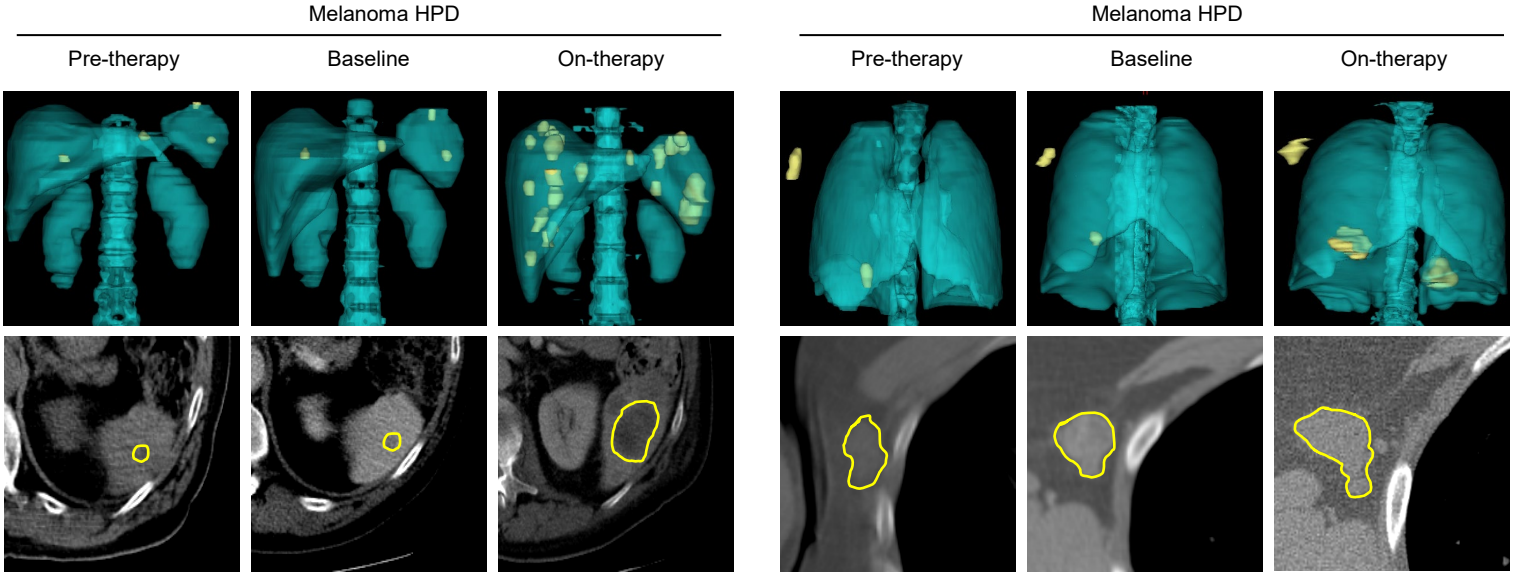
Melanoma HPD
Pre-therapy
Baseline
On-therapy
Melanoma HPD
Pre-therapy
Baseline
On-therapy

L

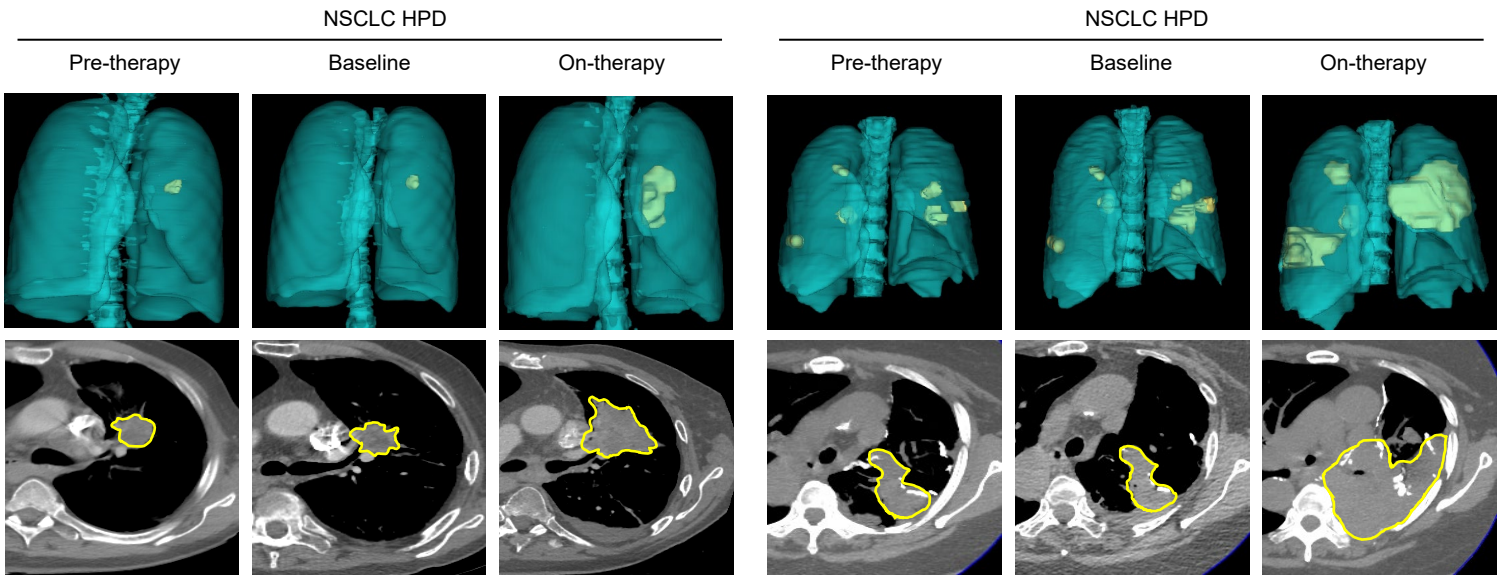
NSCLC HPD
Pre-therapy
Baseline
On-therapy
NSCLC HPD
Pre-therapy
Baseline
On-therapy

M

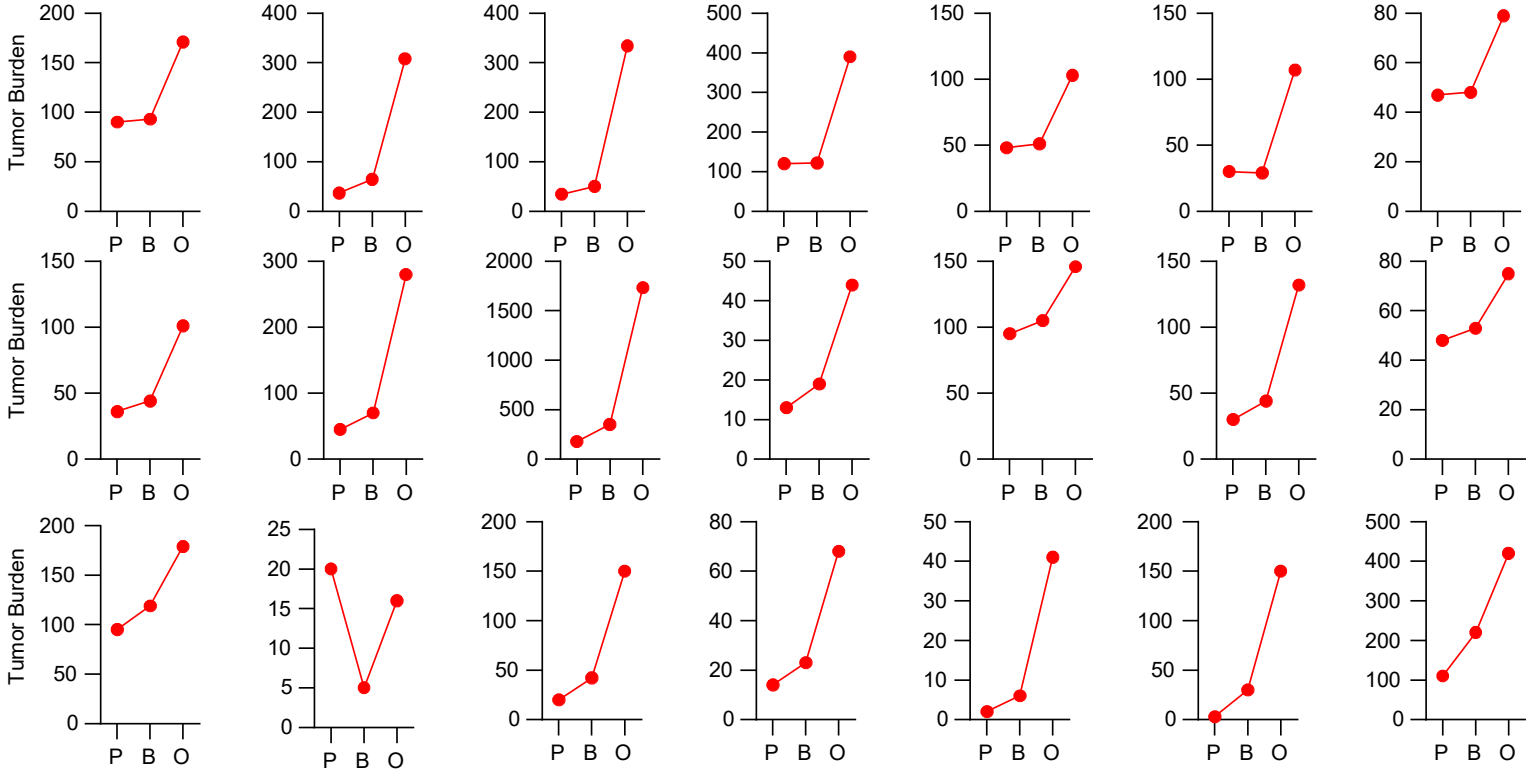

N

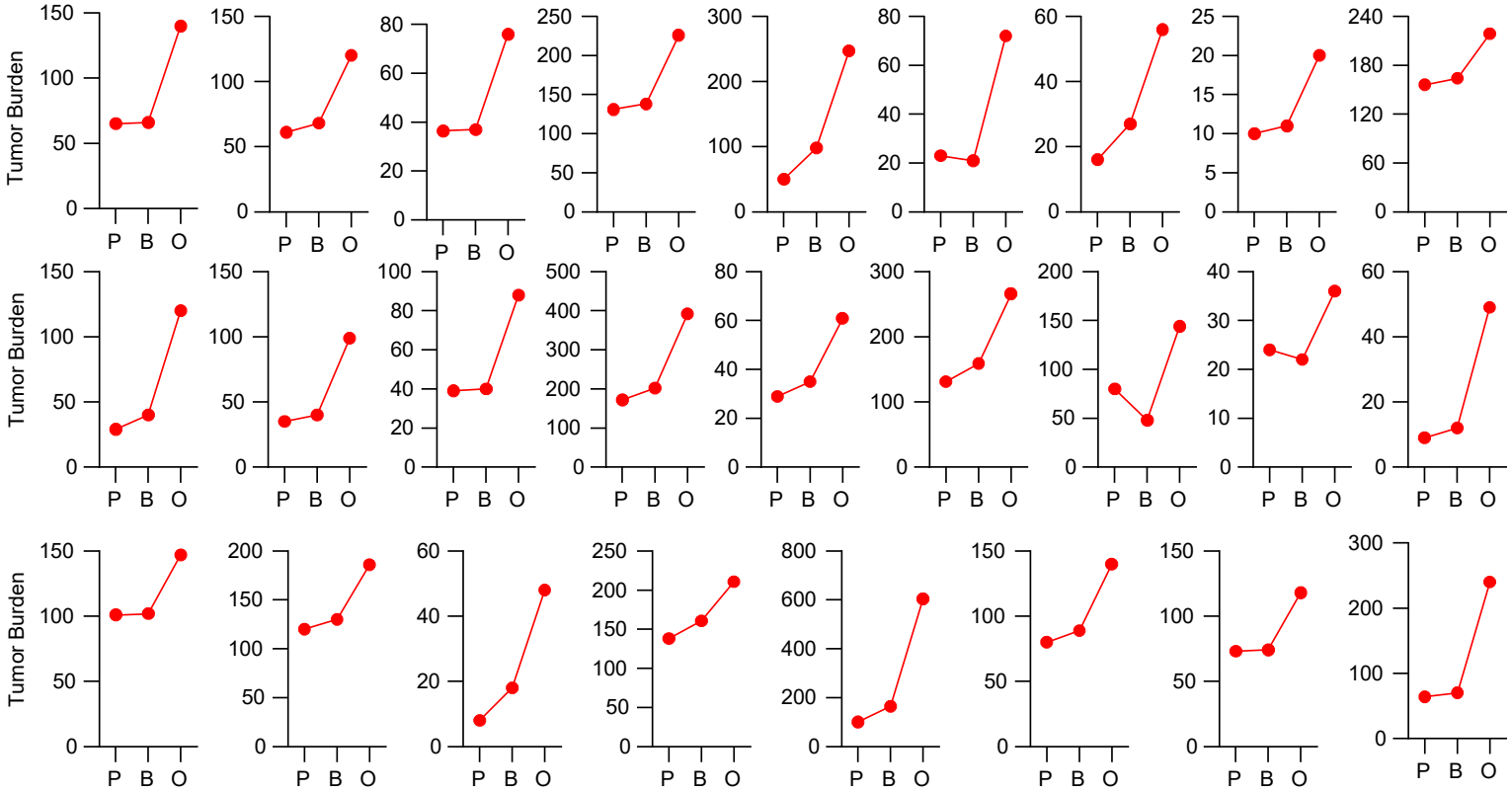

O

Melanoma Immunotherapy Cohort

Subgroup	Number of patients evaluated	HPD Frequency (%) (Mean, SD)	P-value
Age			.46445
≥ median	82		
<median	81		
Performance status			.53041
0	75		
1+	88		
BRAF status			.91376
WT	90		
Mutant	64		
Site of Origin			.18311
Cutaneous	127		
Noncutaneous	36		
Line of therapy			.20807
First line	139		
Second line or higher	24		
ICB Therapy			.10609
Single Agent	116		
Dual Agents	47		

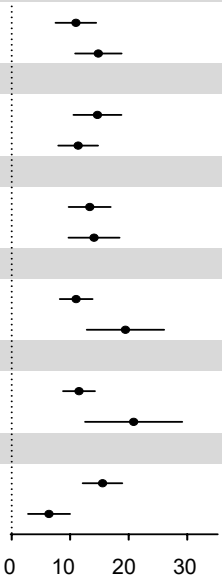

P

NSCLC Immunotherapy Cohort

Subgroup	Number of patients evaluated	HPD Frequency (%) (Mean, SD)	P-value
Age			.38376
< median	100		
≥ median	102		
Performance status			.34836
0-1	158		
2+	44		
Histology			.84312
Adenocarcinoma	135		
Squamous Cell Ca.	52		
Other	15		
Tobacco Use			.28516
Never	33		
Current/Former	169		
Line of therapy			.55734
First line	60		
Second line or higher	142		
Type of therapy			.67080
ICB monotherapy	138		
Chemo + ICB	64		

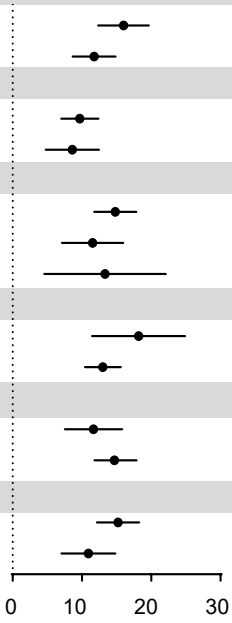

Q

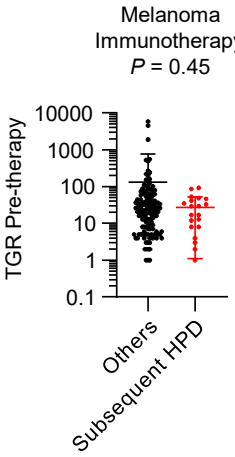

R

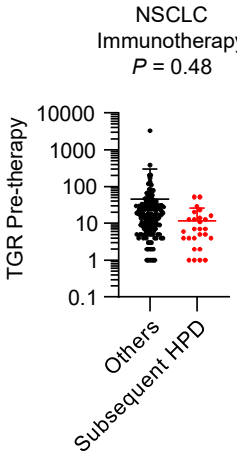

Figure S1: Rapid cancer progression occurs in a subset of patients during immunotherapy. Related to Figure 1.

(A) Multivariable analysis of overall survival (OS) in patients with melanoma (Cohort 1) stratified by type of therapy. RMST at 3 months, HR = 0.900, $P < 0.0001$, Log-rank.

(B) Multivariable analysis of OS in patients with NSCLC (Cohort 2) stratified by type of therapy. RMST at 3 months, HR = 0.942, $P < 0.0001$, Log-rank.

(C) Multivariable analysis of progression-free survival (PFS) in patients with melanoma (Cohort 1) stratified by type of therapy. RMST at 3 months, HR = 0.954, $P = 0.002$, Log-rank.

(D) Multivariable analysis of PFS in patients with NSCLC (Cohort 2) stratified by type of therapy. RMST at 3 months, HR = 0.896, $P = 0.001$, Log-rank.

(E) OS of patients with metastatic melanoma treated with ICB (Cohort 1) stratified by radiographic response, > 50% response n = 41, ≤ 50% response n = 159, Hazard ratio (HR) = 0.1431, $P < 0.0001$ by log-rank test.

(F) OS of patients with metastatic NSCLC treated with ICB (Cohort 2) stratified by stratified by radiographic response, >50% response n = 31; ≤ 50% response n = 181, Hazard ratio (HR) = 0.2678, $P < 0.0001$ by log-rank test.

(G) Tumor growth rate (TGR) of patients with melanoma treated with indicated therapy (Cohort 1). Ratio of TGR following therapy to TGR preceding therapy. Cutoff: More than two-fold increase in TGR (red). targeted therapy n = 96, immunotherapy n = 163. $P = 0.00190$ by Chi squared.

(H) TGR of patients with NSCLC treated with indicated therapy (Cohort 2). Ratio of TGR following therapy to TGR preceding therapy. Cutoff: More than two-fold increase in TGR (red). chemotherapy n = 70, immunotherapy n = 202. $P = 0.04$ by Chi squared.

(I) Frequency of hyperprogression following receipt of immunotherapy (left) or targeted therapy (right) in melanoma patients using indicated criteria from different researchers. paired t test, $P = 0.001$. Data are shown as mean ± s.d.; immunotherapy n = 198, targeted therapy n = 68. Utilizing Champiat et al. definition for HPD: immunotherapy HPD n = 25; targeted therapy n = 4.

(J) Frequency of hyperprogression following receipt of immunotherapy (left) or chemotherapy (right) in NSCLC patients using indicated criteria from different researchers. paired t-test, $P = 0.0001$. Data are shown as mean ± s.d.; immunotherapy n = 161, chemotherapy n = 96. Utilizing Champiat et al. definition for HPD: immunotherapy HPD n = 21; chemotherapy HPD n = 11.

(K-L) Representative cross-sectional and 3D reconstructed computed tomography (CT) images of two patients with metastatic melanoma (**K**) or NSCLC (**L**) with HPD preceding receipt of immunotherapy (left), at baseline preceding immunotherapy (middle), and at first reassessment following immunotherapy (right).

(M-N) Longitudinal tumor burden of individual melanoma (**M**) or NSCLC (**N**) patients with HPD. P, Pre-therapy; B, baseline; O, On-therapy.

(O-P) Proportion of melanoma (**O**) and NSCLC (**P**) patients with hyperprogression stratified by indicated clinicopathologic variables. Chi-squared. Data are shown as mean ± s.d.

(Q-R) Tumor growth rate (TGR) from the period of preceding therapy initiation in patients with melanoma treated with immunotherapy (**Q**) and NSCLC treated with immunotherapy (**R**). Horizontal lines indicate quartiles. Two-tailed t-test.

Table S4: Clinical characteristics of patients with comprehensive sequencing (Cohort 3), Related to Figure 2.

	Total Cohort
Number of Patients	50
Average Age	60.6
Gender	
Male	24 (48%)
Female	26 (52%)
ECOG Performance Status	
0-1	42 (84%)
2+	8 (16%)
Stage at Therapy	
IV	50 (100%)
Tumor Histology	
Melanoma	13 (26%)
NSCLC	5 (10%)
Urothelial Carcinoma	16 (32%)
Sarcoma	7 (14%)
Breast	5 (10%)
Lymphoma	4 (8%)
Therapy	
Atezolizumab	5 (10%)
Ipilimumab	2 (4%)
Nivolumab	8 (16%)
Pembrolizumab	32 (64%)
Combination	3 (6%)

Abbreviations:
ECOG- Eastern Cooperative Oncology Group

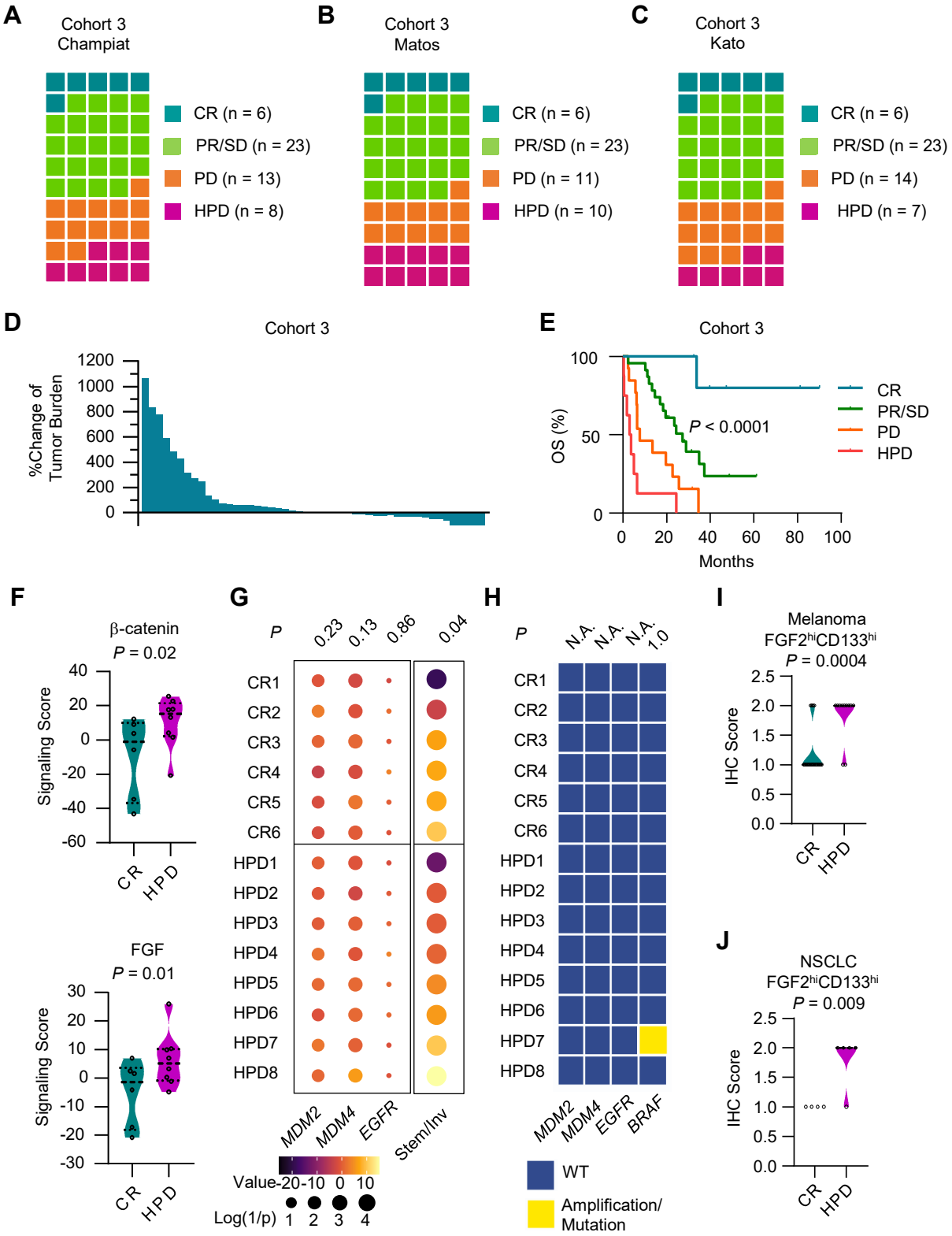
A
Cohort 3
Champiat
CR (n = 6)
PR/SD (n = 23)
PD (n = 13)
HPD (n = 8)
B
Cohort 3
Matos
CR (n = 6)
PR/SD (n = 23)
PD (n = 11)
HPD (n = 10)
C
Cohort 3
Kato
CR (n = 6)
PR/SD (n = 23)
PD (n = 14)
HPD (n = 7)
D
Cohort 3
%Change of Tumor Burden
1200
1000
800
600
400
200
0
E
Cohort 3
OS (%)
100
50
0
P < 0.0001
0
20
40
60
80
100
Months
CR
PR/SD
PD
HPD
F
β-catenin
P = 0.02
Signaling Score
40
20
0
-20
-40
-60
CR
HPD
FGF
P = 0.01
Signaling Score
30
20
10
0
-10
-20
-30
CR
HPD
G
P
0.23
0.13
0.86
0.04
CR1
CR2
CR3
CR4
CR5
CR6
HPD1
HPD2
HPD3
HPD4
HPD5
HPD6
HPD7
HPD8
MDM2
MDM4
EGFR
Stem/Inv
Value -20 -10 0 10
Log(1/p) 1 2 3 4
H
P
N.A.
N.A.
N.A.
1.0
CR1
CR2
CR3
CR4
CR5
CR6
HPD1
HPD2
HPD3
HPD4
HPD5
HPD6
HPD7
HPD8
MDM2
MDM4
EGFR
BRAF
WT
Amplification/ Mutation
I
Melanoma
FGF2hiCD133hi
P = 0.0004
IHC Score
2.5
2.0
1.5
1.0
0.5
0.0
CR
HPD
J
NSCLC
FGF2hiCD133hi
P = 0.009
IHC Score
2.5
2.0
1.5
1.0
0.5
0.0
CR
HPD

Figure S2: Immunogenic and oncogenic pathways correlate in patients with HPD. Related to Figure 2.

(A-C) Best radiographic responses in Cohort 3 based on indicated definitions depicted in a tile diagram. 1 tile represents 1 patient. CR, complete response; PR/SD, partial response/stable disease; PD, progressive disease; HPD, hyperprogressive disease. HPD definition criteria were based on the reports by Drs. Champiat, Matos, or Kato.

(D) Waterfall plot showing change of tumoral burden from initiation of therapy to first surveillance imaging (Cohort 3), Data are shown as percentage change. n = 50.

(E) Overall survival in metastatic patients in Cohort 3 stratified by best radiographic response. HPD definition criteria were based on the report by Dr. Champiat. Log-rank test.

(F) Violin plots displaying β-catenin and FGF signaling scores in Cohort 3 patients stratified by response to immunotherapy. CR n = 6, HPD n = 8. P-values were generated from multivariate mixed effect linear models controlling for biopsy site (fixed effect) and disease type (random effect).

(G) Heat map showing expression levels for *MDM2*, *MDM4*, *EGFR* and stemness and invasiveness gene signature in HPD and CR patients. P-values were generated from multivariate mixed effect linear models controlling for biopsy site (fixed effect) and disease type (random effect).

(H) Tile diagram showed the genetic amplification or mutation of the indicated genes in Cohort 3 patients. Fisher's exact test.

(I-J) IHC scores of $FGF2^{hi}CD133^{hi}$ tumor cells in melanoma (**I**) or NSCLC (**J**) patients with CR or HPD. Chi-square test.

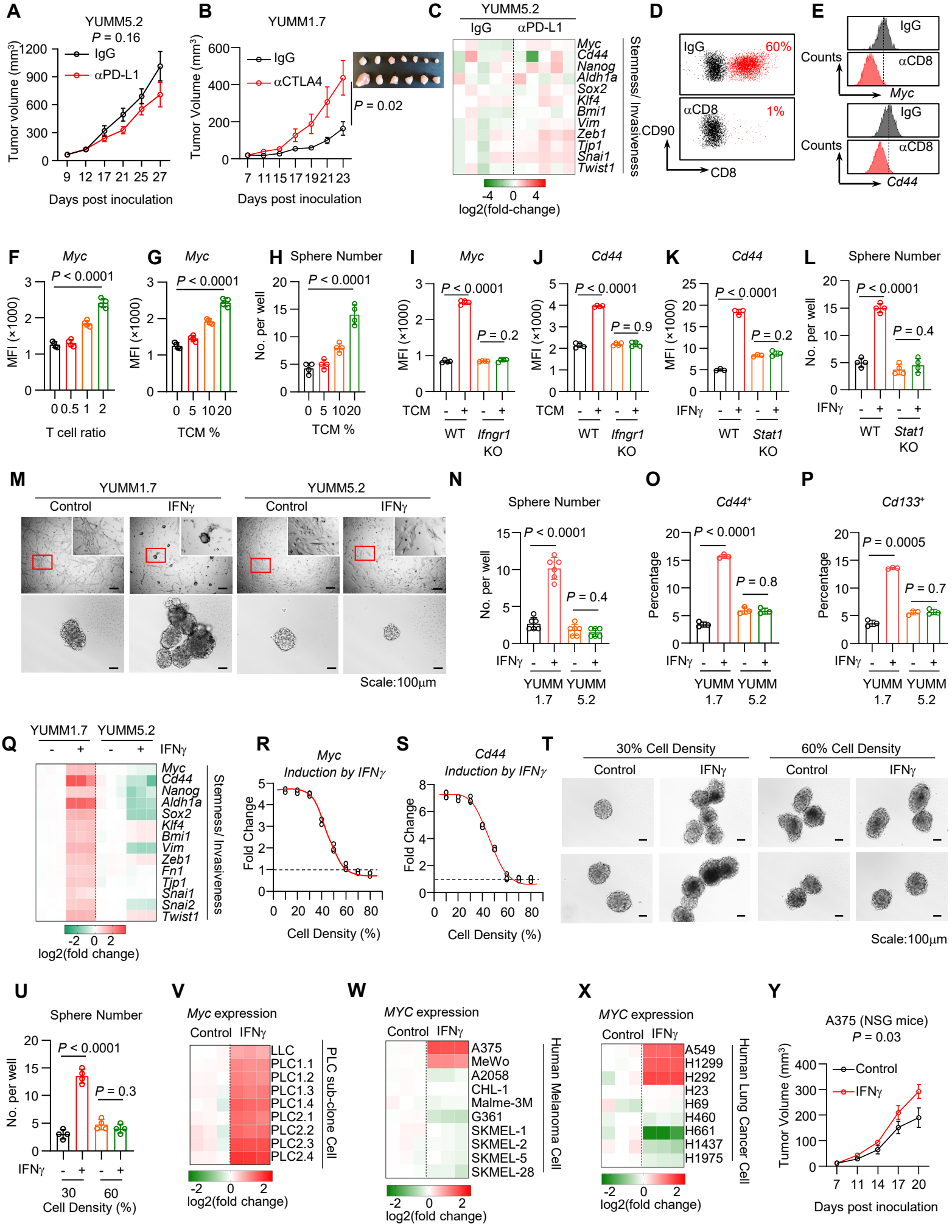
A
YUMM5.2
P = 0.16
IgG
αPD-L1
Tumor volume (mm3)
Days post inoculation
B
YUMM1.7
IgG
αCTLA4
P = 0.02
Tumor Volume (mm3)
Days post inoculation
C
YUMM5.2
IgG
αPD-L1
Myc
Cd44
Nanog
Aldh1a
Sox2
Klf4
Bmi1
Vim
Zeb1
Tjp1
Snai1
Twist1
Stemness/ Invasiveness
log2(fold-change)
D
IgG
60%
αCD8
1%
CD90
CD8
E
IgG
αCD8
Counts
Myc
Cd44
F
Myc
P < 0.0001
MFI (×1000)
T cell ratio
G
Myc
P < 0.0001
MFI (×1000)
TCM %
H
Sphere Number
P < 0.0001
No. per well
TCM %
I
Myc
P < 0.0001
P = 0.2
MFI (×1000)
TCM
WT
Ifngr1 KO
J
Cd44
P < 0.0001
P = 0.9
MFI (×1000)
TCM
WT
Ifngr1 KO
K
Cd44
P < 0.0001
P = 0.2
MFI (×1000)
IFNγ
WT
Stat1 KO
L
Sphere Number
P < 0.0001
P = 0.4
No. per well
IFNγ
WT
Stat1 KO
M
YUMM1.7
YUMM5.2
Control
IFNγ
Scale:100μm
N
Sphere Number
P < 0.0001
P = 0.4
No. per well
IFNγ
YUMM 1.7
YUMM 5.2
O
Cd44+
P < 0.0001
P = 0.8
Percentage
IFNγ
YUMM 1.7
YUMM 5.2
P
Cd133+
P = 0.0005
P = 0.7
Percentage
IFNγ
YUMM 1.7
YUMM 5.2
Q
YUMM1.7
YUMM5.2
IFNγ
Myc
Cd44
Nanog
Aldh1a
Sox2
Klf4
Bmi1
Vim
Zeb1
Fn1
Tjp1
Snai1
Snai2
Twist1
Stemness/ Invasiveness
log2(fold change)
R
Myc
Induction by IFNγ
Fold Change
Cell Density (%)
S
Cd44
Induction by IFNγ
Fold Change
Cell Density (%)
T
30% Cell Density
60% Cell Density
Control
IFNγ
Scale:100μm
U
Sphere Number
P < 0.0001
P = 0.3
No. per well
IFNγ
30
60
Cell Density (%)
V
Myc expression
Control
IFNγ
LLC
PLC1.1
PLC1.2
PLC1.3
PLC1.4
PLC2.1
PLC2.2
PLC2.3
PLC2.4
PLC sub-clone Cell
log2(fold change)
W
MYC expression
Control
IFNγ
A375
MeWo
A2058
CHL-1
Malme-3M
G361
SKMEL-1
SKMEL-2
SKMEL-5
SKMEL-28
Human Melanoma Cell
log2(fold change)
X
MYC expression
Control
IFNγ
A549
H1299
H292
H23
H69
H460
H661
H1437
H1975
Human Lung Cancer Cell
log2(fold change)
Y
A375 (NSG mice)
P = 0.03
Control
IFNγ
Tumor Volume (mm3)
Days post inoculation

Figure S3: $CD8^+$ T cells drive cancer hyperprogression via IFNγ. Related to Figure 3.

(A) YUMM5.2 tumor bearing C57BL/6 mice were treated with control (IgG) or PD-L1 antibody. Tumor growth curves were plotted. Data are shown as mean ± s.d., n = 7 (IgG) or 5 (αPD-L1). Two-tailed t-test.

(B) YUMM1.7 tumor bearing C57BL/6 mice were treated with control (IgG) or CTLA4 antibody. Tumor growth curves were plotted. Data are shown as mean ± s.d., n = 7 (IgG) or 6 (αCTLA4). Two-tailed t-test.

(C) YUMM5.2 tumor bearing C57BL/6 mice were treated with control (IgG) or PD-L1 antibody. On 16^{th} day after tumor inoculation, the indicated gene expression in tumors was determined by qPCR. n = 5 tumors.

(D-E) YUMM1.7 tumor bearing C57BL/6 mice were treated with control (IgG) or CD8 antibody. Tumor infiltrating $CD8^+$ T cells (**D**) and *Myc* (upper) or *Cd44* (lower) expression in $CD45^-$negative tumor cells (**E**) were determined by FACS.

(F-G) YUMM1.7 cells were cultured with indicated ratio of T cells (**F**) or proportion of T cell conditioned medium (TCM) (**G**) for 48 hours. *Myc* expression (MFI) was determined by FACS analysis in $CD45^-CD90^-$ tumor cells. Data are shown as mean ± s.d., n = 4. One-way ANOVA test.

(H) YUMM1.7 cells were cultured with indicated proportion of T cell conditioned medium (TCM) for 48 hours and transferred into 3D-sphere cultures. Tumor spheres were recorded 7 days after 3D-sphere culture. Data are shown as mean ± s.d., n = 4. One-way ANOVA test.

(I-J) WT or *Ifngr1* KO YUMM1.7 cells were cultured with 20% TCM for 48 hours. Tumor intracellular *Myc* (**I**) and surface *Cd44* (**J**) expression was determined by FACS. Data are shown as mean ± s.d., n = 4. Two-tailed t-test.

(K-L) WT or *Stat1* KO YUMM1.7 cells were treated with IFNγ. Surface expression of *Cd44* was determined by FACS 48 hours after treatment (**K**). Tumor spheres were counted on day 7 after 3D-sphere culture (**L**). Data are mean ± s.d., n = 3 (**K**), n = 4 (**L**). Two-tailed t-test.

(M-N) YUMM1.7 and YUMM5.2 cells were treated with IFNγ. Tumor cell morphology in 2D cell culture (upper) or 3D cell culture (lower) was captured after 48 hours treatment (**M**). Tumor spheres were quantified on day 7. Data are shown as mean ± s.d., n = 6. Two-tailed t-test (**N**).

(O-P) YUMM1.7 and YUMM5.2 cells were treated with IFNγ for 48 hours, surface expression of *Cd44* (**O**) or *Cd133* (**P**) were determined by FACS. Data are shown as mean ± s.d., n = 3. Two-tailed t-test.

(Q) YUMM1.7 and YUMM5.2 cells were treated with IFNγ for 48 hours. The indicated gene expression was determined by qPCR. n = 3.

(R-S) Confluent YUMM1.7 cells were trypsinized, counted, seeded at indicated density, and treated with IFNγ for 36 hours. RNA levels of *Myc* (**R**) and *Cd44* (**S**) were determined by qPCR. n =3.

(T-U) YUMM1.7 cells were seeded at 30% or 60% density and treated with IFNγ for 48 hours, followed by 3D-sphere culture. Tumor spheres representative images (**T**) or quantitation (**U**) at day 7 are shown. Data are mean ± s.d., n = 4, Two-tailed t-test.

(V) LLC or PLC cells were treated with IFNγ for 24 hours. *Myc* expression was determined by real-time qRT-PCR. Data are shown as mean ± s.d., n = 3. P value by two-tailed t-test.

(W-X) Human melanoma cell lines (**W**) and human lung cancer cell lines (**X**) were treated with IFNγ for 48 hours. *MYC* expression was determined by qPCR. n = 3.

(Y) A375 tumor-bearing NSG mice were treated with recombinant human IFNγ. Tumor growth curves were plotted. n = 5 (control). n = 6 (IFNγ). Data are shown as mean ± s.d., n = 5. Two-tailed t-test.

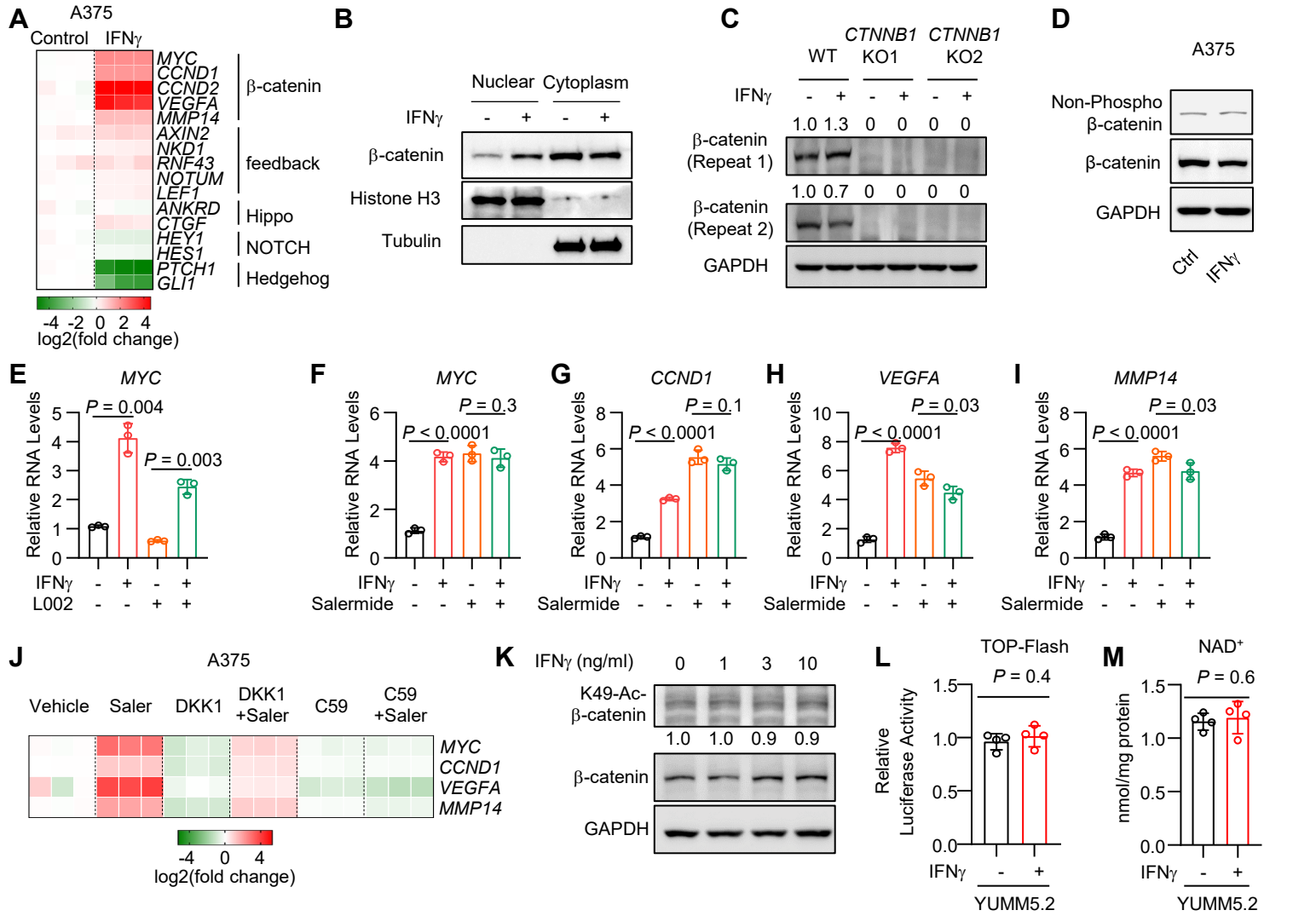

Figure S4: IFNγ reduces NAD⁺ to activate β-catenin acetylation. Related to Figure 4.

(A-B) A375 cells were treated with IFNγ for 36 hours. Indicated transcripts were determined by qRT-PCR. n = 3 (**A**). Indicated proteins were determined in the nuclear or cytoplasmic fractions, respectively. 1 of 2 blots shown (**B**).

(C) Wild type (WT) and *CTNNB1* KO A375 cells were treated with IFNγ for 24 hours. Protein levels of β-catenin (2 repeats) and GAPDH were determined by Western blotting. 1 of 2 Western blots shown.

(D) A375 cells were treated with IFNγ for 24 hours, total or non-phosphorylated β-catenin proteins were determined by Western blot. 1 of 2 Western blots shown.

(E-I). A375 cells were treated with IFNγ, in the presence of L002 (**E**) and Salermide (**F-I**), for 24 hours. β-catenin signaling gene transcripts were determined by qRT-PCR. Data are shown as mean ± s.d., n = 3. Two-tailed t-test.

(J) A375 cells were treated with Salermide (Saler) and DKK1 or Wnt-C59 (C59) for 24 hours. The indicated gene expression was determined by qPCR. n = 3.

(K) A375 cells were treated with IFNγ for 24 hours. Acetylated-β-catenin (K49) was determined by Western blotting. Quantification is indicated. 1 of 3 Western blots shown.

(L) TOP-Flash carrying YUMM5.2 cells were treated with IFNγ for 48 hours. Relative luciferase activity was determined. Data are shown as mean ± s.d., n = 4. Two-tailed t-test.

(M) YUMM5.2 cells were treated with IFNγ for 24 hours. Intracellular NAD⁺ levels were determined by kit. Data are shown as mean ± s.d., n = 4. Two-tailed t-test.

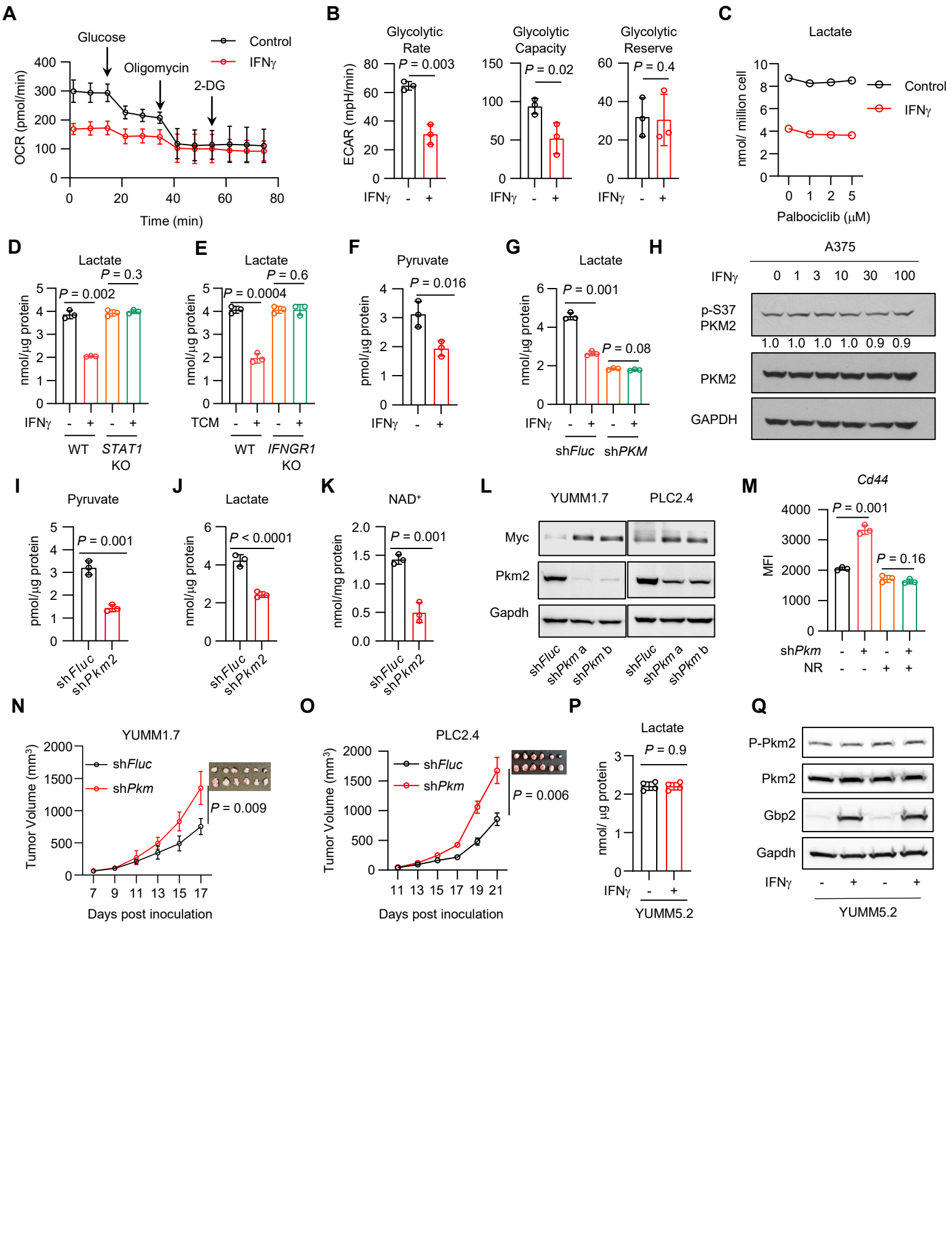
A
Glucose
Oligomycin
2-DG
Control
IFNγ
OCR (pmol/min)
Time (min)
B
Glycolytic Rate
Glycolytic Capacity
Glycolytic Reserve
ECAR (mpH/min)
P = 0.003
P = 0.02
P = 0.4
IFNγ
C
Lactate
nmol/ million cell
Palbociclib (μM)
D
Lactate
P = 0.3
P = 0.002
nmol/μg protein
WT
STAT1 KO
E
Lactate
P = 0.6
P = 0.0004
TCM
IFNGR1 KO
F
Pyruvate
P = 0.016
pmol/μg protein
G
Lactate
P = 0.001
P = 0.08
shFluc
shPKM
H
A375
p-S37 PKM2
PKM2
GAPDH
1.0 1.0 1.0 1.0 0.9 0.9
I
Pyruvate
P = 0.001
shFluc
shPkm2
J
Lactate
P < 0.0001
K
NAD+
P = 0.001
nmol/mg protein
L
YUMM1.7
PLC2.4
Myc
Pkm2
Gapdh
shPkm a
shPkm b
M
Cd44
P = 0.001
P = 0.16
MFI
shPkm
NR
N
YUMM1.7
shFluc
shPkm
P = 0.009
Tumor Volume (mm3)
Days post inoculation
O
PLC2.4
P = 0.006
P
Lactate
P = 0.9
YUMM5.2
Q
P-Pkm2
Pkm2
Gbp2
Gapdh
YUMM5.2

Figure S5: IFNγ regulates PKM2 phosphorylation to alter NAD^+/ β-catenin signaling. Related to Figure 5.

(A) A375 cells were treated with IFNγ for 24 hours. Seahorse analysis showing the oxygen consumption rate (OCR) in control cells and IFNγ-treated cells in the presence of glucose, oligomycin or 2-DG. Data are shown as mean ± s.d., n = 3.

(B) Seahorse analysis showing glycolytic rate, glycolytic capacity, and glycolytic reserve in control cells or IFNγ-treated A375 cells. Data are shown as mean ± s.d., n = 3, P value by two-tailed t-test.

(C) A375 cells were treated with IFNγ and Palbociclib for 24 hours. Lactate production was determined and normalized with cell numbers. n = 3.

(D) WT or *STAT1* A375 KO cells were treated with IFNγ for 48 hours. Lactate production was determined by quantitation kit. Data are shown as mean ± s.d., n = 3, P value by two-tailed t-test.

(E) WT or *IFNGR1* KO A375 cells were treated with T cell conditioned medium (TCM) for 48 hours. Lactate production quantified by kit. Data are shown as mean ± s.d., n = 3. Two-tailed t-test.

(F) Pyruvate levels were detected in A375 cells treated with medium or IFNγ. Data are shown as mean ± s.d., n = 3. Two-tailed t-test.

(G) Control (sh*Fluc*) or *PKM2* knock down (sh*PKM2*) A375 cells were treated with IFNγ for 24 hours. Lactate production quantified by kit. Data are shown as mean ± s.d., n = 3. Two-tailed t-test.

(H) A375 cells were treated with IFNγ. Phosphorylated (S37) and total protein levels of PKM2 were detected by Western blot. Quantification is indicated. 1 of 2 Western blots shown.

(I-K) Pyruvate (**I**), Lactate (**J**), and NAD^+ (**K**) levels in YUMM1.7 sh*Fluc* and sh*Pkm2* cells were quantified by kits. Data are shown as mean ± s.d., n = 3. Two-tailed t-test.

(L) Myc and Pkm2 proteins were detected by Western blot in sh*Fluc* and sh*Pkm2* YUMM1.7 cells, and PLC2.4 cells. 1 of 2 Western blots shown.

(M) sh*Fluc* or sh*Pkm2* YUMM1.7 cells were treated with nicotinamide riboside (NR) for 48 hours. Surface expression of *Cd44* was determined by FACS. Data are shown as mean ± s.d., n = 3. Two-tailed t-test.

(N-O) Tumor growth curves for sh*Fluc* and sh*Pkm2* YUMM1.7 (**N**) or PLC2.4 (**O**) cells. Data are shown as mean ± s.d., n = 6. Two-tailed t-test.

(P-Q) YUMM5.2 cells were treated with IFNγ for 24 hours. Lactate production (**P**) and Pkm2 phosphorylation (**Q**) was determined by kit and Western blot, respectively. IFNγ-responsive Gbp2 protein was utilized as a positive control. Data are shown as mean ± s.d., n = 4. Two-tailed t-test.

Table S5: FGF/ FGFR family members expression upon IFNγ treatment (RNAseq datasets from GSE99299), Related to Figure 6.

	A375 (RPKM)					B16 (RPKM)			
GENE ID	Ctrl		IFNγ		Gene ID	Ctrl		IFNγ	
FGF1	16	13	22	23	Fgf1	32	42	24	25
FGF2	418	370	1170	1171	Fgf2	0	0	1	0
FGF3	0	0	0	0	Fgf3	0	0	0	0
FGF4	0	0	0	0	Fgf4	0	0	0	0
FGF5	95	110	38	38	Fgf5	0	0	0	0
FGF6	0	0	0	0	Fgf6	0	0	0	0
FGF7	3	0	0	0	Fgf7	2	2	3	4
FGF8	0	0	0	0	Fgf8	3	1	0	0
FGF9	0	0	1	0	Fgf9	2	0	1	0
FGF10	0	0	0	0	Fgf10	0	0	0	0
FGF11	12	24	15	22	Fgf11	0	0	0	0
FGF12	36	40	37	30	Fgf12	0	0	0	0
FGF13	73	74	76	40	Fgf13	0	0	0	0
FGF14	0	1	0	1	Fgf14	0	0	0	0
FGF16	0	0	0	0	Fgf15	0	0	0	0
FGF17	0	0	0	0	Fgf16	0	0	0	0
FGF18	1	1	2	1	Fgf17	0	0	0	0
FGF19	2	2	1	2	Fgf18	0	1	0	1
FGF20	1	2	1	1	Fgf20	0	0	0	0
FGF21	3	1	9	3	Fgf21	0	0	0	0
FGF22	1	0	1	1	Fgf22	0	0	0	0
FGF23	0	0	0	0	Fgf23	0	0	0	0
FGFR1	381	462	415	413	Fgfr1	3	0	0	0
FGFR2	4	1	2	0	Fgfr2	0	3	0	1
FGFR3	25	22	9	9	Fgfr3	24	37	31	37
FGFR4	49	63	24	22	Fgfr4	0	1	0	0

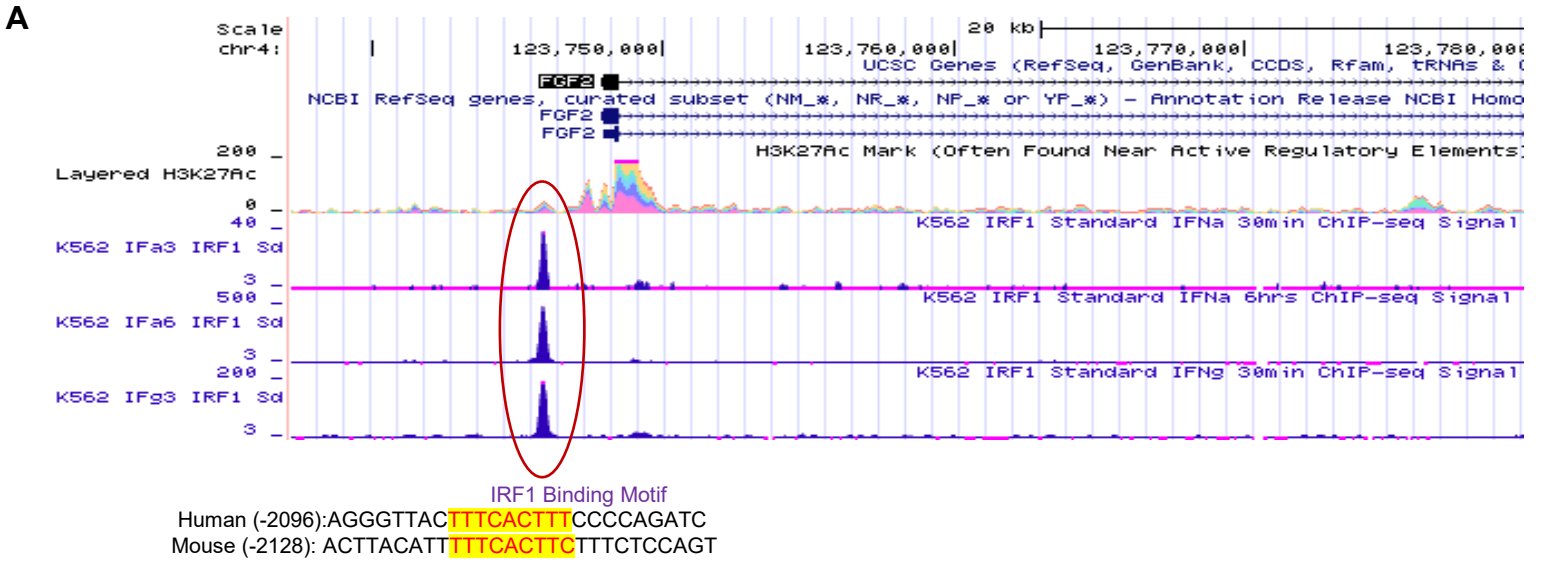
A
Scale
chr4:
123,750,000
123,760,000
123,770,000
20 kb
UCSC Genes (RefSeq, GenBank, CCDS, Rfam, tRNAs &
FGF2
NCBI RefSeq genes, curated subset (NM_*, NR_*, NP_* or YP_*) - Annotation Release NCBI Homo
FGF2
FGF2
H3K27Ac Mark (Often Found Near Active Regulatory Elements)
200
Layered H3K27Ac
0
40
K562 IFa3 IRF1 Sd
K562 IRF1 Standard IFNa 30min ChIP-seq Signal
3
500
K562 IFa6 IRF1 Sd
K562 IRF1 Standard IFNa 6hrs ChIP-seq Signal
3
200
K562 IFg3 IRF1 Sd
K562 IRF1 Standard IFNg 30min ChIP-seq Signal
3
IRF1 Binding Motif
Human (-2096):AGGGTTACTTTCACTTTCCCCAGATC
Mouse (-2128): ACTTACATTTTTCACTTCTTTCTCCAGT

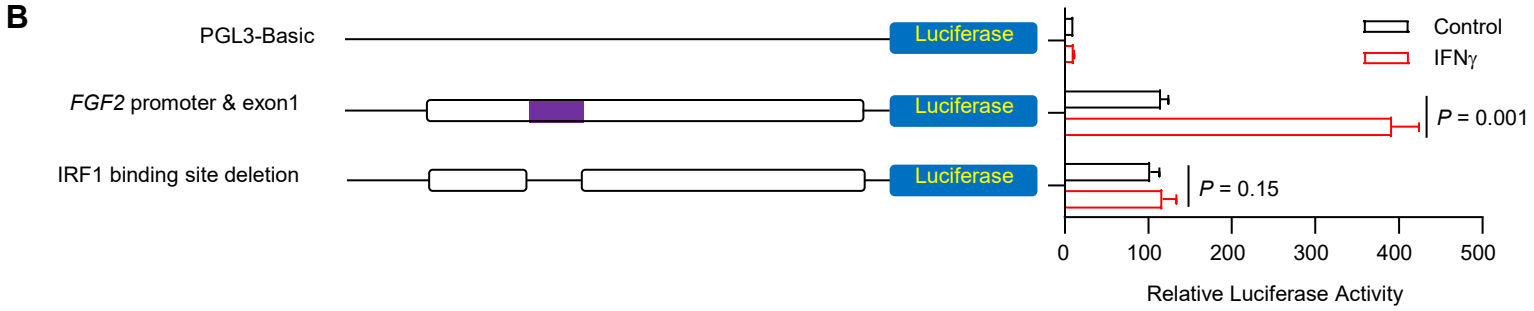
B
PGL3-Basic
Luciferase
FGF2 promoter & exon1
Luciferase
IRF1 binding site deletion
Luciferase
Control
IFNγ
P = 0.001
P = 0.15
0
100
200
300
400
500
Relative Luciferase Activity

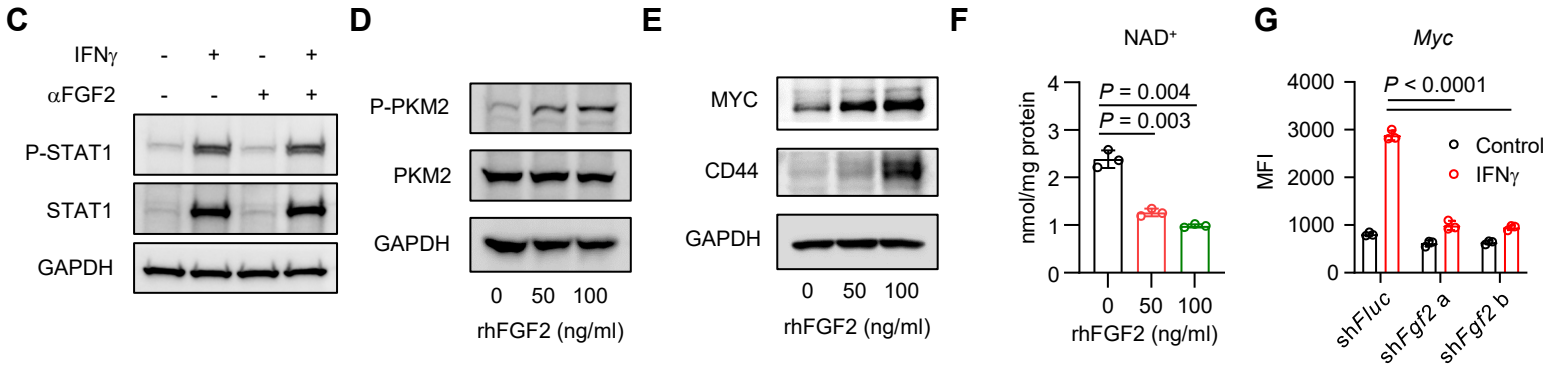
C
IFNγ - + - +
αFGF2 - - + +
P-STAT1
STAT1
GAPDH
D
P-PKM2
PKM2
GAPDH
0 50 100
rhFGF2 (ng/ml)
E
MYC
CD44
GAPDH
0 50 100
rhFGF2 (ng/ml)
F
NAD+
P = 0.004
P = 0.003
nmol/mg protein
0 50 100
rhFGF2 (ng/ml)
G
Myc
P < 0.0001
MFI
Control
IFNγ
shFluc
shFgf2 a
shFgf2 b

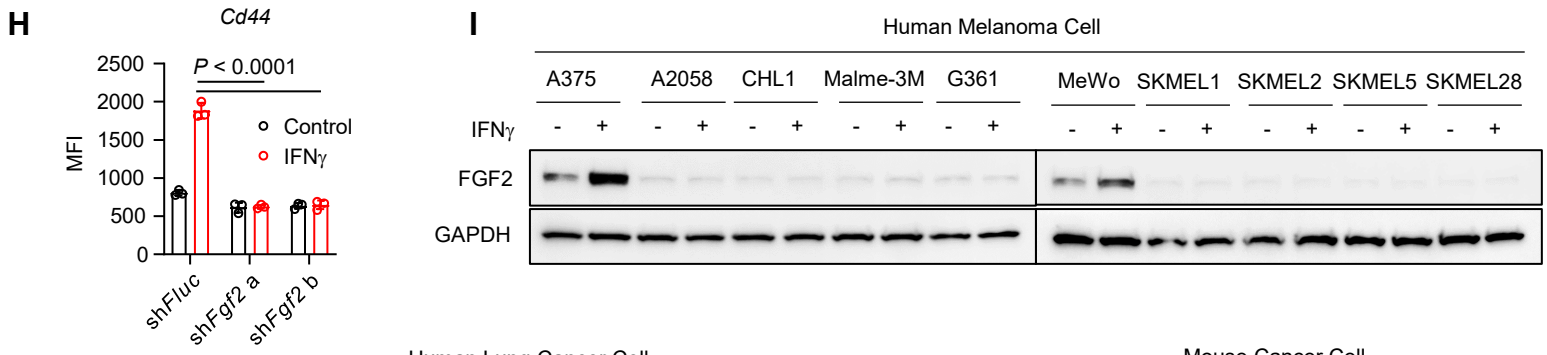
H
Cd44
P < 0.0001
MFI
Control
IFNγ
shFluc
shFgf2 a
shFgf2 b
I
Human Melanoma Cell
A375
A2058
CHL1
Malme-3M
G361
MeWo
SKMEL1
SKMEL2
SKMEL5
SKMEL28
IFNγ
FGF2
GAPDH

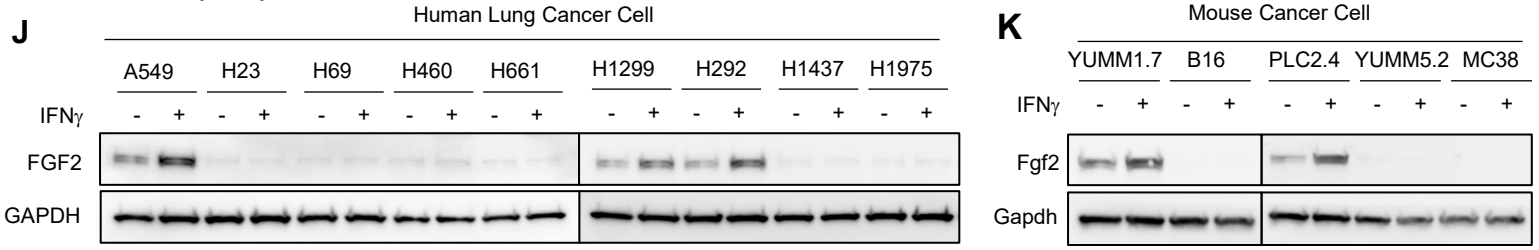
J
Human Lung Cancer Cell
A549
H23
H69
H460
H661
H1299
H292
H1437
H1975
IFNγ
FGF2
GAPDH
K
Mouse Cancer Cell
YUMM1.7
B16
PLC2.4
YUMM5.2
MC38
IFNγ
Fgf2
Gapdh

Figure S6: IFNγ induces FGF2 to control PKM2/ NAD^+/ β-catenin signaling. Related to Figure 6.

(A) IRF1 ChIP-seq datasets in K562 cells were obtained from Encode at UCSC. IRF1 binding motif was found in the *FGF2* promoter in human and mouse.

(B) *FGF2* promoter and exon1 were inserted into PGL3-basic plasmid to generate a *FGF2* promoter reporter. IRF1 binding motif was deleted to generate a mutant reporter. A375 cells carrying *FGF2* promoter reporter or mutant reporter were treated with IFNγ for 24 hours. Luciferase activity was determined by dual luciferase activity assay. Data are shown as mean ± s.d., n = 3. Two-tailed t-test.

(C) A375 cells were treated with IFNγ, in the presence or absence of FGF2 neutralizing antibody (αFGF2). Phosphorylated (Y701) and total protein levels of STAT1 were determined at 24 hours by Western blot.

(D-F) A375 cells were treated with recombinant human FGF2. Phosphorylated PKM2 (**D**), MYC, and CD44 (**E**) were determined by Western blotting. 1 of 2 Western blots shown (**D, E**). NAD^+ levels were quantified by kit (**F**). Data are shown as mean ± s.d., n = 3. Two-tailed t-test (**F**).

(G-H) sh*Fluc* or sh*Fgf2* YUMM1.7 cells were treated with IFNγ for 48 hours. *Myc* (**G**) *or Cd44* (**H**) expression were determined by FACS. Data are shown as mean ± s.d., n = 3. Two-tailed t-test.

(I-K) Human melanoma cells (**I**), human lung cancer cells (**J**), and mouse cancer cells (**K**) were treated with IFNγ for 24 hours. FGF2 protein expression was determined by Western blot.

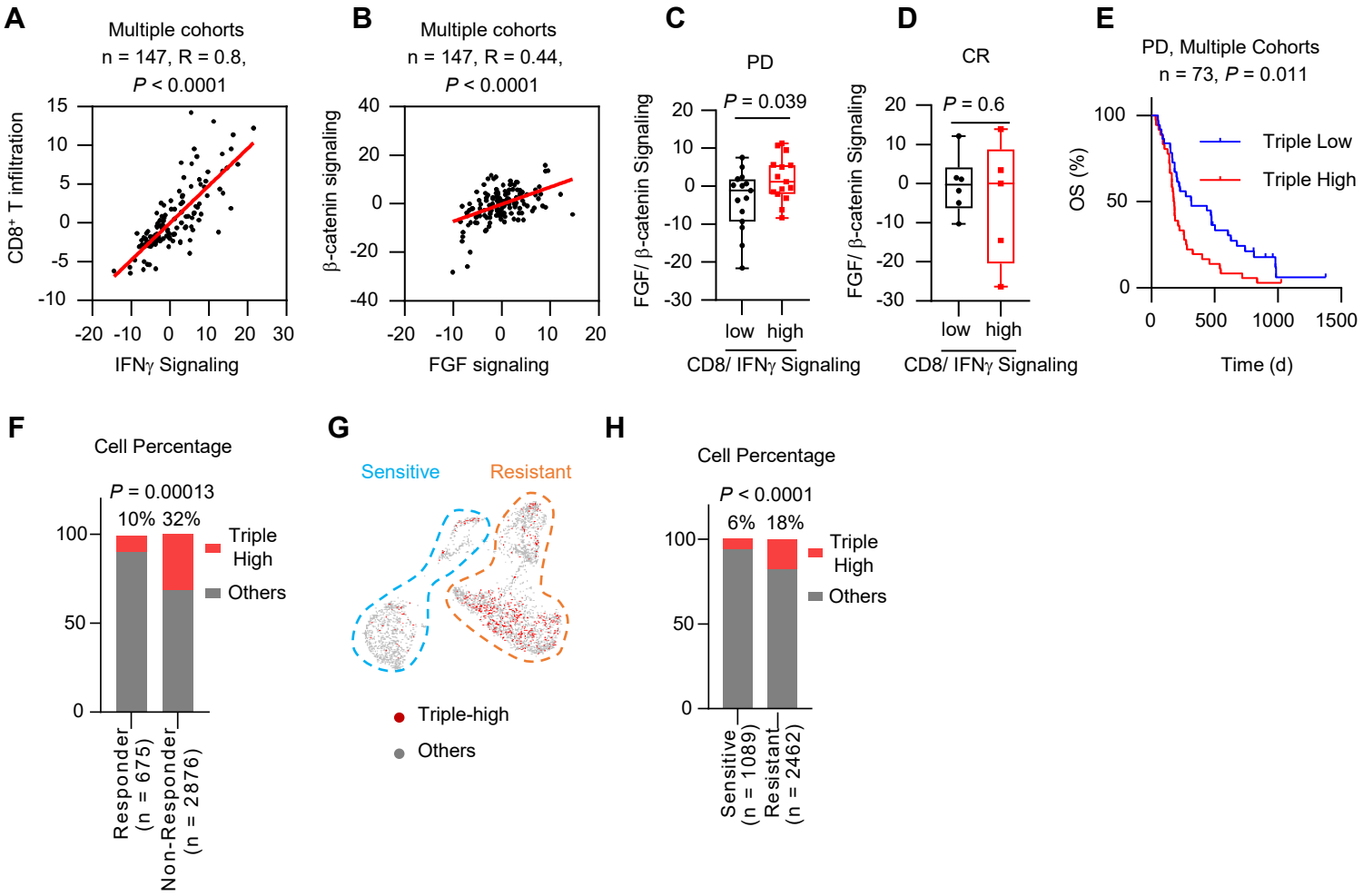

Figure S7: Oncometabolic reprogramming drives cancer hyperprogression during immunotherapy. Related to Figure 6.

(A-B) Correlation between CD8⁺ T cell infiltration and IFNγ signaling (**A**); and FGF signaling and β-catenin signaling (**B**) in 4 public cohorts combined. R and P values were determined by liner regression.

(C-D) Correlation between immunogenic and oncogenic signatures in PD (**C**) and CR (**D**) patients. Patients were divided into low and high CD8/ IFNγ signaling groups. The FGF/ β-catenin signaling levels were plotted. Two-tailed t-test.

(E) Overall survival of patients with PD on immunotherapy from multiple datasets stratified by median IFNγ/ FGF/ β-catenin gene signature scores (triple high vs triple low). HR = 0.55. Log-rank test.

(F) Percentages of tumor cells expressing triple high (IFNγ/ FGF/ β-catenin) gene signature in non-responders and responders to PD-1 therapy are shown. Chi-square test.

(G-H) Tumor cells have different sensitivities to anti-PD-1 therapy. Tumor cells expressing triple high (IFNγ/ FGF/ β-catenin) gene signatures are shown in red (**G**). Percentages of tumor cells expressing triple high (IFNγ/ FGF/ β-catenin) gene signatures in ICB-resistant or -sensitive tumor cells are shown (**H**). Chi-square test.

Table S6: Target sequences for gene knock out or knock down. Related to STAR Methods.

ID	Target sequence
Ms Ifngr1 KO1	ATTAGAACATTCGTCGGTAC
Ms Ifngr1 KO2	CTTGAACCCTGTCGTATGCT
Hm IFNGR1 KO1	GGTACTCCCAATATACGATA
Hm IFNGR1 KO2	GGTCCCTGTTTTTACCGTAG
Ms Stat1 KO1	GGTCGCAAACGAGACATCAT
Ms Stat1 KO2	CCAGTACAGCCGCTTTTCTC
Hm STAT1 KO1	GAGGTCATGAAAACGGATGG
Hm STAT1 KO2	ATTGATCATCCAGCTGTGAC
Hm CTNNB1 KO1	CTAACAGCCGCTTTTCTGTC
Hm CTNNB1 KO2	CAACAGTCTTACCTGGACTC
Hm CTNNB1 KO3	AGTCCTGTATGAGTGGGAAC
shFluc	CGCTGAGTACTTCGAAATGTC
Hm shPKM2 1	AACGCTTGTAGAACTCACTCT
Hm shPKM2 2	AAGAAGATCAACGCCTCACTG
Hm shPKM2 3	GAACTCACTCTGGGCTGTAAC
Hm shPKM2 4	CAACGCTTGTAGAACTCACTC
Ms shPkm2 1	AACGCTTGTAGTGCTCACTCT
Ms shPkm2 2	AACATGCAATAGAGACCAGCT
Ms shPkm2 3	GACTGGAAACCCTGACTTTAT
Ms shFgf2 1	AAGAGAGAGGAGTTGTGTCTA
Ms shFgf2 2	AACGAACTGGGCAGTATAAAC

Table S7: Primers for molecular cloning, Related to STAR Methods.

ID	Primer sequence
FGF2 promoter SacI F	ATATGAGCTCGATGTTGAGCCCCTTGTCATGTG
FGF2 promoter MluI R	ATATACGCGTCGTTTTTGCAGTACAGCCGCTT
Ms FGF2 OE SalI F	ATATGTCGACCATGGCTGCCAGCGGCATCAC
Ms FGF2 OE NotI R	ATATGCGGCCGCTCAGCTCTTAGCAGACATTGGAAGAAACAGTATGGC
CTNNB1 K345R F	GCAGAGTGCTGAGGGTGCTATCTGTCTGCTCTAG
CTNNB1 K345R R	ATAGCACCCTCAGCACTCTGCTTGTGGTCCACAG

Table S8: Primers for qPCR, Related to STAR Methods.

ID	Primer Sequence
Hm ACTB QF	GAGCACAGAGCCTCGCCTTT
Hm ACTB QR	ACATGCCGGAGCCGTTGTC
Hm GBP1 QF	AGCCCTACAACTTCGGAACAG
Hm GBP1 QR	TCTGGATTCGCCATCAGTCG
Hm MYC QF	TACAACACCCGAGCAAGGAC
Hm MYC QR	TTCTCCTCCTCGTCGCAGTA
Hm CCND1 QF	GATGCCAACCTCCTCAACGA
Hm CCND1 QR	GGAAGCGGTCCAGGTAGTTC
Hm VEGFA QF	CTTGCCTTGCTGCTCTACC
Hm VEGFA QR	CACACAGGATGGCTTGAAG
Hm MMP14 QF	AGTTCAGTGCCTACCGAAGAC
Hm MMP14 QR	TGTGTGTGGGTACGTAGGTC
Hm PDL1 QF	ACCTGGCTGCACTAATTGTCTA
Hm PDL1 QR	GGTGACTGGATCCACAACCAA
Hm CD47 QF	GCCTATATCCTCGCTGTGGTT
Hm CD47 QR	TTTGAATGCATTAAGGGGTTCCT
Hm FGF2 QF	GCTGTACTGCAAAAACGGGG
Hm FGF2 QR	AGCCAGGTAACGGTTAGCAC
Hm CD44 QF	AAAACTGCAGCCAACTTCCG
Hm CD44 QR	GAATACACCTGCAAAGCGGC
Hm AXIN2 QF	CAAACTTTCGCCAACCGTGGTTG
Hm AXIN2 QR	GGTGCAAAGACATAGCCAGAACC
Hm CCND2 QF	GAGAAGCTGTCTCTGATCCGCA
Hm CCND2 QR	CTTCCAGTTGCGATCATCGACG
Hm NKD1 QF	GAAGATGGAGAGAGTGAGCGAAC
Hm NKD1 QR	GTCATACAGGGTGAAGGTCCAC
Hm RNF43 QF	GGTTACATCAGCATCGGACTTGC
Hm RNF43 QR	ATGCTGGCGAATGAGGTGGAGT
Hm NOTUM QF	CTACTGGTGGAACGCAAACATGG
Hm NOTUM QR	CGCACCACCTCCTGGATGATG
Hm LEF1 QF	CTACCCATCCTCACTGTCAGTC
Hm LEF1 QR	GGATGTTCCTGTTTGACCTGAGG
Hm ANKRD1 QF	CCTGTGGATGTGCCTACGTT
Hm ANKRD1 QR	ACAGGCGATAAGATGCTCCG
Hm CTGF QF	GAGCAGCTGCAAGTACCAGT
Hm CTGF QR	GTCTTCCAGTCGGTAAGCCG
Hm HEY1 QF	GGCTGGTACCCAGTGCTTTT
Hm HEY1 QR	CCCGAAATCCCAAACTCCGA
Hm HES1 QF	GCCAGTGTCAACACGACACC
Hm HES1 QR	CCTCGTTCATGCACTCGCTG
Hm PTCH1 QF	TCGCTCTGGAGCAGATTTCC
Hm PTCH1 QR	TCTCGAGGTTCGCTGCTTTT
Hm GLI1 QF	CGGCACCCCTTCTCTTGCT
Hm GLI1 QR	CATCGAGTTGAACATGGCGTC
Ms Actb QF	CACTGTCGAGTCGCGTCCA
Ms Actb QR	GACCCATTCCCACCATCACA

Ms Myc QF	GTACCTCGTCCGATTCCACG
Ms Myc QR	GCACCTCTTGAGGACCAGTG
Ms Ccnd1 QF	TCAAGTGTGACCCGGACTG
Ms Ccnd1 QR	CACTACTTGGTGGCTCCCG
Ms Fgf2 QF	AAGCGGCTCTACTGCAAGAA
Ms Fgf2 QR	ACACTTAGAAGCCAGCAGCC
Ms Cd44 QF	TGAGACCTGCAGGTATGGGT
Ms Cd44 QR	GCTGAAGCATTGAAGCAATA
Ms Cdh1 QF	GGTCATCAGTGTGCTCACCTCT
Ms Cdh1 QR	GCTGTTGTGCTCAAGCCTTCAC
Ms Nanog QF	GAACGCCTCATCAATGCCTGCA
Ms Nanog QR	GAATCAGGGCTGCCTTGAAGAG
Ms Aldh1a1 QF	GGAATACCGTGGTTGTCAAGCC
Ms Aldh1a1 QR	CCAGGGACAATGTTTACCACGC
Ms Sox2 QF	AACGGCAGCTACAGCATGATGC
Ms Sox2 QR	CGAGCTGGTCATGGAGTTGTAC
Ms Klf4 QF	CTATGCAGGCTGTGGCAAAACC
Ms Klf4 QR	TTGCGGTAGTGCCTGGTCAGTT
Ms Bmi1 QF	ACTACACGCTAATGGACATTGCC
Ms Bmi1 QR	CTCTCCAGCATTCGTCAGTCCA
Ms Vim QF	CGGAAAGTGGAATCCTTGCAGG
Ms Vim QR	AGCAGTGAGGTCAGGCTTGGAA
Ms Zeb1 QF	ATTCAGCTACTGTGAGCCCTGC
Ms Zeb1 QR	CATTCTGGTCCTCCACAGTGGA
Ms Fn1 QF	CCCTATCTCTGATACCGTTGTCC
Ms Fn1 QR	TGCCGCAACTACTGTGATTCGG
Ms Tjp1 QF	GTTGGTACGGTGCCCTGAAAGA
Ms Tjp1 QR	GCTGACAGGTAGGACAGACGAT
Ms Snai1 QF	TGTCTGCACGACCTGTGGAAAG
Ms Snai1 QR	CTTCACATCCGAGTGGGTTTGG
Ms Snai2 QF	TCTGTGGCAAGGCTTTCTCCAG
Ms Snai2 QR	TGCAGATGTGCCCTCAGGTTTG
Ms Twist1 QF	GATTCAGACCCTCAAACTGGCG
Ms Twist1 QR	AGACGGAGAAGGCGTAGCTGAG
Ms Pcna QF	CAAGTGGAGAGCTTGGCAATGG
Ms Pcna QR	GCAAACGTTAGGTGAACAGGCTC
Ms Mki67 QF	GAGGAGAAACGCCAACCAAGAG
Ms Mki67 QR	TTTGTCCTCGGTGGCGTTATCC
Ms Cdk1 QF	CATGGACCTCAAGAAGTACCTGG
Ms Cdk1 QR	CAAGTCTCTGTGAAGAACTCGCC
Ms Cdk2 QF	TCATGGATGCCTCTGCTCTCAC
Ms Cdk2 QR	TGAAGGACACGGTGAGAATGGC
Ms Cdk4 QF	CATACCTGGACAAAGCACCTCC
Ms Cdk4 QR	GAATGTTCTCTGGCTTCAGGTCC
Ms Cdk6 QF	ACCTCTGGAGTGTCGGTTGCAT
Ms Cdk6 QR	TTCCTCTCCTGGGAGTCCAATG
Ms Cdk7 QF	TGAGAATGGAGTTCTGAAACTGGC
Ms Cdk7 QR	CCACACCATACATCCTAGCTCC
Ms Ccna2 QF	TTGTAGGCACGGCTGCTATGCT
Ms Ccna2 QR	GGTGCTCCATTCTCAGAACCTG

Ms Ccnb1 QF	AGAGGTGGAACTTGCTGAGCCT
Ms Ccnb1 QR	GCACATCCAGATGTTTCCATCGG
Ms Ccne1 QF	AAGCCCTCTGACCATTGTGTCC
Ms Ccne1 QR	CTAAGCAGCCAACATCCAGGAC